



A University of Sussex DPhil thesis

Available online via Sussex Research Online:

<http://sro.sussex.ac.uk/>

This thesis is protected by copyright which belongs to the author.

This thesis cannot be reproduced or quoted extensively from without first obtaining permission in writing from the Author

The content must not be changed in any way or sold commercially in any format or medium without the formal permission of the Author

When referring to this work, full bibliographic details including the author, title, awarding institution and date of the thesis must be given

Please visit Sussex Research Online for more information and further details

UNIVERSITY OF SUSSEX

**Performance of Continuously
Pumped, Passively *Q*-Switched,
Solid State Lasers**

Min Lu

School of Engineering and Design

University of Sussex

A thesis submitted for the degree of

Doctor of Philosophy

2011

Declaration

I confirm that this is my own work and the use of all materials from other sources has been properly and fully acknowledged.

No part of this thesis has already been, or is being currently submitted for any such degree, diploma or other qualification.

Signature:

Date:

This thesis is copyright © 2011 by Min Lu.

List of Related Publications

- [1] M. Lu, C. R. Chatwin, P. M. Birch, R. C. D. Young and W. Wang. The Effect of resonator design parameters on the minimum output pulse width of a passively Q -switched laser. *Asian Journal of Physics*, In Press, 19 (1), 2010.
- [2] M. Lu, C. R. Chatwin, R. C. D. Young and P. M. Birch. Numerical simulation of a CW-pumped Cr:YAG passively Q -switched Yb:YAG pulsed laser. *Optics and Lasers in Engineering*, 49: 617-621, 2009.
- [3] M. Lu, C. R. Chatwin, P. M. Birch, R. C. D. Young and W. Wang. Pulse width performance of a CW pumped passively Q -switched laser taking account of the Q -switch recovery time. *Asian Journal of Physics*, 18 (1): 131-142, 2009.

Acknowledgements

I would like to express my sincere gratitude to my supervisors Prof Chris Chatwin and Dr Rupert Young. It is impossible for me to fulfil my PhD research and finish my thesis without their valuable guidance and support.

Many thanks to all the colleagues in the Industrial Informatics and Manufacturing Systems Research Centre and Department of Engineering and Design, University of Sussex. I learnt a lot from the seminars organised by my group and from the discussions with them.

I would like to thank all the reviewers who reviewed my papers for their suggestions.

Finally, I would like to give my thanks to my husband Xiaoqi Ma and my parents for their continuing help, support and encouragement.

Abstract

This thesis studies the relationship between the pairs of resonator output coupling and intra-cavity absorber initial transmission, and the FWHM (full width at half maximum) pulse duration of a continuously pumped passively Q -switched solid-state laser, when the output energy is pre-determined. Depending on the magnitude of the pumping power, three different rate equation models are used to evaluate the required output coupler reflectivity and absorber initial-transmission pair for the corresponding FWHM pulse duration.

The energy transfer kinetics of the passively Q -switched laser decides the required pumping power; and the pair of output coupler reflectivity absorber transmission pair, determine the build-up time of Q -switching and the repetition rate of the laser system. Hence, the forms of the models are controlled by two conditions: 1) the build-up time of Q -switching; and 2) the recovery time of the absorber.

When the build-up time of Q -switching is relatively short, but the recovery time of the absorber is long, *Model I* is based on the simplified laser rate equations. It is used to evaluate the output coupler reflectivity and absorber initial-transmission pair, which satisfies the pre-determined output energy and FWHM pulse duration. *Model II* is set up to study the case when both the build-up time of Q -switching and the recovery time of the absorber are long. In *Model II*, the laser rate equations are solved using the Runge-Kutta method. *Model III* simulates the case when the recovery time of the absorber is short.

To validate the models, the simulation results of practical passively Q -switched laser systems are compared with experimental results reported in the literature. The agreement of the simulation results with reported experimental results demonstrates the importance of the boundary conditions for the different cases, and verifies the soundness of the models.

Generalizing the simulation results, obtained from different passively Q -switched laser systems with different pumping power and different pre-determined output energy, yields general conclusions which permit a designer to select the correct parameters for a desired laser performance.

Contents

Declaration	i
List of related publications	ii
Acknowledgements	iii
Abstract	iv
Contents	vi
List of tables	x
List of figures	xii
List of symbols, constants and acronyms	xx
1 Introduction	1
1.1 Development of the laser	4
1.2 Solid-state laser materials	12
1.2.1 Host materials	13
1.2.2 Optically active ions	13
1.2.3 Laser material properties and the common laser materials	14
1.3 <i>Q</i> -switched laser	15
1.4 Laser rate equations and the achievement of a passively	

<i>Q</i> -switched solid-state laser	17
1.5 Research methodologies	23
1.6 Contributions	24
1.7 Overview of the thesis	25
2 Foundations for Modelling	27
2.1 Introduction	28
2.2 The definition of Several Key Parameters	28
2.3 The general mathematical analysis of the pulse shape	30
2.4 Numerical simulation	34
2.5 Conclusions	36
3 A Simplified Model of a Passively <i>Q</i>-switched Solid-state Laser System	37
3.1 Introduction	38
3.2 Rate equations	38
3.3 Theoretical Analysis	41
3.3.1 The FWHM pulse width with different pairs of R and T_0	43
3.3.2 The effect of the absorber material (γ_s) on selecting a pair of R and T_0 to get the shorter FWHM pulse width	53
3.4 Modeling	56
3.4.1 A Cr:YAG passively <i>Q</i> -switched Nd:Glass laser	56
3.4.2 A Cr:YAG passively <i>Q</i> -switched Nd:YAG laser	60

3.5 Conclusions	64
4 A Model for a Passively Q-Switched Laser System with a Long Build-up Time	67
4.1 Introduction	68
4.2 Laser rate equations	69
4.3 The effect of the pump power on the output parameters	72
4.4 The simulation and computing steps	77
4.5 The effect of the pump rate	80
4.6 The pump rate and the gain medium	93
4.7 Conclusions	99
5 A Model for a Passively Q-Switched Laser Considering the Recovery Time of the Absorber	101
5.1 Introduction	102
5.2 Theoretical analysis	103
5.3 The simulation results showing the effect of recovery time	108
5.4 The simulation and computing steps	111
5.5 The simulation results of a continuously pumped Cr:YAG passively Q -switched Yb:YAG laser	115
5.6 The pump rate and the gain medium	128
5.7 Conclusions	137
6 Conclusions and Future work	139

6.1 Introduction	140
6.2 Conclusions	140
6.2.1 Models and their boundary conditions	141
6.2.2 Controlling the FWHM pulse duration	145
6.2.3 Programs and their run time	147
6.3 Further work	148
Appendix A The Lagrange Multiplier Technique	150
Appendix B Material Properties	152
B.1 Nd:YAG	152
B.2 Yb:YAG	153
B.3 Cr:YAG	155
References	156

List of Tables

2.1 The parameters of the laser system and materials	34
3.1 The FWHM pulse width t_p as $R = 20\%$ when $E_a = 1$ for $\alpha = 5, 10, 20$ and 50	46
3.2 The FWHM pulse width t_p as $R = 50\%$ when $E_a = 1$ for $\alpha = 5, 10, 20$ and 50	47
3.3 The FWHM pulse width t_p when $R = 20\%$ ($x = 1.61$)	51
3.4 The ranges of R and T_0 when $\alpha = 5, 10, 20, 50$ and $E_a = 0.2, 0.5, 1.5$ and 2	53
3.5 The data for laser system	57
3.6 The material properties for Nd:Glass	57
3.7 The material properties for Cr:YAG	57
3.8 The shortest t_p with its coupling pair of $R(x)$ and $T_0(z_a)$ as $E = 19mJ,$ $49mJ$ and $97mJ$	59
3.9 Material properties of Nd:YAG	61
3.10 The pair of $R(x)$ and $T_0(z_a)$ to achieve the shortest t_p when $E = 3mJ,$ $8mJ$ and $15mJ$ (namely E_a are 0.2, 0.5 and 1) for the Nd:YAG laser system	63

4.1 Material properties of Yb:YAG	73
4.2 Material properties of Cr:YAG	73
4.3 Parameters of the laser cavity	74
4.4 The theoretical and the experimental results	75
4.5 Material properties of Nd:YAG	93
5.1 The extreme points of P_a , E_a and t_p with the corresponding W_p and T_{0_stable}	111
B.1 Properties of Nd:YAG at $25^\circ C$ (with 1% Nd doping)	152
B.2 Properties of Yb:YAG (with 1% Yb doping)	154
B.3 Properties of Cr:YAG	155

List of Figures

1.1 The energy level for a three-level laser medium	18
1.2 The energy level for a four-level laser medium	19
1.3 The energy level system of an absorber	20
1.4 The laser cavity schematic	20
2.1 The Normalized average photon density $\phi(t)$ during the pulse stage	35
2.2 The normalized $n(t)$ and $n_{gs}(t)$ during the pulse stage	36
3.1 When $E_a = 1$, (a) the absorber parameter z_a as a function of the reflectivity parameter x and α (5, 10, 20 and 50), (b) the corresponding small-signal parameter z_l	45
3.2 t_p as the function of x when $E_a = 1$ and $\alpha = 5, 10, 20$ and 50	46
3.3 The adaptive pair of T_0 and R to keep $E_a = 1$ as $\alpha = 5, 10, 20$ and 50	46
3.4 (a) z_a , (b) z_l and (c) t_p as a function of x and α (5, 10, 20 and 50) when $E_a = 0.2$, (d) the proper pairs of R and T_0 to keep $E_a = 0.2$ for $\alpha = 5, 10, 20$ and 50	48
3.5 (a) z_a , (b) z_l and (c) t_p as a function of x and α (5, 10, 20 and 50) when $E_a = 0.5$, (d) the proper pairs of R and T_0 to keep $E_a = 0.5$ for $\alpha = 5, 10, 20$ and 50	48

- 3.6 (a) z_a , (b) z_l and (c) t_p as a function of x and α (5, 10, 20 and 50)
 when $E_a = 1.5$, (d) the proper pairs of R and T_0 to keep $E_a = 1.5$
 for $\alpha = 5, 10, 20$ and 50 49
- 3.7 (a) z_a , (b) z_l and (c) t_p as a function of x and α (5, 10, 20 and 50)
 when $E_a = 2$, (d) the proper pairs of R and T_0 to keep $E_a = 2$
 for $\alpha = 5, 10, 20$ and 50 50
- 3.8 (a) The FWHM pulse width t_p as a function of x and γ_s' (1.1, 1.3, 1.5 and
 1.7) when $E_a = 1.5$, (b) the corresponding pairs of R and T_0 55
- 3.9 (a) The FWHM pulse width t_p as a function of x and γ_s' (1.1, 1.3, 1.5 and
 1.7) when $E_a = 2$, (b) the corresponding pairs of R and T_0 55
- 3.10 (a) The FWHM pulse width t_p as a function of x and γ_s' (1.1, 1.3 and
 1.5) when $E_a = 2.5$, (b) the corresponding pairs of R and T_0 56
- 3.11 (a) The FWHM pulse width t_p as a function of x and γ_s' (1.1 and 1.3)
 when $E_a = 3$, (b) the corresponding pairs of R and T_0 56
- 3.12 (a) The parameter z_l versus x for the cases $E = 19mJ$, $49mJ$ and $97mJ$,
 (b) the corresponding z_a of z_l along x 58
- 3.13 The FWHM pulse width t_p as a function of x
 and different output energy E ($19mJ$, $49mJ$ and $97mJ$) 59
- 3.14 The proper pairs of R and T_0 to keep $E = 19mJ$, $49mJ$ and $97mJ$ 59
- 3.15 The normalized photon density distributions $\phi(t_{pulse})$ for $E = 19mJ$,
 $49mJ$ and $97mJ$ when t_p is the shortest 60
- 3.16 (a) the small-signal parameter z_l and (b) its coupling absorber parameter

- z_a versus the reflectivity parameter x when $E = 3mJ$, $8mJ$ and $15mJ$
(E_a are 0.2, 0.5 and 1) for the Nd:YAG laser system 62
- 3.17 The FWHM pulse width t_p as a function of x when $E = 3mJ$, $8mJ$ and
 $15mJ$ (namely E_a are 0.2, 0.5 and 1) for a Nd:YAG laser system 63
- 3.18 The coupling initial transmission T_0 of the output reflectivity R which to
keep $E = 3mJ$, $8mJ$ and $15mJ$ (namely E_a are 0.2, 0.5 and 1) for a
Nd:YAG laser system 63
- 3.19 The normalized photon density distributions $\phi(t_{pulse})$ $E = 3mJ$, $8mJ$ and
 $15mJ$ (namely E_a are 0.2, 0.5 and 1) for a Nd:YAG laser system 64
- 4.1 The FWHM pulse width t_p as a function of different pump rates W_p for two
models, considering W_p , or not 75
- 4.2 The output energy E_a as a function of different pump rates W_p for two
models, considering W_p , or not 75
- 4.3 The parameter t_p as a function of N_{wp} for two cases, considering W_p in the
rate equations, or not 76
- 4.4 The parameter E_a as a function of N_{wp} for two cases, considering W_p in the
rate equations, or not 76
- 4.5 The programming flowchart to get the required R 's coupling T_0 and the
FWHM pulse width t_p when E_a is known 79
- 4.6 The coupling parameter T_0 (a) of R to keep $E_a = 0.08$, with t_p (b), P_a (c)
and N_{wp} (d) when $W_p = 1 \times 10^3 s^{-1} cm^{-3}$, $1.2 \times 10^3 s^{-1} cm^{-3}$ and
 $1.6 \times 10^3 s^{-1} cm^{-3}$ 84

- 4.7 The coupling parameter T_0 (a) of R to keep $E_a = 0.1$, with t_p (b), P_a (c) and N_{wp} (d) as $W_p = 1 \times 10^3 s^{-1} cm^{-3}$, $1.2 \times 10^3 s^{-1} cm^{-3}$ and $1.6 \times 10^3 s^{-1} cm^{-3}$ 85
- 4.8 The coupling parameter T_0 (a) of R to keep $E_a = 0.3$, with t_p (b), P_a (c) and N_{wp} (d) as $W_p = 1 \times 10^3 s^{-1} cm^{-3}$, $1.2 \times 10^3 s^{-1} cm^{-3}$ and $1.6 \times 10^3 s^{-1} cm^{-3}$ 86
- 4.9 The coupling parameter T_0 (a) of R to keep $E_a = 0.5$, with t_p (b), P_a (c) and N_{wp} (d) as $W_p = 1 \times 10^3 s^{-1} cm^{-3}$, $1.2 \times 10^3 s^{-1} cm^{-3}$ and $1.6 \times 10^3 s^{-1} cm^{-3}$ 86
- 4.10 The distributions of the average photon density in the laser cavity during the pulse time using *Model I* and *Model II* as $R = 50\%$ and $W_p = 1 \times 10^3 s^{-1} cm^{-3}$ for different values of E_a , (a) $E_a = 0.08$, (b) $E_a = 0.1$, (c) $E_a = 0.3$, and (d) $E_a = 0.5$ 88
- 4.11 The coupling parameter T_0 (a) of R to keep $E_a = 0.08$, with t_p (b), P_a (c) and N_{wp} (d) as $W_p = 2 \times 10^3 s^{-1} cm^{-3}$ and $4 \times 10^3 s^{-1} cm^{-3}$ 89
- 4.12 The coupling parameter T_0 (a) of R to keep $E_a = 0.1$, with t_p (b), P_a (c) and N_{wp} (d) as $W_p = 2 \times 10^3 s^{-1} cm^{-3}$ and $4 \times 10^3 s^{-1} cm^{-3}$ 90
- 4.13 The coupling parameter T_0 (a) of R to keep $E_a = 0.3$, with t_p (b), P_a (c) and N_{wp} (d) as $W_p = 2 \times 10^3 s^{-1} cm^{-3}$, $4 \times 10^3 s^{-1} cm^{-3}$ and $8 \times 10^3 s^{-1} cm^{-3}$ 90
- 4.14 The coupling parameter T_0 (a) of R to keep $E_a = 0.5$, with t_p (b), P_a (c) and N_{wp} (d) as $W_p = 2 \times 10^3 s^{-1} cm^{-3}$, $4 \times 10^3 s^{-1} cm^{-3}$ and $8 \times 10^3 s^{-1} cm^{-3}$ 91
- 4.15 The distributions of the average photon density in the laser cavity during the pulse time using *Model I* and *Model II* as R is at the minimum value in Figs. 4.11 - 4.14 and $W_p = 2 \times 10^3 s^{-1} cm^{-3}$ for different values of E_a , (a) $E_a = 0.08$, (b) $E_a = 0.1$, (c) $E_a = 0.3$, and (d) $E_a = 0.5$ 92

- 4.16 For a Nd:YAG laser system, the coupling parameter T_0 (a) of R to keep $E_a = 0.08$, with t_p (b), P_a (c) and N_{wp} (d) as $W_p = 100s^{-1}cm^{-3}$ and $200s^{-1}cm^{-3}$ 96
- 4.17 For a Nd:YAG laser system, the coupling parameter T_0 (a) of R to keep $E_a = 0.1$, with t_p (b), P_a (c) and N_{wp} (d) as $W_p = 100s^{-1}cm^{-3}$, $200s^{-1}cm^{-3}$, $300s^{-1}cm^{-3}$ and $400s^{-1}cm^{-3}$ 96
- 4.18 For a Nd:YAG laser system, the coupling parameter T_0 (a) of R to keep $E_a = 0.3$, with t_p (b), P_a (c) and N_{wp} (d) as $W_p = 200s^{-1}cm^{-3}$, $300s^{-1}cm^{-3}$, $500s^{-1}cm^{-3}$ and $1000s^{-1}cm^{-3}$ 97
- 4.19 For a Nd:YAG laser system, the coupling parameter T_0 (a) of R to keep $E_a = 0.5$, with t_p (b), P_a (c) and N_{wp} (d) as $W_p = 400s^{-1}cm^{-3}$, $500s^{-1}cm^{-3}$ and $1000s^{-1}cm^{-3}$ 98
- 4.20 The distributions of the average photon density in the laser cavity during the pulse time using *Model I* and *Model II* as $R = 50\%$ for different pump rate and different E_a , (a) $E_a = 0.08$ and $W_p = 100s^{-1}cm^{-3}$, (b) $E_a = 0.1$ and $W_p = 100s^{-1}cm^{-3}$, (c) $E_a = 0.3$ and $W_p = 200s^{-1}cm^{-3}$, (d) $E_a = 0.5$ and $W_p = 400s^{-1}cm^{-3}$ 99
- 5.1 The parameters P_a (a), E_a (b), t_p (c) and the initial transmission T_0 (d) at the stable output state as a function of pumping rate W_p 109
- 5.2 The parameters P_a (a), E_a (b), t_p (c) and the initial transmission T_0 (d) at the stable output state as a function of N_{wp} 110
- 5.3 The programming flowchart to get the decided R 's coupling T_0 and the FWHM pulse width t_p when E_a and W_p are known 113

- 5.4 The programming flowchart to get the stable state 114
- 5.5 The output coupler R with its coupling initial transmissions at the first pump cycle T_{0_1st} and at the stable state T_{0_stable} for the cases when the pump rates W_p are $2 \times 10^3 s^{-1} cm^{-3}$, $4 \times 10^3 s^{-1} cm^{-3}$, $6 \times 10^3 s^{-1} cm^{-3}$ and $8 \times 10^3 s^{-1} cm^{-3}$, compared with the results obtained using *Model I* 116
- 5.6 The parameter N_{wp} as a function of R for two cases that one is for the first pump cycle, and the other is for the stable state when the pump rates W_p are $2 \times 10^3 s^{-1} cm^{-3}$, $4 \times 10^3 s^{-1} cm^{-3}$, $6 \times 10^3 s^{-1} cm^{-3}$ and $8 \times 10^3 s^{-1} cm^{-3}$ 117
- 5.7 The FWHM pulse width t_p as a function of R obtained using *Model III* for different pump rate (the pump rates W_p are $2 \times 10^3 s^{-1} cm^{-3}$, $4 \times 10^3 s^{-1} cm^{-3}$, $6 \times 10^3 s^{-1} cm^{-3}$ and $8 \times 10^3 s^{-1} cm^{-3}$) are compared with the data obtained using *Model I* 118
- 5.8 When R is 50% and E_a is 0.08, the distribution of the average photon densities in laser cavity $\phi(t)$ obtained using *Model I* and using *Model III* for the cases when W_p is (a) $2 \times 10^3 s^{-1} cm^{-3}$, (b) $4 \times 10^3 s^{-1} cm^{-3}$, (c) $6 \times 10^3 s^{-1} cm^{-3}$ and (d) $8 \times 10^3 s^{-1} cm^{-3}$ 120
- 5.9 The initial transmissions at the first working cycle T_{0_1st} and at the stable state T_{0_stable} , the parameter N_{wp} , and the FWHM pulse width t_p as a function of R and different W_p ($4 \times 10^3 s^{-1} cm^{-3}$, $6 \times 10^3 s^{-1} cm^{-3}$, $8 \times 10^3 s^{-1} cm^{-3}$ and $10 \times 10^3 s^{-1} cm^{-3}$) as E_a is 0.1 for *Model III*, the corresponding parameters got by *Model I* are plotted as well 123
- 5.10 The initial transmissions at the first working cycle T_{0_1st} and at the stable state T_{0_stable} , the parameter N_{wp} , and the FWHM pulse width t_p as a function of R and different W_p ($8 \times 10^3 s^{-1} cm^{-3}$, $10 \times 10^3 s^{-1} cm^{-3}$,

- $20 \times 10^3 s^{-1} cm^{-3}$ and $30 \times 10^3 s^{-1} cm^{-3}$) as E_a is 0.3 for *Model III*, the corresponding parameters obtained using *Model I* are plotted as well 124
- 5.11 The initial transmissions at the first working cycle T_{0_1st} and at the stable state T_{0_stable} , the parameter N_{Wp} , and the FWHM pulse width t_p as a function of R and different W_p ($8 \times 10^3 s^{-1} cm^{-3}$, $10 \times 10^3 s^{-1} cm^{-3}$, $20 \times 10^3 s^{-1} cm^{-3}$ and $30 \times 10^3 s^{-1} cm^{-3}$) when E_a is 0.5 for *Model III*, the corresponding parameters obtained using *Model I* are plotted as well 126
- 5.12 When R is 50% and E_a is 0.1, the distribution of the average photon densities in laser cavity $\phi(t)$ obtained using *Model I* and using *Model III* for the cases when W_p is (a) $4 \times 10^3 s^{-1} cm^{-3}$, (b) $10 \times 10^3 s^{-1} cm^{-3}$ 127
- 5.13 When R is 50% and E_a is 0.3, the distribution of the average photon densities in laser cavity $\phi(t)$ obtained using *Model I* and using *Model III* for the cases when W_p is (a) $8 \times 10^3 s^{-1} cm^{-3}$, (b) $30 \times 10^3 s^{-1} cm^{-3}$ 127
- 5.14 When R is 50% and E_a is 0.5, the distribution of the average photon densities in laser cavity $\phi(t)$ obtained using *Model I* and using *Model III* for the cases when W_p is (a) $8 \times 10^3 s^{-1} cm^{-3}$, (b) $30 \times 10^3 s^{-1} cm^{-3}$ 128
- 5.15 For a Nd:YAG laser system, the coupling parameter T_{0_1st} , T_{0_stable} (a) - (d) of R to keep $E_a = 0.08$, with N_{Wp_1st} and N_{Wp_stable} (e) - (g) and t_p (d) as W_p is $200 s^{-1} cm^{-3}$, $300 s^{-1} cm^{-3}$, $400 s^{-1} cm^{-3}$ and $500 s^{-1} cm^{-3}$ 130
- 5.16 For a Nd:YAG laser system, the coupling parameter T_{0_1st} , T_{0_stable} (a) - (d) of R to keep $E_a = 0.1$, with N_{Wp_1st} and N_{Wp_stable} (e) - (g) and t_p (d) as W_p is $200 s^{-1} cm^{-3}$, $300 s^{-1} cm^{-3}$, $400 s^{-1} cm^{-3}$ and $1000 s^{-1} cm^{-3}$ 131
- 5.17 For a Nd:YAG laser system, the coupling parameter T_{0_1st} , T_{0_stable} (a) - (d) of R to keep $E_a = 0.3$, with N_{Wp_1st} and N_{Wp_stable} (e) - (g) and t_p (d) as W_p

- is $500s^{-1}cm^{-3}$, $1000s^{-1}cm^{-3}$, $2000s^{-1}cm^{-3}$ and $3000s^{-1}cm^{-3}$ 133
- 5.18 For a Nd:YAG laser system, the coupling parameter T_{0_1st} , T_{0_stable} (a) - (d) of R to keep $E_a = 0.5$, with N_{Wp_1st} and N_{Wp_stable} (e) - (g) and t_p (d) as W_p is $1000s^{-1}cm^{-3}$, $2000s^{-1}cm^{-3}$, $3000s^{-1}cm^{-3}$ and $4000s^{-1}cm^{-3}$ 134
- 5.19 For a Nd:YAG laser system, when R is 50% and E_a is 0.08, the distribution of the average photon densities in laser cavity $\phi(t)$ obtained using *Model I* and using *Model III* for the cases when W_p is (a) $200s^{-1}cm^{-3}$, (b) $500s^{-1}cm^{-3}$ 135
- 5.20 For a Nd:YAG laser system, when R is 50% and E_a is 0.1, the distribution of the average photon densities in laser cavity $\phi(t)$ obtained using *Model I* and using *Model III* for the cases when W_p is (a) $200s^{-1}cm^{-3}$, (b) $1 \times 10^3 s^{-1}cm^{-3}$ 135
- 5.21 For a Nd:YAG laser system, when R is 50% and E_a is 0.3, the distribution of the average photon densities in laser cavity $\phi(t)$ obtained using *Model I* and using *Model III* for the cases when W_p is (a) $500s^{-1}cm^{-3}$, (b) $3 \times 10^3 s^{-1}cm^{-3}$ 136
- 5.22 For a Nd:YAG laser system, when R is 50% and E_a is 0.5, the distribution of the average photon densities in laser cavity $\phi(t)$ obtained using *Model I* and using *Model III* for the cases when W_p is (a) $1 \times 10^3 s^{-1}cm^{-3}$, (b) $4 \times 10^3 s^{-1}cm^{-3}$ 136

List of Symbols, Constants and Acronyms

Symbols

ϕ (cm^{-3})	Average photon density in the laser cavity
n (cm^{-3})	Instantaneous population inversion density of the gain medium
n_{gs} (cm^{-3})	Instantaneous population densities of the absorber ground state
n_{es} (cm^{-3})	Instantaneous population densities of the absorber excited state
σ (cm^2)	Laser stimulated emission cross-section
σ_{gs} (cm^2)	Absorber ground state absorption cross-section
σ_{es} (cm^2)	Absorber excited state absorption cross-section
γ	Inversion reduction factor of the gain media
γ_s	Inversion reduction factor of the absorber media
R	Reflectivity of the output mirror
L	Remaining two way dissipative (none useful) optical loss
l (cm)	Length of the gain media
l_s (cm)	Length of the absorbing media
n_{s0} (cm^{-3})	Absorber total population density
l' (cm)	Optical length of resonator

W_p ($s^{-1}cm^{-3}$)	Volumetric pump rate into the upper level
n_{tot} (cm^{-3})	Doping concentration of the gain medium
τ_{21} (μs)	Spontaneous emission lifetimes of the upper level of the gain medium
τ_s (μs)	Spontaneous emission lifetimes of the upper level of the absorber
n_i (cm^{-3})	Initial population inversion density at the start of Q -switching
n_f (cm^{-3})	Final inversion population density at the end of Q -switching
n_t (cm^{-3})	Instantaneous population inversion density of gain media when the output power is at the peak point
G_0^2	Round-trip unsaturated small signal power gain
T_0	Initial transmission of an absorber
n_{gsi} (cm^{-3})	Initial density of the absorbing state at ground level of the absorber at the beginning of the Q -switching
n_{esi} (cm^{-3})	Initial population density in the absorber's excited state at the beginning of the Q -switching
c (m/s)	Speed of light
ϕ_{max} (cm^{-3})	Maximum value of the photon density in the laser resonator at the lasing stage
$t_r = \frac{2l'}{c}$ (ns)	Round-trip transit time of light in the resonator of optical length l'
$z_l = 2\sigma l_i = \ln(G_0^2)$	Small-signal parameter
$z_a = 2\sigma_{gs} l_s n_{gsi} = -\ln(T_0^2)$	Absorber parameter
$x = \ln\left(\frac{1}{R}\right)$	Reflectivity parameter
$\rho = \ln\left(\frac{n_i}{n_f}\right)$	Final population parameter

$$n_{ii} = \frac{n_i}{n_i}$$

Peak point population parameter

$$E_a = \ln\left(\frac{1}{R}\right) \ln\left(\frac{n_i}{n_f}\right)$$

Output energy parameter

$$P_a = c\gamma\sigma \ln\left(\frac{1}{R}\right) \phi_{\max}$$

Peak power parameter

Constants

$$h = 6.626 \times 10^{-34} (Js)$$

Planck constant

$$c = 2.998 \times 10^8 (m/s)$$

Speed of light in vacuum

Acronyms

FWHM Full width at half maximum

LD Laser diode

CW Continuous wave

Chapter 1

Introduction

The Laser is one of the most important technologies created in the late twentieth century. After it was invented in 1958, the technologies based on lasers were developed for different applications. Some applications of lasers, such as materials processing and pulsed holography, require high laser power with nanosecond pulses. Compared with other types of lasers, passively Q -switched solid-state lasers do not require high voltages or complex control mechanisms to achieve high peak power, high repetition rates and short nanosecond pulse durations. They are used widely for scientific, industrial and military applications, including materials processing, measurement, holography, medicine, and laser printers. This research focuses on understanding and controlling the performance of passively Q -switched solid-state lasers.

A continuously pumped passively Q -switched laser produces a continuous train of pulses at a fixed repetition rate; in a stable operational state one pulse in the pulse train is representative of the output properties of the laser. When the properties of the laser resonator are decided, the output properties of a continuously pumped passively Q -switched laser, such as the output energy, the pulse duration, and the peak power, can be controlled by selecting the pumping power, and an absorber/output coupler pair.

Due to their importance, Q -switched lasers are the focus of significant research activity. Numerical models of passively Q -switched lasers have been reported by Ref. [Degnan, 1995], [Xiao, 1997], [Liu, 2001], [Li, 2006a]. The experimental results and theoretical analysis of a continuously pumped passively Q -switched laser have been reported in Refs. [Langrock, 2002], [Li, 2004], [Li, 2005b], [Mercer, 2007]. International research has focused on the optimization of the output coupler and the transmission of the saturable absorber to maximize output energy and efficiency. In the research of maximizing output energy, the magnitude of the pulse width of the laser system isn't considered. However, some applications require control of the output pulse duration with a pre-determined output energy.

As indicated in the first paragraph, passively Q -switched lasers have a wide range of applications. Passively Q -switched laser systems with high output energies in short pulse widths have applications for material processing, micromachining, marking & cutting of extremely hard materials (such as diamonds), nonlinear optics, supercontinuum generation, time-resolved fluorescence measurements, DNA-analysis, lidar (a detection system that works on the principle of radar, but uses light from a laser) and laser ranging, pollution monitoring, ignition of explosives, combustion engines and gas mixtures.

Continuously pumped passively Q -switched lasers are frequently used for welding and cutting. These laser systems have high average powers and high pulse energies with a short pulse width. Compared with other industrial systems, passively Q -switched laser systems provide advantages such as high precision and less chance of material warping. Passively Q -switched laser systems with shorter pulse widths can reduce the heat-affected zone of the materials (reducing the heat transfer within materials), and enlarge the range of workpiece materials.

Passively Q -switched laser systems can provide very short pulse durations to satisfy the requirements of laser micromachining for which it delivers great flexibility, high resolution and precision; for micromachining it is a developing technology for high precision microfabrication, which includes laser micro drilling, micro milling, scribing and dicing, and laser micro cutting. When the pulse width is shorter than the heat induction time of the workpiece material, material warping is minimized. Currently many research groups are working to get ultra-short pulse lasers which can be used to photoetch the components onto CPU chips.

However, some applications such as the removal of tattoos and the removal/reduction of hyperpigmentation require a passively Q -switched laser which can produce long-pulse-durations, high-pulse-power at low repetition rates.

In these examples, the pulse duration and output energy of laser systems are key design issues. Different applications of passively Q -switched lasers have different requirements for the magnitude of the pulse width. In commercial product design, the materials for the gain medium and the saturable absorber are mature, for example, Nd:YAG and Yb:YAG are normally used as the gain medium, Cr:YAG is the most popular material for the absorber. It is unnecessary to develop new materials to control the FWHM pulse duration of passively Q -switched lasers. Based on the known technology and materials, it is possible to achieve the required output performance by the selection of several components, such as the output coupler, the absorber's initial transmission, the length of the laser cavity, and the pump source. This research focuses on the optimization of resonator and material parameters to satisfy these important performance requirements. The thesis gives direction to achieve the expected FWHM pulse width of a passively Q -switched laser and satisfy the predefined output energy requirements.

1.1 Development of the laser

LASER is an acronym for **L**ight **A**mplification by the **S**timulated **E**mission of **R**adiation which was established by Gordon Gould in 1957. It is a mechanism for emitting electromagnetic radiation, typically UV light, visible light or IR light, via the process of stimulated emission. The emitted laser light is (usually) a spatially coherent, narrow low-divergence beam, which can be manipulated with lenses. In a coherent beam of electromagnetic energy, all the waves have the same frequency and phase. Laser light is generally a narrow spectrum of near-monochromatic light; yet, there are lasers that emit a broad spectrum of light, or emit different wavelengths of light simultaneously.

In 1917, Albert Einstein first proposed the process that makes lasers possible called "Stimulated Emission" which is a process that acts on a population

inversion to stimulate the emission of radiation from an excited level (induced by the presence of radiant energy at the same frequency) to a lower level. The stimulated radiation is coherent with the stimulating photons.

The precursor to the laser was the **MASER** (**M**icrowave **A**mplification by **S**timulated **E**mission of **R**adiation). The maser amplified electromagnetic radiation of much longer wavelengths in the microwave range (thus the M instead of L in maser). The first maser was created by Charles H. Townes and his colleagues [Gordon, 1954] who succeeded in producing an inverted population by isolating excited ammonia molecules [Bertolotti, 1983]. Nikolai Basov and Alexander Prokhorov [Bertolotti, 1983] of the USSR first developed the system with more than two energy levels which can release stimulated emission without falling to the ground state, thus maintaining a population inversion, and achieving a continuous output.

In 1960, the first working laser, a "pink" ruby bar ($\text{Cr}^{3+}:\text{Al}_2\text{O}_3$) with two parallel end faces acting as the resonator and a pulsed photographic flashlamp as an optical pumping source, was built by Theodore. H. Maiman [Maiman, 1960], [Hecht, 1992]. Soon afterwards, in 1960, Peter Sorokin and Mirek Stevenson [Hecht, 1992] developed the first 4-level laser (uranium doped calcium fluoride) which was capable in theory of continuous output, although in the solid state a continuous output could not be achieved. Since 1960, laser systems have enjoyed rapid and steady development.

After the invention of the ruby laser in 1960, the research and development of lasers focused on obtaining laser action from as many materials as possible. Hence, lasers based on gas, liquid and solid media with a wide variety of different operating properties were demonstrated.

From 1960-1969, there were many significant achievements with solid-state lasers. In 1961, E. Snitzer working in American Optical Corporation

demonstrated the first neodymium-glass laser (Nd:glass laser) in a millimeter-scale rod, which was essentially the first fiber laser [Snitzer, 1961]. In the same year, L. F. Johnson and K. Nassau at Bell Labs reported the first neodymium-doped solid-state laser operating at $1.06 \mu\text{m}$ [Johnson, 1961]. Soon after, it was also invented at Bell Labs where Ralph R. Soden, Scotch Plains, and Le Grand G. Van Uitert demonstrated the first continuous wave operation of a rare earth doped crystal laser (a Nd:CaWO₄ laser) at room temperature, and was granted a patent on this in 1965 [Soden,1965]. The first fiber amplifier using a spring-shaped coil of fiber slipped around a linear flashlamp was demonstrated in 1964 by C. J. Koester and E. Snitzer at American Optical [Koester, 1964].

During the 1960's, the research into solid-state lasers focused on the development of new inorganic hosts for laser materials based on various rare earths. The main host YAG was investigated at Bell Labs during this period. It must be mentioned that in 1964, the first Nd:YAG (neodymium ions doped yttrium aluminium garnet) laser was invented by Joseph E. Geusic, R. G. Smith, H. M. Markos etc. at Bell Labs [Geusic, 1964]. Nd:YAG has good thermal, mechanical and optical properties which led to Nd:YAG being the most versatile and widely used active material for solid-state lasers.

In the 1960s, the semiconductor laser was developed. The concept of a semiconductor laser was introduced by Basov [Basov, 1964]. He suggested that the stimulated emission of radiation could occur in semiconductors by the recombination of carriers injected across a p-n junction. The first pulsed semiconductor laser emitting infrared light was invented by Robert Hall and researchers at General Electric Labs in November 1962 [Hall, 1962]. One month later, Nick Holonyak and Sam Bevacqua of GE reported a red light diode made from GaAs alloyed with phosphorus. In the same year, laser action in a semiconductor material was also demonstrated separately by M. I. Nathan [Nathan, 1962], N. Holonyak Jr [Holonyak Jr. 1962] and T. M. Quist [Quist, 1962]. About 10 years later, the continuous operation, room temperature,

semiconductor laser was achieved. The laser diode (LD) is also used as the pump source for other lasers. In 1962, the LD pumped solid-state laser was proposed, and was demonstrated in 1963 by Robert Keyes and Theodore Quist at MIT Lincoln Labs [Keyes, 1964]. The first LD pumped solid-state laser operated at cryogenic temperatures, but the promise of the approach was recognized.

Gas and liquid lasers, which play a very important role, also had a very fast development in 1960s. Just before the end of 1960, the first gas laser (using helium-neon gas) operating at $1.15 \mu\text{m}$, was invented by Ali Javan, William Bennett, and Donald Herriott at Bell Labs [Javan, 1961]. The helium-neon (He-Ne) gas laser was the first laser to emit a continuous beam, and its lasing action could be initiated by an electric discharge rather than the intense discharge of photons from a flashlamp [Siegman, 1986]. One year later (in 1962), the first visible continuous wave He-Ne gas laser was reported by Alan White and J. Dane Rigden at Bell Labs [White, 1962]. This He-Ne gas laser was operating in the red at 632.8 nm . In 1964, the red He-Ne laser was used by Emmett Leith and Juris Upatnieks at the University of Michigan to make the first three-dimensional laser holograms which was displayed at a conference of the Optical Society of America. Spectra-Physics and Optics Technology Inc. were soon manufacturing red He-Ne lasers to sell for research and commercial applications. After the invention of the He-Ne laser, the first high power CO_2 laser operating at nominal wavelengths centring around 9.4 and $10.6 \mu\text{m}$ was demonstrated in 1964 by C. K. N. Patel at Bell Labs [Patel, 1964]. Due to its high efficiency, the CO_2 laser went on to become one of the main industrial work horses; it is commonly found with power levels of 5 to 10kW , exceptionally people have built 100kW systems.

The chemical laser is an important branch of gas lasers. The first chemical laser was invented in 1965 by George Pimentel and his colleagues at University of California, Berkley [Kasper, 1965], [Arnold, 1973]. Today, the most common chemical lasers are the chemical oxygen iodine laser (COIL), all gas-phaser iodine laser (AGIL), the hydrogen fluoride laser (HF laser), the deuterium

fluoride laser (DF laser), and the deuterium fluoride-carbon dioxide laser (DF-CO₂ laser). The HF and DF lasers are operating in the mid-infrared region, while the COIL and DF-CO₂ lasers are transfer lasers. Chemical lasers can produce high power continuous wave output which reaches megawatt power levels [Spencer, 1969], [Mirels, 1972].

The dye laser (a kind of liquid laser) was also invented in the 1960s. In 1966, Peter Sorokin and J. R. Lankard reported the first dye laser at IBM [Schafer, 1966], then Fritz P. Schaefer independently invented a dye laser at the Max Planck Institute in the same year [Brackmann, 2000]. Mary L. Spaeth demonstrated the first tunable dye laser at Hughes Research Labs [Brackmann, 2000]. Dye lasers can be pumped by incoherent or laser sources, both pulsed and continuous wave (CW) [Peterson, 1970], [Shank, 1975]. Compared to gases and most solid state lasing media, the output of a dye laser is always coherent radiation tunable over a specific spectral region with an ultra narrow line width or ultra short pulse. The wide bandwidth makes dye lasers particularly suitable for tunable lasers and pulsed lasers [Aldag, 2005].

In 1960s, the mode-locked technology was demonstrated. In 1963, Logan E. Hargrove, Richard L. Fork, and M. A. Pollack conceived and carried out the first experiments that demonstrated mode-locking by a He-Ne with an acousto-optic modulator (the first mode locked acousto-optic *Q*-switch). The effect produced is coupling of the optical cavity modes to produce intense, short, and periodic optical pulses. The mode-locking principle has since been used to accomplish even further reductions in pulse duration. Mode locking is fundamental for laser communications and is the basis for femtosecond lasers.

The laser cavity was studied in the 1960s. The theoretical analysis of the optical resonator was published in 1961 by A. G. Fox and T. Li in the Bell system technical journal [Fox, 1961].

In the 1970s, laser research focused on the engineering improvements and applications of lasers. The system lifetime and reliability were improved in this decade. The construction of large Nd:glass lasers began at many research facilities. At the same time, the solid-state lasers were readily accepted as versatile research tools in many laboratories. Progress in the operation of holmium-, thulium-, and erbium-doped crystals was achieved from 1970 to 1978.

The semiconductor laser had a fast development in the 1970s. In 1970, the first continuous wave semiconductor laser operating at room temperature was reported by Z. Alferov, Mort Panish and Izuo Hayashi at Ioffe Physico-Technical Inst. [Alferov, 1970]. Charles H. Henry proposed the idea of the quantum well in 1972. Two years later (in 1974), Charles H. Henry, R. Dingle, and W. Wiegmann observed and reported the quantum levels in *Physical Review Letters* [Dingle, 1974]. In 1976, Jim Hsieh and C. Shen demonstrated the first room-temperature InGaAsP diode laser operation at $1.25 \mu\text{m}$, at MIT Lincoln Labs [Hsieh, 1977].

The first excimer laser based on Xenon (Xe) was produced in 1970 by N. Basov and his colleagues at Lebedev Labs in Moscow [Basov, 1970]. Then, J. J. Ewing and Charles Brau made the first rare gas halide excimer laser in 1974 at Avco Everet Labs. Soon after, the excimer laser became a common laser in material processing, and medical devices.

During the 1980s, the practical use of laser-based systems began to appear. Starting from 1979, and into the 1980s, a number of tunable lasers were discovered. A breakthrough in tunable lasers was the invention of the alexandrite laser based on $\text{Cr}^{3+}:\text{BeAl}_2\text{O}_4$ crystal. Then the Ti:Sapphire laser was invented by P. Moulton at MIT Lincoln Labs in 1982 [Moulton, 1986]. In 1989, the Ti:Sapphire laser became a commercial product.

The performance of diode lasers was improved during the 1980s. In 1985, K. Iga demonstrated the first room-temperature operation vertical-cavity surface-

emitting semiconductor lasers (VCSELs) [Iga, 1985]. After this, laser diodes became commercially available with output powers of several watts. Another two kinds of the common commercial semiconductor lasers are the vertical-external-cavity surface-emitting lasers (VECSELs) [Iga, 2000], and the external-cavity diode lasers [Welch, 2000].

From 1985 to 1987, the commercial diode-pumped Nd:YAG lasers experienced rapid development. During this period, new schemes for holmium lasers which produced efficient systems capable of delivering high-output energy at room temperature were introduced.

In the 1990s, the research and the development of lasers focused on making lasers with operational characteristics optimized for specific applications. In 1991, the mode locking of the Ti:Sapphire laser was reported. From 1993 - 1998, the colquiriite family of crystals, Cr⁴⁺-doped garnets and forsterite were demonstrated as sources for tunable lasers.

In 1994, Jerome Faist, Federico Capasso, Deborah L. Sivco, and Carlo Sirtori etc. demonstrated the first quantum cascade multiple wavelength laser at Bell Labs [Faist, 1994]. After this, the technology was developed extensively, which makes quantum-cascade lasers excellent sources for most applications from the mid-IR to the terahertz band.

The first petawatt laser using a revolutionary laser was demonstrated at Lawrence Livermore National Labs in 1996. The laser reached a 1.25 petawatts peak power.

In 1997, Wolfgang Ketterle and his colleagues reported the first pulsed atom laser which was the interference between two colliding condensates at MIT [Andrews, 1997].

In the recent decade, many types of lasers covering a wide range of wavelengths and over a wide variety of output power levels were developed. A generation of compact, robust, reliable micro-lasers, waveguide lasers, and thin disk lasers were invented for commercial laser systems.

In 2004, O. Boyraz and B. Jalali demonstrated the first silicon Raman laser at the University of California, Los Angeles [Boyraz, 2004].

In 2006, John Bowers reported the first silicon laser at the University of California, Santa Barbara [Fang, 2006]. One year later (in 2007), the first mode-locked silicon evanescent laser was reported by the same group [Koch, 2007].

In addition to the usual liquid state, dye lasers are available as solid state dye lasers (SSDL), which are based on solid media (for example, the dye doped in a polymer matrix). The first continuous-wave operation of a solid-state dye laser was achieved by R. Bornemann in 2006 [Bornemann, 2006]. An unusual kind of the dye laser is the organic semiconductor dye laser, which is an organic dye embedded into an organic semiconductor [Klinkhammer, 2009].

After the first petawatt laser was made, the Lawrence Livermore National Labs demonstrated the first 10 Petawatt laser in 2010.

Observing the recent fifty-year history of the laser and the development of the technologies based on laser systems, it is noted that the application of the laser system and the corresponding technologies were rapidly invented in the laboratory, then emerged out of the lab and into use in a wide variety of practical applications. The improvement of the laser system and the research into laser applications ran parallel to the demonstration of new laser systems.

The first supermarket barcode scanner (a red He-Ne gas laser), which was the first use of lasers in the daily lives of the general population was used on 26th of

June, 1974 in Troy, Ohio. The laser has a wide variety of applications in modern society, such as medicine (eye surgery, dentistry, bloodless surgery, cosmetic surgery), industry including material processing (cutting, welding, brazing, bending) and non-contact measurement, military (marking targets, blinding troops, electro-optical countermeasures), spectroscopy, holography, laser printer, disc player reader, photochemistry, inter-ferometry and optical communication.

1.2 Solid-state laser materials

The solid-state laser is the most important branch of the laser family. The flexibility of solid-state lasers leads to a wide variety of applications. Solid-state lasers can be found in manufacturing, in hospitals, in research laboratories, in military systems, and in our daily life.

The wide range of active materials and their flexible size and shape are the factors that results in the wide application of the solid-state lasers. Materials which can be used as a gain medium for laser operation must have the properties to amplify light by stimulated emission. A solid-state material should satisfy the general properties of the laser material, which must possess sharp fluorescent lines, strong absorption bands, and high quantum efficiency for the fluorescent transition of interest. Generally, a solid-state laser material is a host crystal or glass doped with a small amount of optically active ions, and the optical transitions occur between states of inner, incomplete electron shells [Sennaroglu, 2007]. The spectroscopic properties of the laser transition are characterized by its upper level lifetime, emission cross section, and gain bandwidth, these properties determine the way the laser system may be designed and operated [Cheo, 1989].

A material which is suitable for solid-state laser applications must possess appropriate chemical, mechanical, thermal, and optical properties, which are determined by the inherent properties of the host material, the properties of the

optically active ions, and the mutual interaction between the host and the dopant ions [Staliunas, 2003].

1.2.1 Host materials

Normally, the solid-state host materials consist of crystalline solids and glasses.

A laser host material must satisfy the following criteria:

- 1) The crystal must be rugged and stable with respect to operational environment, and be robust to thermal, photo, and mechanical changes. Here, the most important parameters are thermal conductivity, hardness, and fracture strength. The crystal must have a high stress-fracture limit, a small thermal expansion and stress-optic coefficients to stop lensing, and be hard for good polishing.
- 2) The crystal must possess favourable optical properties. It must have minimum scattering centres, a minimum parasitic absorption at lasing and pump wavelengths, and a low index of refraction to maximize the stimulated emission cross section.
- 3) The crystal must have a lattice that can accept the dopant ions and that have local crystal fields of symmetry and the strength needed to induce the desired spectroscopic properties.
- 4) The crystal must be easily and economically produced with high quality in a large size.

Today, the materials used for the host includes: 1) glasses, 2) Oxides, 3) sapphire (Al_2O_3), 4) garnets, such as YAG, 5) Aluminate (YAlO or YAP), 6) Oxysulfide, 7) phosphates and silicates, 8) tungstates, molybdates, vanadates, and beryllates, 9) fluorides, and 10) ceramics.

1.2.2 Optically active ions

The optically active ions suitable for doping must deliver [Erneux, 2010]:

- 1) an efficient absorption of pump radiation;

- 2) an efficient internal conversion to a metastable-state population with small quantum defect;
- 3) an appropriate energy storage time in the metastable-state to utilize all pump energy;
- 4) an efficient radiative emission at the laser wavelength with high quantum efficiency;
- 5) no absorption at the lasing wavelength;
- 6) an emission linewidth compatible with desired tenability and stimulated emission probability;
- 7) an ion-ion interaction compatible with maximum pumping and minimum quenching.

The most important optically active ions used for doping are rare earth ions (such as Nd^{3+} , Eu^{3+} , Er^{3+} , Yb^{3+}), actinide ions, and transition metal ions (such as Cr^{3+}) [Arkin, 2002].

1.2.3 Laser material properties and the common solid-state laser

The solid-state laser material can be characterised by the following properties:

- 1) laser data, including lasing wavelength, halfwidth of the laser transition, pumping wavelength, wavelength below which colour centre generation has been observed or is possible, effective cross section of stimulated emission, temperature coefficient of the refractive index, nonlinear refractive index;
- 2) mechanical properties, including specific weight, Poisson number, Young's modulus, fracture tension, fracture tension due to microcracks in the material, fracture toughness, Knoop hardness as an indicator for polishing the material;
- 3) crystal properties, including melting temperature, concentration in atom per cent, concentration in weight percentage, conversion factors for the calculation of the absolute ion number, elasto-optical coefficients from the literature.

There are large numbers of solid state materials in which laser action can be achieved, but few types are widely used. The commercial solid-state laser used in some applications include: 1) ruby laser, 2) Nd:Lasers, 3) Er:Lasers, 4) tunable lasers and 5) Yb:YAG laser. The ruby laser is not very common due to its low efficiency.

1.3 *Q*-switched laser

Q-switching, also known as **giant pulse formation**, is a technique by which a laser can be made to produce a pulsed beam of light [Drexhage, 1972], [Koechner, 2006]. The technique allows the production of light pulses with extremely high peak power. *Q*-switching is achieved by putting a *Q*-switch in the laser resonator. When the cavity *Q* is lower, the energy is stored in the amplifying medium by optical pumping, and the cavity losses are high, hence lasing action cannot occur. After a certain time the stored energy in the amplifying medium will exceed the threshold level, and the medium is gain saturated. At this moment, the resonator losses are low, and the cavity *Q* is changed from low to high. The stored energy is suddenly released as a short laser pulse.

In 1958, Gordon Gould first proposed *Q*-switching. Three years later (in 1961), *Q*-switching used an electrically switched Kerr cell shutter in a ruby laser to concentrate the output of the laser into a single pulse; this was discovered by R. W. Hellwarth and F. J. McClung [McClung, 1962]. In 1963, W. G. Wagner and B. A. Lengyel first described the theory of the *Q*-switched laser [Wagner, 1963].

There are two main kinds of *Q*-switching: Active *Q*-switching and Passive *Q*-switching. The active *Q*-switching is based on an active loss modulation with a *Q*-switch. The pulse repetition rate is externally controlled. Typical Active *Q*-

switches are mechanical Q -switches, electro-optical Q -switches (a Pockels cell or Kerr cell), and acousto-optic Q -switches.

As an alternative to the active Q -switched laser, the passively Q -switched laser gives low cost, reliable operation without high voltages. In the cavity, a passive Q -switch consists of an optical element whose transmission increases when the intensity of light exceeds some threshold. Initially, the loss of the material is high, as the fluence increases, the material becomes more transparent, and then at high fluence levels the material bleaches, which results in a high transmission. When this kind of material with high absorption at the laser wavelength is set in the laser cavity, it will prevent laser oscillation, but still permit some lasing once a large amount of energy is stored in the gain medium. As the laser power increases and exceeds the round-trip losses, the material saturates. The resonator loss reduces rapidly, and the power increases faster. This results in the absorber being in a state with low losses to allow efficient extraction of the stored energy by the laser pulse. After the pulse, the absorber recovers to the high loss state. Then the next pulse is delayed until the energy in the gain medium is fully replenished.

Historically, the passive Q -switched laser was studied for the CO₂ laser for the generation of high intensity pulses [Vasilenko, 1975]. Today, with the development of microchip solid state lasers, passive Q -switched microchip lasers have led to practical applications. The passive Q -switched microchip laser deliver extremely short high-peak-power pulses without the need for an additional external pulse generator [Chen, 2000]. The short pulse widths are useful for high precision optical ranging with applications in automated production.

Saturable absorbers which have been widely used for the passive Q -switching of solid state lasers include dye films [Drexhage, 1972], colour centers [Morris, 1990] [Dong, 1993] [Chen, 2000], and doped crystals [Spariosu, 1993] [Sillard,

1998]. The passively Q -switched lasers with organic dyes (dye films or colour centers) used for saturable absorbers have poor durability which results from the degradation of the light sensitive organic dye, and the low thermal limits of plastic materials. Hence, the applications of the passive Q -switched lasers were limited. The crystal doped with the absorber ions or containing colour centers improved the durability and reliability of passive Q -switched lasers. $F_2:LiF$ colour center crystal was the first new material used as the absorber besides the organic dyes in 1990. Now $Cr^{4+}:YAG$ is employed as the most popular absorber material for passively Q -switched lasers. The Cr^{4+} ions provide a high absorption cross section at the laser wavelength.

1.4 Laser rate equations and the achievement of a passively Q -switched solid-state laser

The important thing for laser research is to study the laser behaviour, and to give sufficiently accurate results to permit performance design. The laser rate equations can be employed to describe the dynamic behavior of a laser such as average and peak power, Q -switched pulse shape, and pulse duration. A set of simultaneous differential equations describe the population inversion and the radiation density within a laser medium. In real laser systems the pumping and laser processes involve a large number of energy levels. So a laser rate equation model can be very complex. In general, each laser has its own set of rate equations. However, the main features of the lasers can be studied using a three-level or four-level optically pumped energy level system. Between the three-level and four-level systems, there are the quasi-three-level or quasi-four-level lasers.

An optically pumped three-level laser is shown in Fig. 1.1. In this diagram, all ions of the laser medium are in the lowest level 1 (ground level E_1). Ions are raised to level 3 (pump band E_3) by the pump light. Most of the excited ions are

transferred quickly to level 2 (E_2). Then the ions return to the ground level by emitting a photon. In Fig. 1.1, W_{13} is the pump parameter. τ_{31} and τ_{21} are the life times of E_3 and E_2 , respectively. τ_{21} is the relaxation time from E_2 to E_1 . And the lifetime of E_2 is larger than the relaxation time from E_2 to E_1 , namely $\tau_{21} \gg \tau_{32}$.

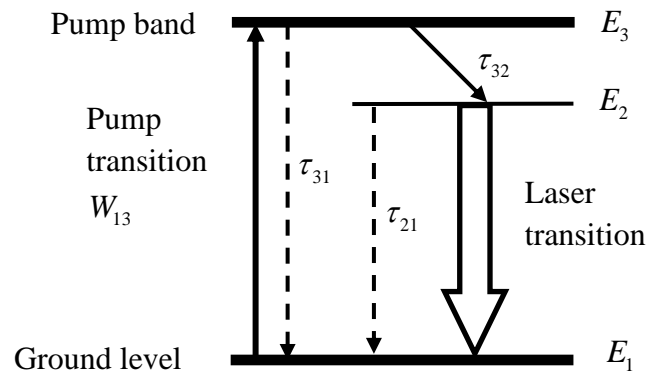


Figure 1.1 The energy level for a three-level laser medium

A four-level laser system has the lower laser level above the ground state by an energy gap. Hence, the four-level laser system requires less energy to generate population inversion compared to the three-level laser system. Fig. 1.2 shows the four-level laser system which is characteristic of the rare earth ions in glass or crystalline host materials. The ions pumped by the pump light are raised to level 3 (pump level E_3). Then they are transferred rapidly to level 2 (E_2). The laser transition happens when the ions transfer from level 2 to level 1 (terminal level E_1). Finally, the ions return to level 0 (ground level E_0) which is under the terminal level E_1 . τ_{30} , τ_{31} , τ_{20} and τ_{21} are the life times of $E_3 \rightarrow E_0$, $E_3 \rightarrow E_1$, $E_2 \rightarrow E_0$ and $E_2 \rightarrow E_1$, respectively. τ_{32} and τ_{10} are the relaxation times of $E_3 \rightarrow E_2$ and $E_1 \rightarrow E_0$, respectively. W_{03} is the pump parameter.

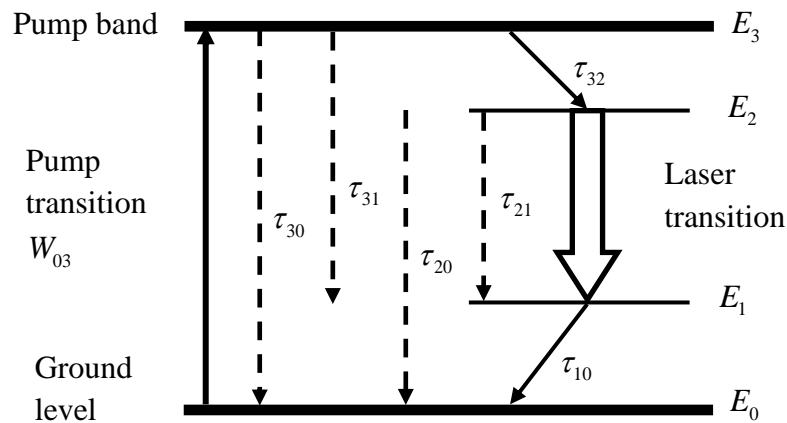


Figure 1.2 The energy level for a four-level laser medium

In the so-called quasi-three-level or quasi-four-level lasers, the laser transition terminates at a level close to the ground level. Compared with the four-level laser system, the three-level lasers and the quasi-three-level lasers need high pump intensities to exceed the threshold. But this disadvantage can be overcome if there are other favourable characteristics of the laser materials. The ruby laser which is still used in some applications is the typical three-level laser system. The Yb:YAG laser is a quasi-three-level laser, which is a very important laser for high power applications. The Nd:YAG laser is an example of a four-level laser system.

As the absorber is inserted in the laser cavity, the performance of the saturable absorber has to be considered in the laser rate equations. M. Hercher used a four-level model to describe the excited state absorption of a saturable absorber [Wagner, 1963]. The material selected as the saturable absorber can be presented as a simple energy level system shown in Fig. 1.3, which includes the excited state. In Fig. 1.3, σ_{gs} and σ_{es} are the ground state and excited state absorption cross sections, respectively. Compared with the upper state time τ_s , the

relaxation times of $E_4 \rightarrow E_2$ and $E_3 \rightarrow E_2$, τ_{42} and τ_{32} , are very fast. In some cases, this energy level system can be simplified as a two-level energy system.

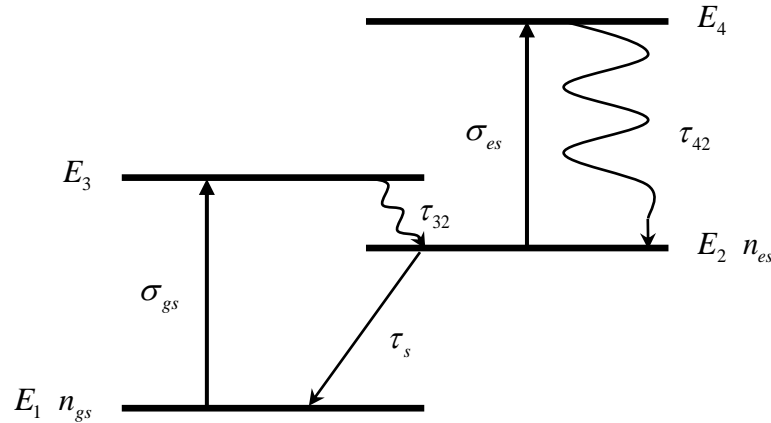


Figure 1.3 The energy level system of an absorber

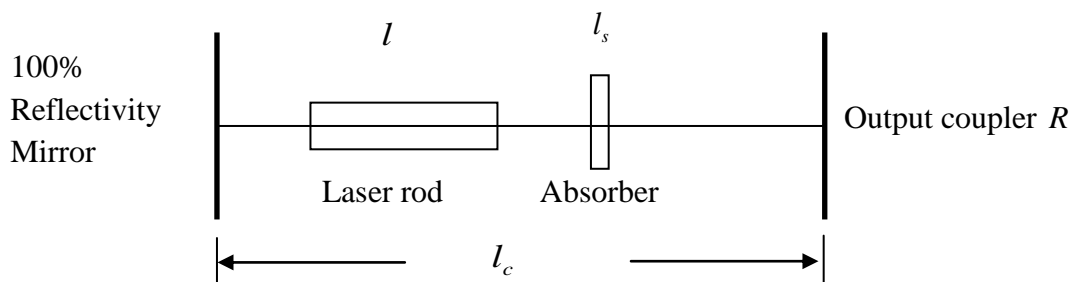


Figure 1.4 The laser cavity schematic

A. Szabo and R. A. Stein [Szabo, 1965] first derived the rate equations for the passively Q -switched laser. A continuously pumped passively Q -switched laser system can be considered as a laser medium with an inter cavity saturable absorber as show in Fig. 1.4. According to the analysis of the previous paragraphs, the laser rate equations for a three or four level gain medium, which includes the excited state of the saturable absorber and the pump power, can be represented by:

$$\frac{d\phi}{dt} = \frac{\phi}{t_r} [2\sigma nl - 2\sigma_{gs} n_{gs} l_s - 2\sigma_{es} n_{es} l_s - \ln(\frac{1}{R}) - L] \quad (1.1a)$$

$$\frac{dn}{dt} = W_p (n_{tot} - n) - \gamma\sigma c\phi n - \frac{n}{\tau_{21}} \quad (1.1b)$$

$$\frac{dn_{gs}}{dt} = -\gamma_s \sigma_{gs} c\phi n_{gs} + \frac{n_{s0} - n_{gs}}{\tau_s} \quad (1.1c)$$

$$n_{gs} + n_{es} = n_{s0} \quad (1.1d)$$

where, ϕ is the photon density, n is the instantaneous population inversion density, n_{gs} and n_{es} are the instantaneous population densities of the absorber ground and excited state respectively, σ is the laser stimulated emission cross-section, σ_{gs} and σ_{es} are the absorber ground and excited state absorption cross-sections respectively, γ and γ_s are the inversion reduction factors of the gain medium and absorber respectively, R is the reflectivity of the output mirror, L is the remaining two way dissipative (none useful) optical loss, l and l_s are the lengths of the gain and absorbing media respectively, $t_r = \frac{2l'}{c}$ is the round-trip transit time of light in the resonator of optical length l' , W_p is the volumetric pump rate into the upper level and is proportional to the CW pump power, n_{tot} is the doping concentration of the gain medium, n_{s0} is the absorber total population density, τ_{21} and τ_s are the spontaneous emission lifetimes of the upper level of the gain medium and the absorber, respectively. l_c in Fig.1.4 is the length of laser cavity.

The output performance of the laser system such as the output energy E , the peak power P_{\max} and the approximate FWHM pulse duration t_p of the passively Q -switched laser pulse can be written as:

$$E = \frac{h\nu A}{2\sigma\gamma} \ln(\frac{1}{R}) \ln(\frac{n_i}{n_f}) \quad (1.2a)$$

$$P_{\max} = \frac{h\nu A l'}{t_r} \ln(\frac{1}{R}) \phi_{\max} \quad (1.2b)$$

$$t_p = \frac{E}{P_{\max}} \quad (1.2c)$$

where, A is the cross-sectional area of the laser beam, h is Plank's constant, ν is the frequency of the laser EM field.

A design procedure that presents the optimization of a passively Q -switched laser was developed by Degnan [Degnan, 1995]. In his model, the design curves of the optimized output reflectivity and initial absorber transmission were presented as a function of two dimensionless variables: one is the ratio of the logarithmic round-trip small signal gain divided by the dissipative (nonuseful) round-trip loss, and the other is the ratio of the absorber cross section to laser stimulated emission cross section. Several variables are defined to compare the passively and actively Q -switched results. The Lagrange multiplier method (see Appendix A) is applied to get a unique choice of output coupler and unsaturated absorber initial transmission which maximizes the output energy. The theoretical results of the variables were plotted. The performance of different absorber mediums can also be given by the curves.

G. Xiao improved Degnan's theory and established a generalized model by introducing the excited state absorption of the absorber into the laser rate equations [Xiao, 1997]. The variables defined by Degnan were modified by introducing the effect of the excited state of an absorber. An additional experimental confirmation was presented by a Cr:YAG passively Q -switched Nd:Glass laser [Xiao, 1998].

A continuous wave (cw) pumped passively Q -switched laser was described by [Agnesi, 1998] and [Agnesi, 2000]. A cw diode-pumped passively Q -switched solid-state laser is used to get short, high peak power laser pulses. The experimental results shown in [Liu, 2003], [Voitikov, 2005] and [Li, 2006a] report that the pulse energy varies with the pump power. As pump power increases, the pulse energy increases at first, and then begins to decrease after

reaching its maximum value. During this process, the repetition rate increases with pump power. These results were totally different to the conclusion based on Morris and Pollock's investigation. It shows that the pump power affects the performance of a laser system, such as the output pulse energy, peak power and the FWHM pulse duration. Li [Li, 2006a] explained this phenomenon by the recovery time of an absorber, and summarized the solutions for the passively Q -switched laser rate equations by considering the finite recovery time of an absorber in the model.

1.5 Research methodologies

To control the FWHM pulse duration of a passively Q -switched solid-state laser system, rigorous research was undertaken. The factors which affect the output pulse duration were first confirmed. The optical elements in the laser resonator, the output reflectivity, the initial transmission of an absorber, the materials of the gain medium and the saturable absorber, and the length of the laser cavity all affect the pulse duration. The simplest way to control the output pulse duration is to select a proper pair of output-reflectivity and absorber initial-transmission.

When the other parameters are determined, the laser rate equations are employed to study the effect of the output-reflectivity and the absorber initial-transmission. The laser rate equations have different mathematical expressions with different preconditions. Two main mechanisms affect the expressions for the laser rate equations: 1) the buildup time of the Q -switch, and 2) the recovery time of the absorber. Based on the different initial conditions for each laser pulse, different models are developed.

Three models have been developed, then the Runge-Kutta method is applied to solve the different groups of differential equations, and plot the numerical results. Studying a practical laser system and plotting the simulation results is used to

present general conclusions. According to the simulation data, the scope of application of the models is demonstrated. Here, Matlab was used to do simulation.

1.6 Contributions

This thesis studies the FWHM pulse duration of a passively Q -switched solid-state laser system based on the selection of a proper pair of output-coupler and absorber whilst the output energy is kept at the required value. The selection of the gain medium is considered as well. The study gives a reliable, low-cost, and simple method to control the FWHM pulse duration of a passively Q -switched laser system without changing the output energy.

Previous research has focused on maximizing the output energy of a passively Q -switched laser. As shown in Section 1.4, Degnan developed a general model to obtain the optimized output energy of a passively Q -switched laser system. Xiao improved his model by introducing the excited state of absorber into laser rate equations. In these models, the pump rate and the recovery time of absorber were neglected. But some industrial applications have requirements on both the output energy and output pulse performance. In this thesis, the pulse performance of a passively Q -switched laser was studied for the cases when the effects of the pump rate and recovery time of absorber were considered in the models.

Considering the different preconditions, three models based on the laser rate equations are set up to study the effect of a proper pair of output-coupler and absorber on the performance of a laser system. The preconditions that control the required model characteristics are the following: 1) the build-up time of the Q -switching; and 2) the recovery time of the absorber.

Model I is based on the suppositions that 1) the buildup time of the Q -switched laser pulse is short enough to neglect the effect of the pump power in the lasing stage; and 2) the recovery time of the absorber is long enough that the most atoms of the absorber can return to the ground level before the beginning of next Q -switch. In *Model I*, the effect of the pump power is negligible, which results in the modified expressions for the laser rate equations.

Model II is set up for the case where the first supposition of *Model I* isn't satisfied. When the build-up time is long, and the recovery time of the absorber allows most atoms of the absorber to return to the ground level at the beginning of next Q -switching, a laser system can reach the stable output working state after the first few pumping and pulse cycles. In *Model II*, the pump power must be considered in the laser rate equations. The Runge-Kutta method is used to solve the laser rate equations to obtain the numerical results.

Model III improves *Model II* by considering that the recovery time of the absorber compared with the finite decay time of the upper level. Hence, the initial population density of the absorber's ground level at the beginning of Q -switching is affected by the recovery time of the absorber. Furthermore, the initial transmission affects the initial condition of the Q -switching and the output parameters of a laser system are affected.

The simulation results from the three models are compared to show the scope of application for the models.

1.7 Overview of the thesis

The chapters with their contents are reviewed in the following paragraphs.

Chapter 2 provides the preparation work for setting up the models. The key variables are defined and explained in this chapter. The differences between the

variables of this thesis and ones given by Degnan are explained. The theoretical method to show the shape of the pulse is introduced in this chapter.

Chapter 3 gives the conditions satisfied by *Model I*. The precondition of *Model I* yields the corresponding simplified laser rate equations. The simulation results are demonstrated using a Cr:YAG passively *Q*-switched Nd:Glass laser [Xiao, 1998].

Chapter 4 is based on *Model II* and shows the effect of the pump power on the selection of the output reflectivity and the coupling initial transmission, and the value of the pulse duration. A continuously pumped Cr:YAG passively *Q*-switched Yb:YAG laser and a passively *Q*-switched Nd:YAG laser are used to present the simulation data.

Chapter 5 presents the recovery time of an absorber as one of the mechanisms that affects the output performance of a *Q*-switched laser system. The initial transmission is affected by the finite recovery time. The laser system given by [Li, 2006] is employed to show the results.

Chapter 6 provides the general conclusions from the research. Some ideas for the further research are reported in the final section of this chapter.

Chapter 2

Foundations for Modelling

2.1 Introduction

Before analyzing the effects of a pair of output reflector and initial transmission, on the FWHM pulse width; several key parameters are defined in terms of a single dimensionless parameter to simplify the expressions for the equations.

The pulse shape and the temporal width of the passively Q -switched solid-state laser are studied in the case when the build-up time of the Q -switched laser pulse is quite short compared with the pumping and relaxation times of the laser medium, hence the pumping and spontaneous decay of the laser medium during the pulse stage can be ignored. The simplified laser rate equations are used to establish the general theoretical approach. The theoretical results of a Cr:YAG passively Q -switched laser are verified using experimental data.

2.2 The definition of Several Key Parameters

Degnan defined some key parameters in his model to compare the passively and actively Q -switched results [Degnan, 1995]. The remaining non-useful optical loss in the laser resonator was contained in the definitions of Degnan's key parameters. Xiao improved Degnan's model by introducing the excited state of an absorber [Xiao and Bass, 1997]. Hence, in Xiao's model the losses including the loss of the excited state and the non-useful optical loss replaced the non-useful optical loss in Degnan's model, and were considered in the definitions of the key parameters. In this thesis, the loss of the excited state changes with different absorbers used to get the pre-determined output energy. Hence, for convenience, to show the effect of the excited state of an absorber, the losses will not be processed as a part of the key parameters. Therefore, the definition of the parameter will only present its physical significance.

The parameter z_l is defined as

$$z_l = 2\sigma l n_i = \ln(G_0^2) \quad (2.1)$$

here, n_i is the initial population inversion density at the start of Q -switching, σ is the laser stimulated emission cross-section, l is the length of the gain, and G_0^2 is the round-trip unsaturated small signal power gain. z_l shows the initial condition of the laser system's lasing stage, and is named the *small-signal parameter*.

The parameter z_a is given as

$$z_a = 2\sigma_{gs} l_s n_{gsi} = -\ln(T_0^2) \quad (2.2)$$

where: n_{gsi} is the initial density of the absorbing state at ground level of the absorber, σ_{gs} is the absorber ground state absorption cross-section, l_s is the length of the absorbing media, T_0 is the initial transmission of an absorber. According to the definition, the parameter z_a describes the initial state of the absorber at the beginning of Q -switching. Hence, z_a is named the *absorber parameter*.

The parameter to show the output reflectivity is defined as the *reflectivity parameter* x by

$$x = \ln\left(\frac{1}{R}\right) \quad (2.3)$$

where, R is the reflectivity of the output mirror.

The parameter ρ is named the *final population parameter*, and illustrates the stimulated emission population density of the gain medium at the lasing stage,

$$\rho = \ln\left(\frac{n_i}{n_f}\right) \quad (2.4)$$

where, n_f is the final inversion population density at the end of Q -switching.

The *peak point population parameter* n_{ii} is defined by

$$n_{ii} = \frac{n_t}{n_i} \quad (2.5)$$

where, n_t is the instantaneous population inversion density when the output power reaches the maximum value.

Eq. 1.2 (a) gives the expression of the output energy of a laser system, and yields the *output energy parameter* E_a

$$E_a = \ln\left(\frac{1}{R}\right) \ln\left(\frac{n_i}{n_f}\right) \quad (2.6a)$$

Substituting Eq. 2.3 and Eq. 2.4, Eq. 2.6 (a) is written as

$$E_a = x\rho \quad (2.6b)$$

And the *peak power parameter* P_a can be obtained from Eq. 1.2 (b)

$$P_a = c\gamma\sigma \ln\left(\frac{1}{R}\right) \phi_{\max} \quad (2.7)$$

where: c is the speed of light, γ accounts for the effects of level degeneracies on the gain medium, ϕ_{\max} is the maximum value of the photon density in the laser resonator at the lasing stage.

The parameters defined in this section will be used in the next chapters, and they will not be explained again.

2.3 The general mathematical analysis of the pulse shape

When the build-up time of the Q -switched laser pulse is quite short compared with the pumping and relaxation times of the laser medium, the behaviour of the passively Q -switched solid-state laser system during the pulse stage can be

described by the simplified laser rate equations given in Chapter 1. Now the rate equations including the excited state of the absorber are

$$\frac{d\phi}{dt} = \frac{\phi}{t_r} [2\sigma n l - 2\sigma_{gs} n_{gs} l_s - 2\sigma_{es} n_{es} l_s - \ln\left(\frac{1}{R}\right) - L] \quad (2.8a)$$

$$\frac{dn}{dt} = -\gamma\sigma c\phi n \quad (2.8b)$$

$$\frac{dn_{gs}}{dt} = -\gamma_s \sigma_{gs} c\phi n_{gs} \quad (2.8c)$$

$$n_{gs} + n_{es} = n_{s0} \quad (2.8d)$$

here: ϕ is the average photon density in the laser cavity, n is the instantaneous population inversion density, n_{gs} and n_{es} are the instantaneous population densities of the absorber ground and excited state respectively, σ is the laser stimulated emission cross-section, σ_{gs} and σ_{es} are the absorber ground and excited state absorption cross-sections respectively, γ and γ_s are the inversion reduction factors of the gain medium and absorber respectively, R is the reflectivity of the output mirror, L is the remaining two way dissipative (none useful) optical loss, l and l_s are the lengths of the gain and absorbing media respectively, $t_r = \frac{2l'}{c}$ is the round-trip transit time of light in the resonator of optical length l' , n_{s0} is the absorber total population density.

Dividing Eq. 2.8 (b) by Eq. 2.8 (c) and integrating, the relation between n and n_{gs} is given by,

$$n_{gs} = n_{gsi} \left(\frac{n}{n_i}\right)^\alpha \quad (2.9)$$

where, n_i is the initial inversion population density of the gain medium at the beginning of the Q -switching, n_{gsi} is the initial population density in the absorber's ground state at the beginning of the Q -switching, and α is defined as

$$\alpha = \frac{\gamma_s \sigma_{gs}}{\gamma \sigma}, \quad (2.10)$$

The parameter α shows the relationship between the gain medium and the absorber. The initial condition for Q -switching is obtained by setting the left hand side of Eq. 2.8 (a) to zero

$$2\sigma l n_i - 2\sigma_{gs} l_s n_{gsi} - 2\sigma_{es} l_s n_{esi} - [\ln(\frac{1}{R}) + L] = 0 \quad (2.11)$$

where n_{esi} is the initial population density in the absorber's excited state at the beginning of the Q -switching. Assuming that the repetition rate of the laser system is slow enough to let most of the atoms of the absorber be at the ground level at the beginning of Q -switching yields

$$n_{esi} \approx 0, \quad (2.12)$$

gives

$$n_{gsi} \approx n_{s0}. \quad (2.13)$$

Hence, Eq. 2.11 is rewritten as

$$2\sigma l n_i - 2\sigma_{gs} l_s n_{s0} - [\ln(\frac{1}{R}) + L] = 0 \quad (2.14)$$

Eq. 2.14 is also used to calculate the value of the initial inversion population density of the gain medium n_i .

Substituting Eq. 2.9 into Eq. 2.8 (a) and dividing Eq. 2.8 (a) by Eq. 2.8 (b) yields

$$\frac{d\phi}{dn} = -\frac{l}{\gamma l'} \left[1 - \frac{(\sigma_{gs} - \sigma_{es}) l_s n_{gsi}}{\sigma l n} \left(\frac{n}{n_i}\right)^\alpha - \frac{\ln(\frac{1}{R}) + L + 2\sigma_{es} n_{s0} l_s}{2\sigma n l} \right] \quad (2.15)$$

which can be integrated to yield

$$\phi(n) = \frac{l}{\gamma l'} \left\{ n_i - n - \frac{\gamma l_s n_{gsi}}{\gamma_s l} \left[1 - \left(\frac{n}{n_i}\right)^\alpha \right] - \frac{\ln(\frac{1}{R}) + L + 2\sigma_{es} l_s n_{s0}}{2\sigma l} \ln\left(\frac{n_i}{n}\right) \right\} \quad (2.16)$$

$$\text{here, } \gamma_s' = \gamma_s \frac{1}{1 - \sigma_{es}/\sigma_{gs}}.$$

At the end of Q -switching, $\phi(n) \approx 0$. Hence, the final inversion population density n_f at this moment is

$$1 - \frac{n_f}{n_i} - \frac{\gamma l_s n_{gsi}}{\gamma_s' l n_i} \left[1 - \left(\frac{n_f}{n_i} \right)^\alpha \right] - \frac{\ln\left(\frac{1}{R}\right) + L + 2\sigma_{es} l_s n_{s0}}{2\sigma n_i l} \ln\left(\frac{n_i}{n_f}\right) = 0 \quad (2.17)$$

When the output power is at its peak point, the instantaneous population inversion density n_i is shown by setting the left side of Eq. 2.8 to zero

$$\frac{n_i}{n_i} = \frac{\alpha \gamma l_s n_{gsi}}{\gamma_s' l n_i} \left(\frac{n_i}{n_i} \right)^\alpha + \frac{\ln\left(\frac{1}{R}\right) + L + 2\sigma_{es} l_s n_{s0}}{2\sigma l n_i} \quad (2.18)$$

The expression for t during the pulse stage is given by Eq. 2.8 (b)

$$dt = - \frac{dn}{\gamma c \sigma n \phi(n)} \quad (2.19)$$

Substituting Eq. 2.16 into Eq. 2.19 and integrating both sides of Eq. 2.19 yields:

$$t = - \frac{l'}{c \sigma l n_i} \int \frac{dn}{\left\{ \left(1 - \frac{n}{n_i} \right) - \frac{\gamma l_s n_{gsi}}{\gamma_s' l n_i} \left[1 - \left(\frac{n}{n_i} \right)^\alpha \right] - \frac{\ln\left(\frac{1}{R}\right) + L + 2\sigma_{es} l_s n_{s0}}{2\sigma l n_i} \ln\left(\frac{n_i}{n}\right) \right\} n} \quad (2.20)$$

When the output pulse shape of a laser system is known, the FWHM pulse width obtained from the pulse shape is more accurate than the one calculated by the approximate expression given by Eq. 1.2 (c).

In order to simplify the analysis and discussion, an additional variable n_m is defined as

$$n_m = \frac{n}{n_i} \quad (2.21)$$

Substituting the defined variables z_l , z_a , x , ρ , n_i and n_m into Eq. 2.14, Eq. 2.16, Eq. 2.17, Eq. 2.18, Eq. 2.20 and assuming that $n_{s0} \approx n_{gsi}$ yields the following expression

$$z_l - z_a - x - L = 0 \quad (2.22a)$$

$$\alpha z_l (1 - \rho - e^{-\rho}) - \frac{\gamma_s}{\gamma_s'} z_a (1 - \alpha \rho - e^{-\alpha \rho}) = 0 \quad (2.22b)$$

$$n_{ii} = \frac{\gamma_s}{\gamma_s'} \frac{z_a}{z_l} n_{ii}^\alpha + \frac{x + L + \frac{\sigma_{es}}{\sigma_{gs}} z_a}{z_l} = 1 - \frac{\gamma_s}{\gamma_s'} \frac{z_a}{z_l} (1 - n_{ii}^\alpha) \quad (2.22c)$$

$$\phi(n) = \frac{z_l}{2\gamma\sigma l'} \left\{ 1 - \frac{n}{n_i} - \frac{\gamma_s}{\gamma_s'} \frac{z_a}{\alpha z_l} \left[1 - \left(\frac{n}{n_i}\right)^\alpha \right] - \frac{x + L + \frac{\sigma_{es}}{\sigma_{gs}} z_a}{z_l} \ln\left(\frac{n_i}{n}\right) \right\} \quad (2.22d)$$

and

$$t = -\frac{t_r}{z_l} \int \left[(1 - n_m) - \frac{1}{\alpha} \frac{\gamma}{\gamma_s'} \frac{z_a}{z_l} (1 - n_m^\alpha) + \frac{x + L + \frac{\sigma_{es}}{\sigma_{gs}} z_a}{z_l} \ln(n_m) \right]^{-1} \frac{dn_m}{n_m}. \quad (2.22e)$$

2.4 Numerical simulation

The numerical simulation results of a Nd:Glass laser passively Q -switched by Cr:YAG [Xiao and Bass, 1998] verifies the model built up in this chapter. The data applied in the simulation are listed in Table 2.1.

Table 2.1 The parameters of the laser system and materials

Size of Nd:Glass	3mm×75mm
Stimulated emission cross-section of Nd:Glass (σ)	$4.4 \times 10^{-20} \text{ cm}^2$ [Xiao and Bass, 1998]
Level degeneracies effect of Nd:Glass (γ)	1
Refractive index of Nd:Glass	1.56
Length of Cr:YAG (l_s)	1.8mm
Initial transmission of Cr:YAG (T_0)	47%
Ground absorption cross-section of Cr:YAG (σ_{gs})	$7 \times 10^{-18} \text{ cm}^2$ [Koechner, 2006]
Excited state absorption cross-sections of Cr:YAG (σ_{es})	$2 \times 10^{-18} \text{ cm}^2$ [Koechner, 2006]
Level degeneracies effect of Cr:YAG (γ_s)	1

Length of the laser cavity	19cm
Reflectivity of the output coupler (R)	50%
Remaining dissipative optical loss (L)	0.04

Since the values of the ground and excited state absorption cross-sections of Cr:YAG are used the data in Ref. [Koechner, 2006], the parameter α is 160 now, and not the same as shown in Ref. [Xiao and Bass, 1998]. Fig. 2.1 shows the simulation result of the average photon density in the laser cavity $\phi(t)$ during the pulse stage. For the convenience of the analysis, the data used in Fig. 2.1 are the normalized data of $\phi(t)$ ($\phi(t)/\phi_{\max}$). In Fig. 2.1, two dot lines are plotted to show two special values of the average photon density: the maximum value ($\phi(t)/\phi_{\max} = 1$), and the half maximum value ($\phi(t)/\phi_{\max} = 0.5$). Measuring the interval between two points cut by the half-maximum dot line gets that the simulation FWHM pulse width is $9.2ns$. The experimental value shown in Ref. [Xiao and Bass, 1998] was $10.5ns$. The fact that the theoretical result approaches the experimental result proves that the model can be used to simulate the pulse shape when the build-up time of the Q -switched laser pulse is quite short compared with the pumping and relaxation times of the laser medium. The corresponding normalized $n(t)$ and $n_{gs}(t)$ are plotted in Fig. 2.2.

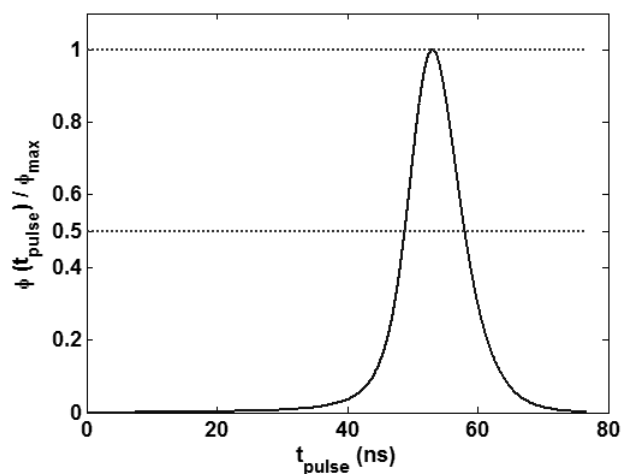


Figure 2.1 The Normalized average photon density $\phi(t)$ during the pulse stage

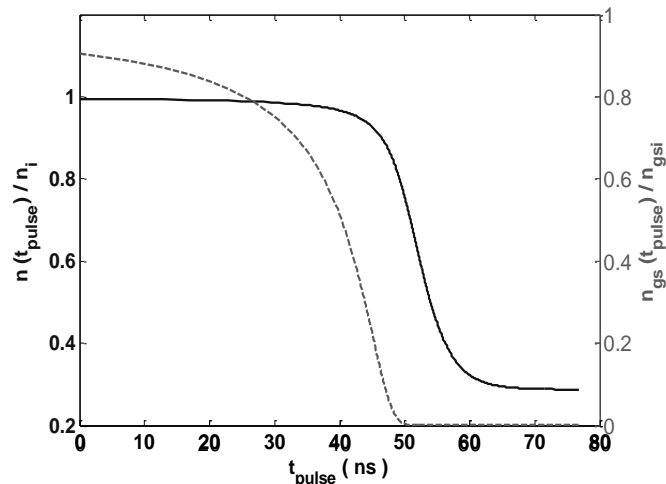


Figure 2.2 The normalized $n(t)$ and $n_{gs}(t)$ during the pulse stage

2.5 Conclusions

Several key parameters are defined in this chapter. The physical significance of each defined parameter is shown by the definition.

A simulation method based on the laser rate equations is applied to describe the output pulse shape of a passively Q -switched solid-state laser for the case when the build-up time of the Q -switched laser pulse is quite short compared to the pumping and relaxation times of the laser medium, and the initial population density of the ground level of an absorber is nearly equal to the absorber's total population density. The FWHM pulse width can be obtained from the pulse shape. The simulation results for a Cr:YAG passively Q -switched Nd:Glass laser agrees with the experimental results. This method is used in Chapter 3 to predict the pulse shape.

Chapter 3

A Simplified Model of a Passively Q - switched Solid-state Laser System

3.1 Introduction

The theoretical analysis based on the simplified laser rate equations is used to study the factors affecting the FWHM pulse width of the passively Q -switched solid-state laser in the case when the output energy is kept to a pre-determined value. Here, the factors studied includes: the output reflectivity and absorber initial-transmission pair, the gain medium and the absorber material. A simplified model which is named as *Model I* in Chapter One is constructed on the following assumptions that: 1) the build-up time of the Q -switched laser pulse is short enough to neglect the effect of the pump power during the lasing stage; 2) most atoms excited to the upper level of the absorber will return to the ground level by the beginning of next Q -switch. A Cr:YAG passively Q -switched Nd:Glass laser is used to demonstrate the numerical results. Then, the Nd:Glass material in the laser cavity is replaced with Nd:YAG to assist in understanding the effect of the gain medium.

3.2 Rate equations

In *Model I*, the assumption that most of the atoms of the absorber will return to the ground level before the beginning of the next Q -switching results in the initial conditions for each pumping and lasing cycle being the same, hence the pumping cycle doesn't affect the output of the laser system for this case. Hence, the study of the pumping cycle can be ignored in *Model I*. At the lasing stage, the first assumption mentioned in Section 3.1 results in the effect of the pump power being negligible in the rate equations. Hence, considering the excited state of the absorber, the simplified rate equations to describe the lasing process are:

$$\frac{d\phi}{dt} = \frac{\phi}{t_r} [2\sigma nl - 2\sigma_{gs} n_{gs} l_s - 2\sigma_{es} n_{es} l_s - \ln\left(\frac{1}{R}\right) - L] \quad (3.1a)$$

$$\frac{dn}{dt} = -\gamma\sigma c\phi n \quad (3.1b)$$

$$\frac{dn_{gs}}{dt} = -\gamma_s \sigma_{gs} c \phi n_{gs} \quad (3.1c)$$

$$n_{gs} + n_{es} = n_{s0} \quad (3.1d)$$

where ϕ is the photon density, n is the instantaneous population inversion density, n_{gs} and n_{es} are the instantaneous population densities of the absorber ground and excited state respectively, σ is the laser stimulated emission cross section, σ_{gs} and σ_{es} are the absorber ground and excited state absorption cross sections respectively, γ and γ_s are the inversion reduction factors of the gain medium and absorber respectively, R is the reflectivity of the output mirror, L is the remaining two way dissipative (none useful) optical loss, l and l_s are the lengths of the gain and absorbing media respectively, $t_r = \frac{2l'}{c}$ is the round-trip transit time of light in the resonator of optical length l' , n_{s0} is the absorber total population density.

From the analysis completed in Chapter 2, the following relationships can be obtained:

$$n_{gs} = n_{gsi} \left(\frac{n}{n_i}\right)^\alpha \quad (3.2a)$$

$$2\sigma l n_i - 2\sigma_{gs} l_s n_{gsi} - \left[\ln\left(\frac{1}{R}\right) + L\right] = 0 \quad (3.2b)$$

$$\phi(n) = \frac{l}{\gamma l'} \left\{ n_i - n - \frac{\gamma l_s n_{gsi}}{\gamma_s l} \left[1 - \left(\frac{n}{n_i}\right)^\alpha \right] - \frac{\ln\left(\frac{1}{R}\right) + L + 2\sigma_{es} l_s n_{s0}}{2\sigma l} \ln\left(\frac{n_i}{n}\right) \right\} \quad (3.2c)$$

$$1 - \frac{n_f}{n_i} - \frac{\gamma l_s n_{gsi}}{\gamma_s l n_i} \left[1 - \left(\frac{n_f}{n_i}\right)^\alpha \right] - \frac{\ln\left(\frac{1}{R}\right) + L + 2\sigma_{es} l_s n_{s0}}{2\sigma n_i l} \ln\left(\frac{n_i}{n_f}\right) = 0 \quad (3.2d)$$

$$\frac{n_i}{n_i} = \frac{\alpha \gamma l_s n_{gsi}}{\gamma_s l n_i} \left(\frac{n_i}{n_i}\right)^\alpha + \frac{\ln\left(\frac{1}{R}\right) + L + 2\sigma_{es} l_s n_{s0}}{2\sigma l n_i} \quad (3.2e)$$

where, n_i is the initial population inversion density at the start of Q -switching, n_{gsi} is the initial density of the ground level of the absorber by the beginning of

the Q -switching, which is assumed to be equal to n_{s0} in *Model I*. n_f is the final inversion population density at the end of Q -switching. n_t is the instantaneous population inversion density when the output power is at its peak point. The parameters α and γ_s' are defined as

$$\alpha = \frac{\gamma_s \sigma_{gs}}{\gamma \sigma}, \quad (3.3a)$$

and

$$\gamma_s' = \gamma_s \frac{1}{1 - \sigma_{es}/\sigma_{gs}}. \quad (3.3b)$$

As shown in Chapter 1, the output energy, the output peak power and an expression for the approximate FWHM (full width at half maximum) pulse width of the laser output are:

$$E = \frac{h\nu A}{2\sigma\gamma} \ln\left(\frac{1}{R}\right) \ln\left(\frac{n_i}{n_f}\right) \quad (3.4a)$$

$$\begin{aligned} P_{\max} &= \frac{h\nu A l'}{t_r} \ln\left(\frac{1}{R}\right) \phi_{\max} \\ &= \frac{h\nu A l}{\gamma t_r} \ln\left(\frac{1}{R}\right) \left\{ n_i - n_t - \frac{\gamma_s l_s n_{gsi}}{\gamma_s' l n_i} \left[1 - \left(\frac{n_t}{n_i}\right)^\alpha \right] - \frac{\ln\left(\frac{1}{R}\right) + L + 2\sigma_{es} l_s n_{s0}}{2\sigma l} \ln\left(\frac{n_i}{n_t}\right) \right\} \end{aligned} \quad (3.4b)$$

$$t_p = \frac{E}{P_{\max}} \quad (3.4c)$$

where, A is the cross-sectional area of the laser beam, h is Plank's constant and ν is the frequency of the laser EM field.

Substituting the expression for ϕ_{\max} into the definition of the peak power parameter P_a (Eq. 2.7) yields

$$P_a = \frac{1}{t_r} x \left[z_l (1 - n_{ii}) - \frac{\gamma_s}{\gamma_s'} \frac{z_a}{\alpha} (1 - n_{ii}^\alpha) + (x + L + \frac{\sigma_{es}}{\sigma_{gs}} z_a) \ln(n_{ii}) \right]. \quad (3.5)$$

Substituting the variables z_l , z_a , x , ρ , n_{ii} , E_a , P_a into Eq. 3.3 and Eq. 3.4 gives

$$z_l - z_a - x - L = 0 \quad (3.6a)$$

$$\phi(n) = \frac{z_l}{2\sigma\gamma l'} \left\{ 1 - \frac{n}{n_i} - \frac{\gamma_s}{\gamma_s'} \frac{z_a}{\alpha z_l} \left[1 - \left(\frac{n}{n_i} \right)^\alpha \right] - \frac{x + L + \frac{\sigma_{es}}{\sigma_{gs}} z_a}{z_l} \ln \left(\frac{n_i}{n} \right) \right\} \quad (3.6b)$$

$$\alpha z_l (1 - \rho - e^{-\rho}) - \frac{\gamma_s}{\gamma_s'} z_a (1 - \alpha \rho - e^{-\alpha \rho}) = 0 \quad (3.6c)$$

$$n_{ii} = \frac{\gamma_s}{\gamma_s'} \frac{z_a}{z_l} n_{ii}^\alpha + \frac{x + L + \frac{\sigma_{es}}{\sigma_{gs}} z_a}{z_l} = 1 - \frac{\gamma_s}{\gamma_s'} \frac{z_a}{z_l} (1 - n_{ii}^\alpha) \quad (3.6d)$$

$$E = \frac{h\nu A}{2\sigma\gamma} x \rho = \frac{h\nu A}{2\sigma\gamma} E_a \quad (3.6e)$$

$$\begin{aligned} P_{\max} &= \frac{h\nu A}{2\sigma\gamma t_r} x z_l \left[1 - n_{ii} - \frac{\gamma_s}{\gamma_s'} \frac{z_a}{\alpha z_l} (1 - n_{ii}^\alpha) \right] + \frac{x + L + \frac{\sigma_{es}}{\sigma_{gs}} z_a}{z_l} \ln(n_{ii}) \\ &= \frac{h\nu A}{2\sigma\gamma} P_a \end{aligned} \quad (3.6f)$$

$$\begin{aligned} t_p &= \frac{E}{P_{\max}} = t_r \frac{x \rho}{x \left[z_l (1 - n_{ii}) - \frac{\gamma_s}{\gamma_s'} \frac{z_a}{\alpha} (1 - n_{ii}^\alpha) \right] + (x + L + \frac{\sigma_{es}}{\sigma_{gs}} z_a) \ln(n_{ii})} \\ &= \frac{E_a}{P_a} \end{aligned} \quad (3.6g)$$

3.3 Theoretical Analysis

As shown in Eq. 3.6 (g), the value of the FWHM pulse width of a laser system is presented by two variables E_a and P_a . Eq. 2.6 and Eq. 3.5 show E_a and P_a are decided by the following factors: 1) the length of the laser cavity, 2) the materials of the gain medium and absorber, and 3) the output reflectivity and the initial transmission. It is noted that the factors 2) and 3) can be expressed by the parameters α and γ_s' , the reflectivity parameter x and the absorber parameter z_a , respectively.

As the gain medium and the absorber are already decided, it is convenient for the designer to select the different output coupler and absorber pair to achieve the required pulse width, and pre-determined output energy. Hence, the study of the factors affecting the pulse width can focus on the output reflectivity R and the initial transmission T_0 (which can be represented by the reflectivity parameter x and the absorber parameter z_a , respectively). But other factors, such as the gain medium and the absorber material (namely the parameters α and γ_s'), will be discussed in this chapter as well.

Before the discussion, a precondition has to be mentioned again that the output energy of the laser system E shouldn't be affected by the different pairs of output coupler and absorber when the gain medium and the absorber material are pre-selected. Assuming that the cross-sectional area of the laser beam A does not change greatly and the gain medium is decided when the gain medium is selected, results in the simplification that the output energy parameter E_a can be used instead of E in the model, and its value is invariant along R (the reflectivity parameter x) and T_0 (the absorber parameter z_a).

When the laser cavity mode, the output energy E , the laser gain medium and the absorber are determined by a designer, the output energy parameter E_a can be calculated by Eq. 1.2 (a) and Eq. 2.6 (a). As the value of E_a is known, the values of R , its coupling T_0 and the corresponding FWHM pulse width t_p can be calculated by the following steps:

- 1) An output coupler R is selected by the designer at first, and the value of x is given by Eq. 2.3;
- 2) The value of parameter ρ is obtained from

$$\rho = \frac{E_a}{x} ; \quad (3.8)$$

- 3) By Eq. 3.6 (a) and Eq. 3.6 (c), z_a and z_l can be expressed by the variables x and ρ as

$$z_a = \frac{\alpha(x+L)(1-\rho-e^{-\rho})}{\frac{\gamma_s}{\gamma_s'}(1-\alpha\rho-e^{-\alpha\rho})-\alpha(1-\rho-e^{-\rho})} \quad (3.9a)$$

and

$$\begin{aligned} z_l &= z_a + x + L \\ &= \frac{\frac{\gamma_s}{\gamma_s'}(x+L)(1-\alpha\rho-e^{-\alpha\rho})}{\frac{\gamma_s}{\gamma_s'}(1-\alpha\rho-e^{-\alpha\rho})-\alpha(1-\rho-e^{-\rho})}. \end{aligned} \quad (3.9b)$$

Now T_0 is given by the definition of the absorber parameter z_a (Eq. 2.2) as

$$T_0 = e^{-z_a/2}; \quad (3.10)$$

4) After the values of z_l and z_a have been given, the parameter n_{ii} is calculated by Eq. 3.6 (d). When n_{ii}^α is small enough to be ignored, Eq. 3.6 (d) can be simplified to

$$n_{ii} \approx 1 - \frac{\gamma_s}{\gamma_s'} \frac{z_a}{z_l} \quad (3.11)$$

5) Substituting Eq. 3.9 and Eq. 3.11 into Eq. 3.6 (g) yields the FWHM pulse width t_p .

For the case that studying the effect of the gain medium or the absorber as the laser cavity is pre-decided, the simulation steps are the same as Steps 1-5, but the value of α or γ' , which is decided by the gain medium and the absorber, is different.

3.3.1 The FWHM pulse width with different pairs of R and T_0

In the simulation, the absorber used is Cr:YAG. Using the material parameters of Cr:YAG shown in Chapter 2 gives $\gamma_s = 1$ and $\gamma_s' \approx 1.4$. The remaining two way dissipative (none useful) optical loss is assumed to be $L = 0.04$. The round-trip transit time of light in the resonator is set as $t_r = 1ns$.

Fig. 3.1 plots the variables z_a and its coupling parameter z_l as a function of x and for different values of α (5, 10, 20 and 50) when $E_a = 1$. According to the variables' definition, z_a (the absorber parameter) represents the initial transmission of an absorber, and z_l (the small-signal parameter) represents the initial condition of the laser system.

Fig. 3.1 (a) shows z_a monotonically decreases along x for the cases that the values of α are 5, 10, 20 and 50, when the output energy parameter $E_a = 1$. It is noted that the change of z_a along x can be divided into two parts: the sharp change part and the gentle change part. When x is away from its minimum value shown in Fig. 3.1 (a), the coupling z_a decreases sharply from its maximum value. Once x is greater than 1, the change of z_a becomes gentle versus x . As an example, for the case when α is 20, z_a decreases from 4.5 to 1.2 when x increases from 0.39 to 1, and as x increases from 1 to 2.3, z_a changes from 1.24 to 1.

The data for the small-signal parameter z_l for different values of α are plotted in Fig. 3.1 (b). It can be observed that the curves of z_l for all the cases of α have the same trend along x . Affected by both the reflectivity parameter x and the absorber parameter z_a , the curve of z_l decreases along x firstly, then reaches its minimum point, after that it is upward sloping.

In both Figs. 3.1 (a) and 3.1 (b), the differences between the curves for the cases that the values of α are 5, 10, 20 and 50, are diminishing as x is close to its minimum value (namely when the output reflectivity has its highest data). It can be imagined that as x is selected to be a minimum value, the values of its corresponding FWHM pulse duration t_p for the cases that $\alpha = 5, 10, 20$ and 50, is nearly the same.

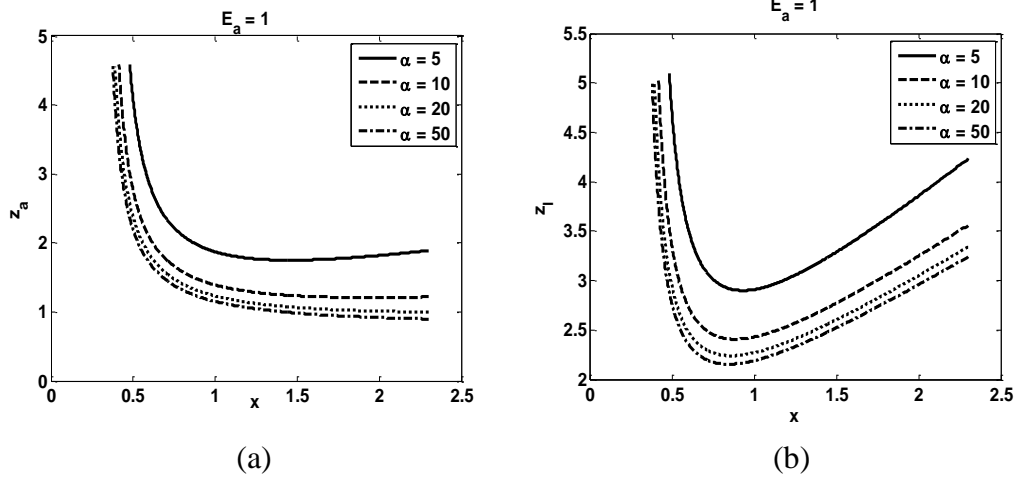


Figure 3.1 When $E_a = 1$, (a) the absorber parameter z_a as a function of the reflectivity parameter x and α (5, 10, 20 and 50), (b) the corresponding small-signal parameter z_l

The corresponding FWHM pulse width t_p as a function of x and for different values of α (5, 10, 20 and 50) are plotted in Fig. 3.2. To show the parameters visually, the adaptive pairs of T_0 (calculated by the absorber parameter z_a) and R (obtained from the reflectivity parameter x) to keep $E_a = 1$ are shown in Fig. 3.3. For the convenience of the comparison, Tables 3.1 and 3.2 list two groups of the approximate FWHM pulse width t_p which result from two selected output couplers $R = 20\%$ and $R = 50\%$ and their coupling absorber initial transmissions T_0 when α is 5, 10, 20 and 50, respectively. Table 3.1 shows when the reflectivity of an output coupler R is relatively low, the shorter FWHM pulse width t_p can be obtained by employing a group of gain medium and absorber resulting in a bigger α . It is noted that when the output reflectivity is close to its maximum value, for the cases that $\alpha = 5, 10, 20$ and 50, the FWHM pulse width t_p approaches its minimum value, and the differences between the corresponding t_p are negligible.

The analysis of Figs. 3.2 - 3.3 and Tables 3.1 and 3.2 shows the shorter t_p can be achieved by the following methods. One is to select a higher output reflectivity (x is lower) when the gain medium and the absorber have been decided. The second is to use a group of gain medium and absorber which leads to a bigger α .

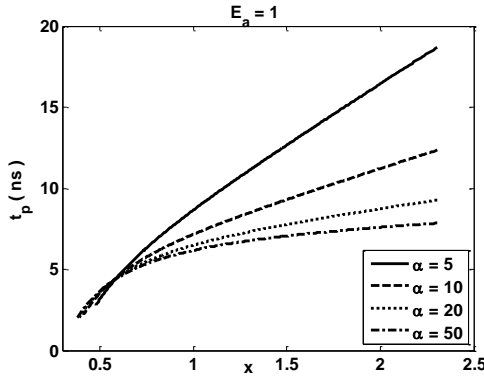


Figure 3.2 t_p as the function of x when $E_a = 1$ and $\alpha = 5, 10, 20$ and 50

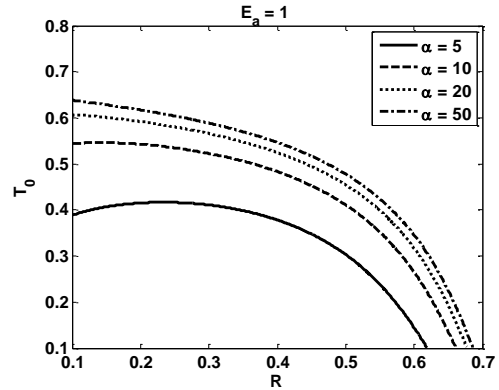


Figure 3.3 The adaptive pair of T_0 and R to keep $E_a = 1$ as $\alpha = 5, 10, 20$ and 50

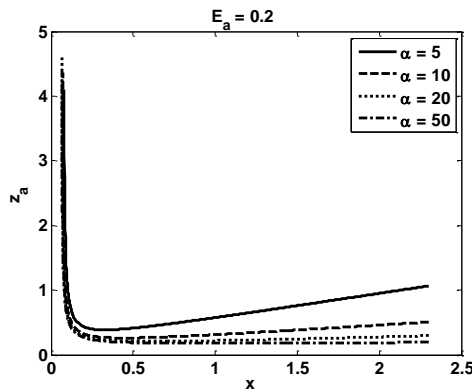
Table 3.1 The FWHM pulse width t_p as $R = 20\%$ when $E_a = 1$ for $\alpha = 5, 10, 20$ and 50

$E_a = 1$			
α	R ($x = \ln(\frac{1}{R})$)	T_0 ($z_a = -2\ln(T_0)$)	t_p (ns)
5	20% ($x = 1.61$)	0.42 ($z_a = 1.76$)	13.5
10	20% ($x = 1.61$)	0.54 ($z_a = 1.2$)	9.7
20	20% ($x = 1.61$)	0.60 ($z_a = 1.04$)	8.0
50	20% ($x = 1.61$)	0.62 ($z_a = 0.97$)	7.2

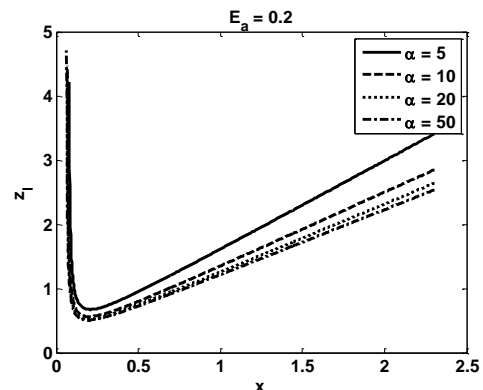
Table 3.2 The FWHM pulse width t_p as $R=50\%$ when $E_a=1$ for $\alpha=5, 10, 20$ and 50

$E_a = 1$			
α	$R \left(x = \ln\left(\frac{1}{R}\right) \right)$	$T_0 \left(z_a = -2\ln(T_0) \right)$	$t_p \text{ (ns)}$
5	50% ($x = 0.7$)	0.30 ($z_a = 2.38$)	5.73
10	50% ($x = 0.7$)	0.41 ($z_a = 1.78$)	5.38
20	50% ($x = 0.7$)	0.45 ($z_a = 1.57$)	5.18
50	50% ($x = 0.7$)	0.48 ($z_a = 1.47$)	5.08

To study the effect of the output energy on the output reflectivity and initial transmission pair, and the corresponding FWHM pulse duration, Figs. 3.4 - 3.7 plot the parameters z_a , its corresponding z_l and the FWHM pulse duration t_p as a function of x and for different values of α ($\alpha=5, 10, 20$ and 50) when $E_a=0.2, 0.5, 1.5$ and 2. The proper pairs of output reflectivity R and its coupling initial transmission T_0 to keep $E_a=0.2, 0.5, 1.5$ and 2 for the case that $\alpha=5, 10, 20$ and 50 are plotted in Figs. 3.4 - 3.7 as well.



(a)



(b)

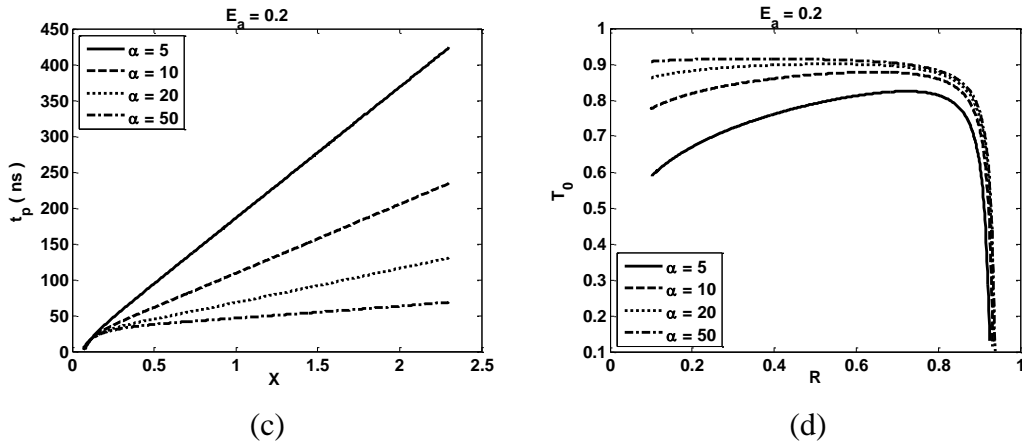


Figure 3.4 (a) z_a , (b) z_l and (c) t_p as a function of x and α (5, 10, 20 and 50) when $E_a = 0.2$, (d) the proper pairs of R and T_0 to keep for $\alpha = 5, 10, 20$ and 50

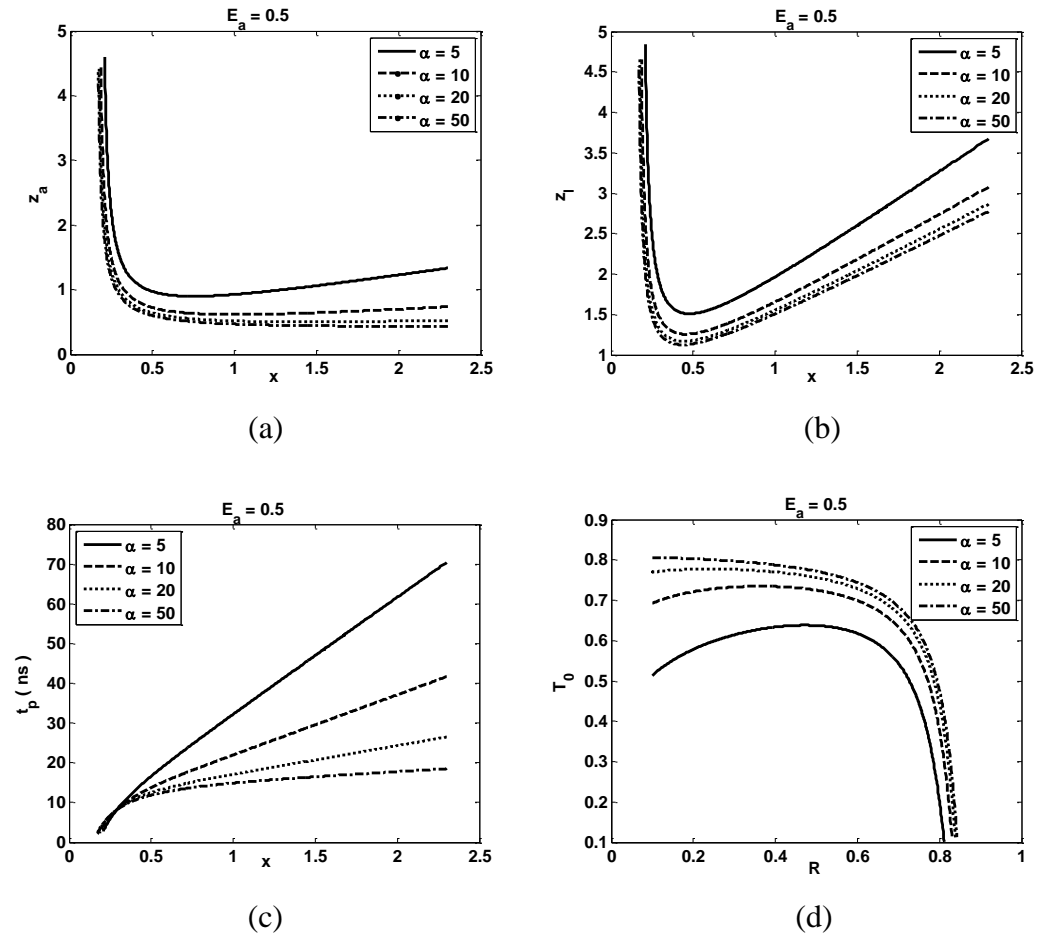


Figure 3.5 (a) z_a , (b) z_l and (c) t_p as a function of x and α (5, 10, 20 and 50) when $E_a = 0.5$, (d) the proper pairs of R and T_0 to keep $E_a = 0.5$ for $\alpha = 5, 10, 20$ and 50

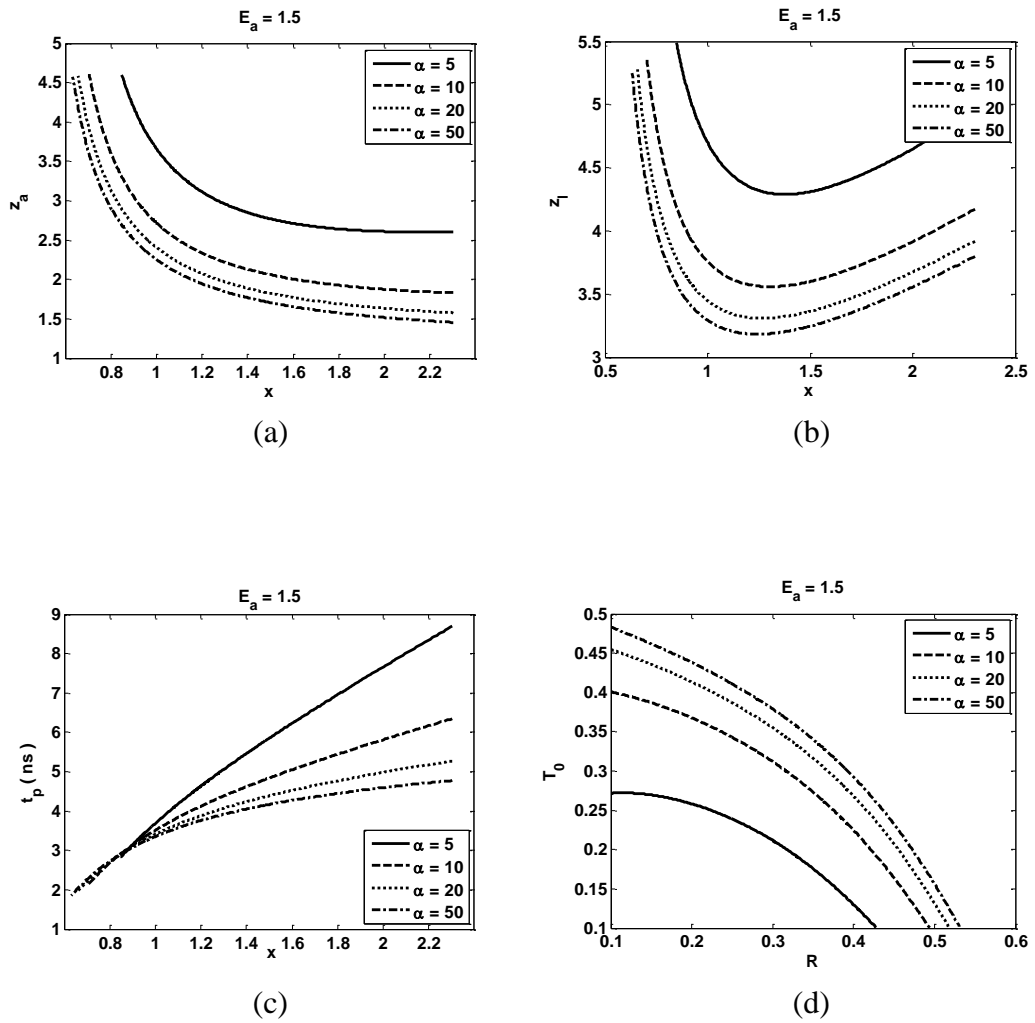
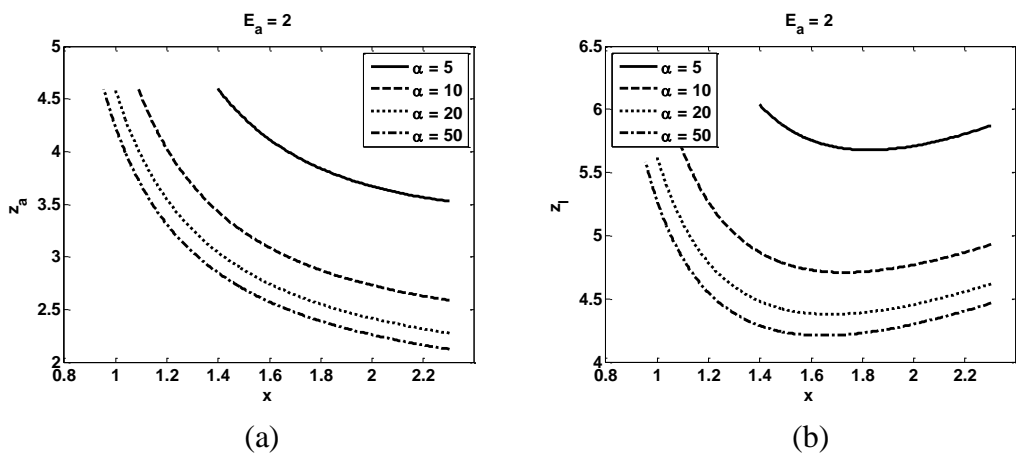


Figure 3.6 (a) z_a , (b) z_l and (c) t_p as a function of x and α (5, 10, 20 and 50) when $E_a = 1.5$, (d) the proper pairs of R and T_0 to keep $E_a = 1.5$ for $\alpha = 5, 10, 20$ and 50



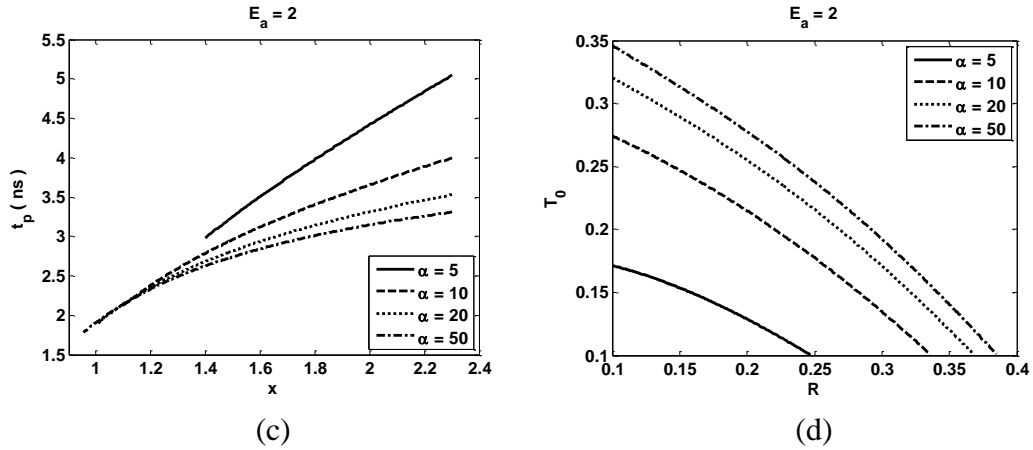


Figure 3.7 (a) z_a , (b) z_l and (c) t_p as a function of x and α (5, 10, 20 and 50) when $E_a = 2$, (d) the proper pairs of R and T_0 to keep $E_a = 2$ for $\alpha = 5, 10, 20$ and 50

Fig. 3.4 (a) and Fig. 3.5 (a) show when E_a is relatively low the parameter, z_a doesn't decrease monotonically with x as given in Fig. 3.1 (a), and follows a decrease-valley-increase process. This situation is especially obvious for the cases when α is 5 or 10. In Fig. 3.4 (a) and Fig. 3.5 (a), z_a decreases sharply as x is far away from its minimum value, and the curves of z_a for small α approach one with bigger α . When E_a is higher, such as 1.5 and 2 shown in Fig. 3.6 and Fig. 3.7, z_a decreases monotonically and gently as x is increasing compared with the lower output energy.

In Figs. 3.4 (b) - 3.7 (b), the small gain parameter z_l whose value is determined by x and its coupling z_a follows a decrease-valley-increase process along x the same as it shown in Fig. 3.1 (b).

The FWHM pulse width t_p as a function of x and different values of α for the cases that $E_a = 0.2, 0.5, 1.5$ and 2 are plotted in Figs. 3.4 (c) - 3.7 (c). It is noted that t_p decreases along x , and for a selected x , it is shorter with a higher α . But

the curves of t_p for different α approach each other as x is close to its smallest value. Comparing Figs. 3.4 - 3.7, the FWHM pulse width t_p produced by a selected output coupler is normally shorter when the output energy E_a is higher. As an example, Table 3.3 shows a group of E_a (0.2, 0.5, 1.5 and 2) and its corresponding FWHM pulse width t_p as $\alpha = 5, 10, 20$ and 50 when $R = 20\%$.

Table 3.3 The FWHM pulse width t_p when $R = 20\%$ ($x = 1.61$)

	$E_a = 0.2$		$E_a = 0.5$		$E_a = 1.5$		$E_a = 2$	
α	T_0 (z_a)	t_p (ns)	T_0 (z_a)	t_p (ns)	T_0 (z_a)	t_p (ns)	T_0 (z_a)	t_p (ns)
5	0.67 (0.80)	2.97×10^2	0.58 (1.10)	50	0.26 (2.70)	6.3	0.13 (4.10)	3.5
10	0.82 (0.40)	1.67×10^2	0.72 (0.65)	31	0.37 (2.0)	5.1	0.21 (5.10)	3.1
20	0.88 (0.25)	97	0.78 (0.50)	22	0.41 (1.77)	4.5	0.26 (4.54)	2.9
50	0.91 (0.18)	56	0.80 (0.44)	17	0.44 (1.65)	4.3	0.28 (4.30)	2.89

As shown in Figs. 3.4 (d) - 3.7 (d), the number of the pairs of R and T_0 which can be employed in the system is reducing when E_a is increasing. And the smaller α will aggravate this situation. It is easy to explain this phenomenon that when the laser system is required to provide higher output energy, more energy is needed to be stored in the gain medium before lasing, and then it will be released in a short time. According to the operating principle of passive Q -switching, compared with the lower output energy case, the initial loss from the absorber must have a relatively high value before bleaching occurs, as the output reflectivity is fixed. Here, the high loss of the absorber means the value of the

absorber initial transmission is low. It demonstrates that for the same output reflectivity, the coupling absorber initial transmission for the high output energy is smaller than for the low output energy. Hence, the highest output reflectivity for the low output energy case may not have the coupling initial transmission to satisfy the high output energy. Then the available range of the output reflectivity for the high output energy is smaller than the low output energy. Therefore, the selection range for the coupling absorber initial transmission is reduced as well. As shown in Eq. 3.9, when the output energy is decided, the value of α affects the selected output reflectivity and its coupling absorber initial transmission, and thereby affects the small signal parameter. A smaller α results in a smaller coupling initial transmission T_0 for a determined output reflectivity R , which means the high output reflectivity that has the coupling absorber initial transmission to keep the pre-determined output energy for the high α , will not have the corresponding absorber initial transmission for the low α . Therefore, the available range of the R and T_0 pair decreases.

The available values of R and its corresponding T_0 for the case $\alpha = 5, 10, 20, 50$ and $E_a = 0.2, 0.5, 1.5, 2$ are shown in Table 3.4. It can be assumed that the pairs of gain medium and absorber which lead to a lower α cannot work for a much higher E_a . For example, if $\alpha = 5$, it is hard for a laser system to get $E_a > 2$. When $E_a = 2$, the best situation, that for the case $\alpha = 50$, the ranges of R and T_0 are 0.1–0.38 and 0.1–0.35, will still result in a very high optical loss and a high initial inversion density. It is known that a high initial inversion density will result in significant amplified spontaneous emission prior to lasing, and the output energy cannot reach the required value. Hence, the ideal practical guide for a designer is to employ an output coupler with high reflectivity.

Table 3.4 The ranges of R and T_0 when $\alpha = 5, 10, 20, 50$ and $E_a = 0.2, 0.5, 1.5$ and 2

	$E_a = 0.2$		$E_a = 0.5$	
α	R	T_0	R	T_0
5	0.1–0.93	0.1–0.82	0.1–0.82	0.1–0.64
10	0.1–0.93	0.1–0.88	0.1–0.83	0.1–0.73
20	0.1–0.94	0.1–0.90	0.1–0.84	0.1–0.78
50	0.1–0.94	0.1–0.92	0.1–0.84	0.1–0.81
	$E_a = 1.5$		$E_a = 2$	
α	R	T_0	R	T_0
5	0.1–0.42	0.1–0.27	0.1–0.25	0.1–0.17
10	0.1–0.49	0.1–0.40	0.1–0.34	0.1–0.27
20	0.1–0.52	0.1–0.45	0.1–0.37	0.1–0.32
50	0.1–0.53	0.1–0.48	0.1–0.38	0.1–0.35

3.3.2 The effect of the absorber material (γ_s') on selecting a pair of R and T_0 to get the shorter FWHM pulse width

Now the effect of the material of the absorber (γ_s') on R and its coupling T_0 is studied. It is hoped to get a higher output reflectivity and reduce the optical loss and initial inversion density. Before the study, the parameter α showing the relation between the gain medium and absorber material is set as 20.

Figs. 3.8 (a) - 3.11 (a) plot the FWHM pulse width t_p as a function of the output coupler parameter x and the absorber material parameter γ_s' (1.1, 1.3, 1.5 and 1.7) when E_a is required to be 1.5, 2, 2.5 and 3. The reflectivity of the output coupler R and its coupling absorber initial transmission T_0 are shown in Figs. 3.8 (b) - 3.11 (b).

As shown in Figs. 3.8 (a) and (b), there exist proper pairs of R and T_0 for the cases that γ_s' is 1.1, 1.3, 1.5 and 1.7, to keep $E_a = 1.5$. It is found in Fig. 3.8 (a) that when the laser systems with different γ_s' operate with the corresponding highest output reflectivity, they have nearly the same output FWHM pulse width. For one determined output coupler, a laser system with a bigger absorber material parameter γ_s' needs a smaller coupling initial transmission T_0 , and has a shorter FWHM pulse width. It is obvious that the available range of R is reduced with γ_s' 's increase. As shown in the figure, when γ_s' is 1.7, the maximum available R is 33%; but when $\gamma_s' = 1.1$, the highest available reflectivity R is 80%.

Comparing the results shown in Figs. 3.8 - 3.11, it is found that there are no couples of R and T_0 that satisfy the requirements $E_a = 2.5$ or $E_a = 3$ for the case that $\gamma_s' = 1.7$. Although there are the theoretical data of R and T_0 to keep $E_a = 2$ as $\gamma_s' = 1.7$, it is not practically feasible.

Figs. 3.9 - 3.11 give the same conclusions as given by Fig. 3.8 that for the same output coupler R the FWHM pulse width t_p achieved by an absorber with a bigger γ_s' is shorter than one produced by the smaller γ_s' . But the bigger absorber material parameter γ_s' results in a narrower adaptive ranges of R and T_0 . With E_a 's increasing, the adaptive ranges of R and T_0 from each γ_s' are

reducing. When the output energy E_a is required as a higher value, only an absorber with smaller γ_s' can satisfy the requirement.

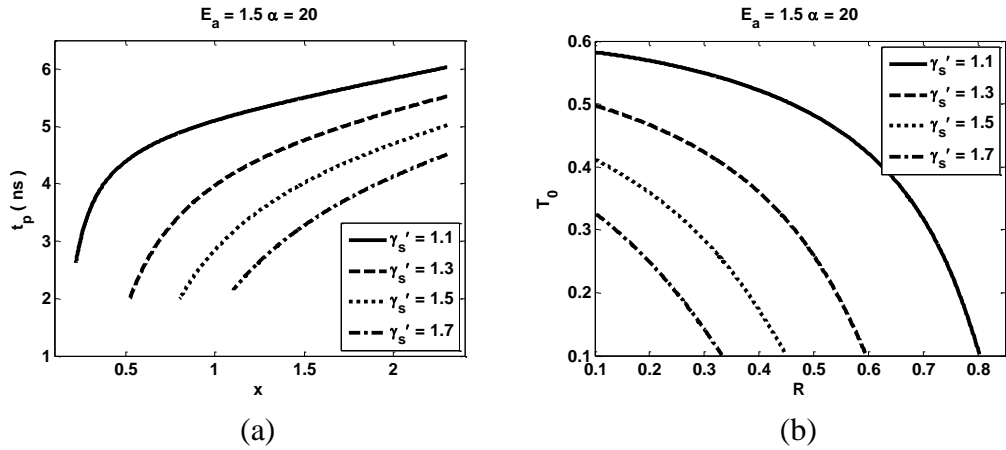


Figure 3.8 (a) The FWHM pulse width t_p as a function of x and γ_s' (1.1, 1.3, 1.5 and 1.7) when $E_a = 1.5$, (b) the corresponding pairs of R and T_0

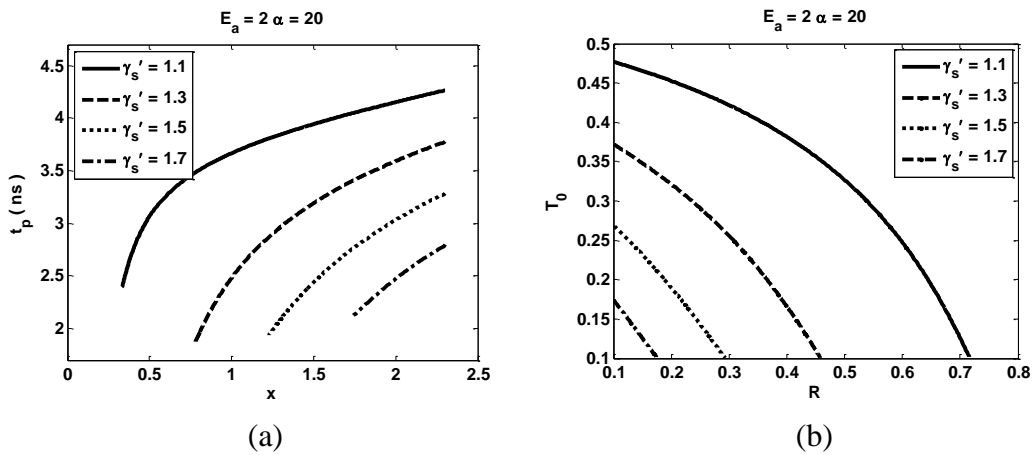


Figure 3.9 (a) The FWHM pulse width t_p as a function of x and γ_s' (1.1, 1.3, 1.5 and 1.7) when $E_a = 2$, (b) the corresponding pairs of R and T_0

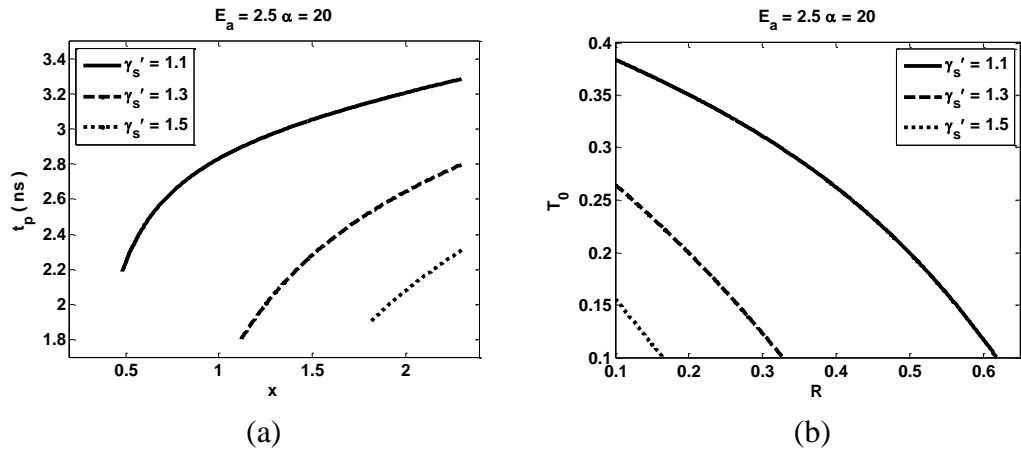


Figure 3.10 (a) The FWHM pulse width t_p as a function of x and γ_s' (1.1, 1.3 and 1.5) when $E_a = 2.5$, (b) the corresponding pairs of R and T_0

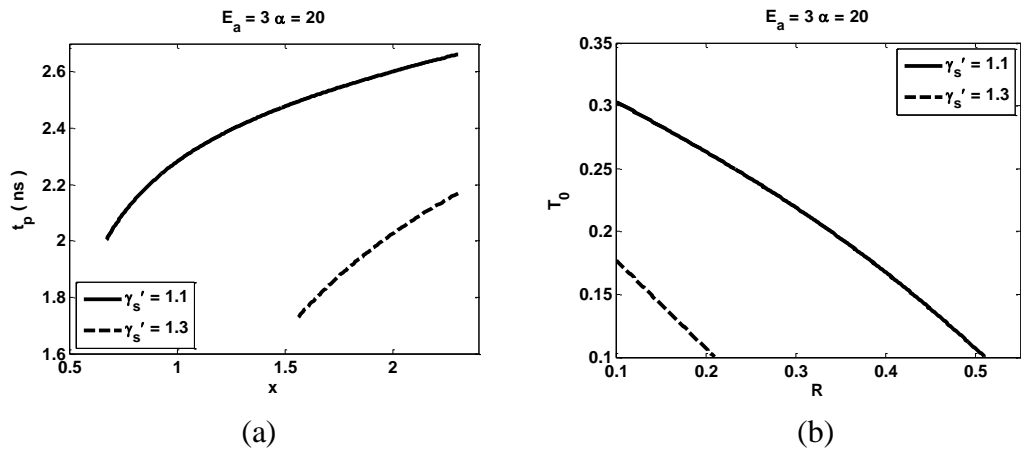


Figure 3.11 (a) The FWHM pulse width t_p as a function of x and γ_s' (1.1 and 1.3) when $E_a = 3$, (b) the corresponding pairs of R and T_0

3.4 Modeling

3.4.1 A Cr:YAG passively Q -switched Nd:Glass laser

A Cr:YAG passively Q -switched Nd:Glass laser [Xiao and Bass, 1998] is used to show the simulation results for a practical case. The data of this laser system are

listed in the following Tables. For this material system, $\alpha \approx 160$ which is calculated using Eq. 2.10.

Table 3.5 The data for laser system

l_c (length of cavity) (mm)	λ (the wave length of output laser) (μm)	L (the remaining two none useful optical loss)	The laser beam diameter (mm)
190	1.054	0.04	2.4

Table 3.6 The material properties for Nd:Glass

l (length of laser rod) (mm)	Radius of laser rod (mm)	σ (cm^2)	γ
75	3	4.4×10^{-20}	1

Table 3.7 The material properties for Cr:YAG

σ_{gs} (cm^2)	σ_{es} (cm^2)	γ_s
7×10^{-18}	2×10^{-18}	1

An output coupler with a reflectivity that is too low will result in a high inversion population which leads to a significant amplified spontaneous emission prior to lasing. Hence, to avoid this problem, in the modeling the reflectivity of the output coupler is required to be $R > 40\%$. In the modeling, the value of the output energy parameter E_a is set as 0.2, 0.5 and 1. And the corresponding output energy E can be calculated as $19mJ$, $49mJ$ and $97mJ$ by Eq. 3.6 (e) and the measured laser beam size.

The small gain parameter z_l and its corresponding absorber parameter z_a versus x for the cases when $E = 19mJ$, $49mJ$ and $97mJ$ are plotted in Fig. 3.12. The parameter z_l follows a decrease-valley-increase process with x 's increasing. This phenomenon is obvious for the cases $E = 19mJ$ and $49mJ$. The plot of z_a

decreases monotonically along x , and it is noted that, as x approaches its minimum value, z_a changes sharply.

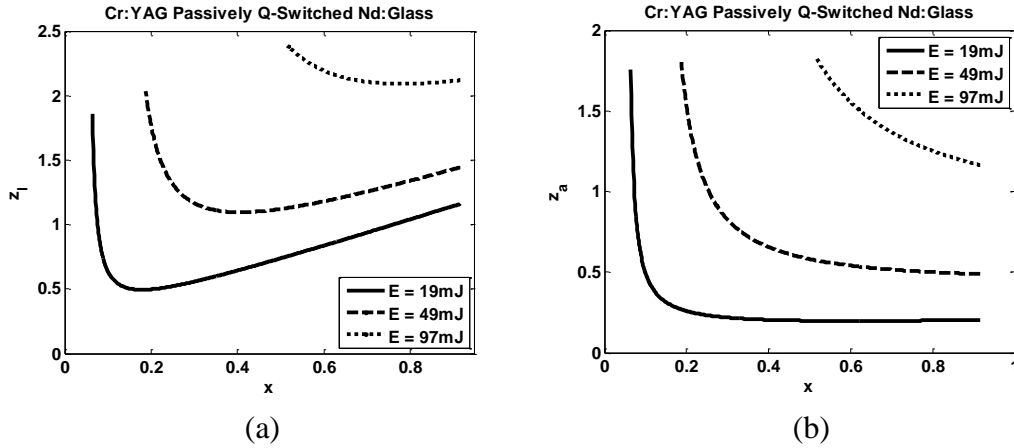


Figure 3.12 (a) The parameter z_l versus x for the cases $E = 19\text{mJ}$, 49mJ and 97mJ , (b) the corresponding z_a of z_l along x

The FWHM pulse width t_p as a function of x and different output energy E (19mJ , 49mJ and 97mJ) is plotted in Fig. 3.13. Fig. 3.14 plots the proper pairs of R and T_0 to keep the output energy as 19mJ , 49mJ and 97mJ . It is found that normally the parameter t_p for the higher output energy has a smaller value, but the values of the shortest FWHM pulse widths t_p for the cases $E = 19\text{mJ}$, 49mJ and 97mJ don't have a great difference. For one deterministic output energy, selecting an output coupler with higher reflectivity whose coupling T_0 is lower is one way to get a shorter FWHM pulse width. For the convenience of observation, the shortest FWHM pulse width t_p with its corresponding pair of $R(x)$ and T_0 (z_a) as $E = 19\text{mJ}$, 49mJ and 97mJ are listed in Table 3.8. It is observed in Table 3.8 that the values of T_0 to get the shortest t_p for different output energies is around 0.41, and the corresponding R has great difference.

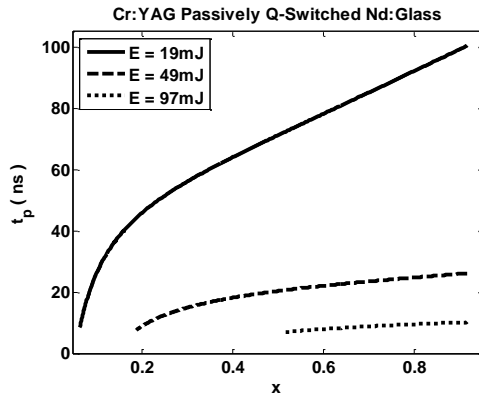


Figure 3.13 The FWHM pulse width t_p as a function of x and different output energy E ($19mJ$, $49mJ$ and $97mJ$)

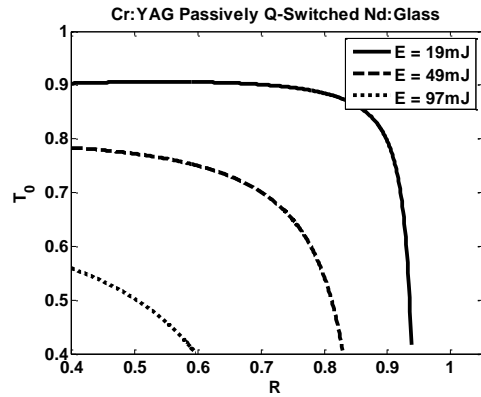


Figure 3.14 The proper pairs of R and T_0 to keep $E = 19mJ$, $49mJ$ and $97mJ$

Table 3.8 The shortest t_p with its coupling pair of $R(x)$ and $T_0(z_a)$ as $E = 19mJ$, $49mJ$ and $97mJ$

E	$19mJ$	$49mJ$	$97mJ$
$R (x = \ln(\frac{1}{R}))$	0.93 ($x = 0.06$)	0.83 ($x = 0.18$)	0.60 ($x = 0.52$)
$T_0 (z_a = -2\ln(T_0))$	0.42 ($z_a = 1.75$)	0.41 ($z_a = 1.80$)	0.40 ($z_a = 1.83$)
$t_p (ns)$	8.4	7.7	6.9

Fig. 3.15 plots the normalized photon density distributions (ϕ) along the pulse time for different output energy when t_p is the shortest. The figure shows that the shape of the pulses for different output energies are nearly the same.

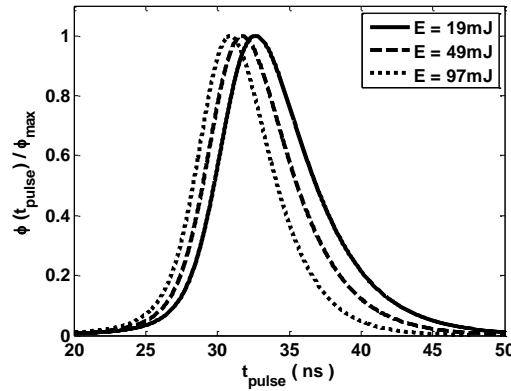


Figure 3.15 The normalized photon density distributions $\phi(t_{pulse})$ for $E = 19mJ$, $49mJ$ and $97mJ$ when t_p is the shortest

3.4.2 A Cr:YAG passively Q -switched Nd:YAG laser

In Section 3.3.1, it is noted that the parameter α can affect the selection of the output reflectivity and absorber initial transmission pair to keep the pre-determined output energy parameter E_a , and further affect the FWHM pulse duration. By the definition of α shown in Eq. 2.10, it is known that the value of α is determined by the material characteristics of the gain medium and the absorber. When the material of the absorber is held constant; α is only affected by the gain medium. Today, the most popular absorber material is Cr:YAG but the number of the materials used as the gain medium of a passively Q -switched laser system is very large. Hence, the study of the parameter α can be transferred to the study of the material of the gain medium.

Here, a same size Nd:YAG gain material is in place of the Nd:Glass gain material in Xiao's laser system to show the effect of the gain medium (the parameter α) on the selection of the output reflectivity and initial transmission pair, and the FWHM pulse duration. The material properties of Nd:YAG are listed in Table 3.9. Now, $\alpha = 25$.

Table 3.9 Material properties of Nd:YAG

Parameters	Nd:YAG
l (length of laser rod)(mm)	75
Radius of laser rod(mm)	3
Emission cross section (σ)	$2.8 \times 10^{-19} \text{ cm}^2$
Effect of level degeneracies (γ)	1

As done in Section 3.4.1, the output energy parameter E_a is set to be 0.2, 0.5 and 1, respectively. Here, the size of the laser beam is assumed to be same as the Nd:Glass laser system described in Section 3.4.1. Compared with the Nd:Glass, the different value of the Nd:YAG material's emission cross section σ leads to the different value of the term $\frac{h\nu A}{2\sigma\gamma}$ in Eq. 3.6 (e). Hence, even though the output energy parameter E_a of the Nd:YAG laser is assigned to be the same as for the Nd:Glass laser (0.2, 0.5 and 1), the corresponding values of the output energy E are $3mJ$, $8mJ$ and $15mJ$ which are much smaller than the output energies of the Nd:Glass laser system ($19mJ$, $49mJ$ and $97mJ$) shown in Section 3.4.1.

Fig. 3.16 plots the small gain parameter z_l and its corresponding absorber parameter z_a versus x for the cases that $E = 3mJ$, $8mJ$ and $15mJ$ (the values of E_a are 0.2, 0.5 and 1, respectively). The same as for the Nd:Glass laser, the parameter z_l for the Nd:YAG laser decreases along x firstly, then reaches its minimum point, after which it increases (it can be said that z_l follows a decrease-valley-increase process along x). The curve of z_a decreases monotonically along x . It is noted that the corresponding z_l and z_a for a fixed value of x for the Nd:YAG laser system is nearly same as for the Nd:Glass laser system. The simulation results agree with the theoretical results obtained in Section 3.3.1.

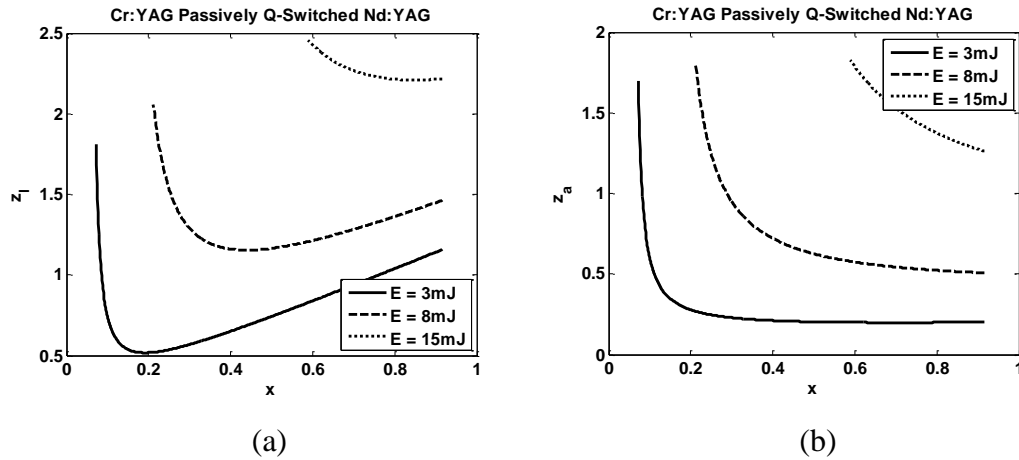


Figure 3.16 (a) the small-signal parameter z_l and (b) its coupling absorber parameter z_a versus the reflectivity parameter x when $E = 3\text{mJ}$, 8mJ and 15mJ (E_a are 0.2, 0.5 and 1) for the Nd:YAG laser system

Fig. 3.17 plots the FWHM pulse width t_p as a function of x for the different output energy $E = 3\text{mJ}$, 8mJ and 15mJ (namely E_a are 0.2, 0.5 and 1). Compared with the Nd:Glass laser system shown in Fig. 3.13, the curve of t_p for the Nd:YAG laser system has the same trend of changing, but in the Nd:YAG laser system the value of t_p for the same x is longer than for the Nd:Glass laser system. However, the difference between two laser systems is negligible when x is close to its minimum value.

For convenience of observation, the output reflectivity R and initial transmission T_0 pairs to keep the output energy $E = 3\text{mJ}$, 8mJ and 15mJ (namely E_a are 0.2, 0.5 and 1) are plotted in Fig. 3.18. The range of selection of R and T_0 pairs to keep the pre-determined output energy parameter E_a is wider for the Nd:Glass laser system than for the Nd:YAG laser system. Observing Figs. 3.17 and 3.18 shows that the shortest FWHM pulse duration t_p can be obtained by using the

highest output reflectivity R . The R and T_0 pairs which result in the shortest FWHM pulse width in Fig. 3.17 for the different output energies are listed in Table 3.10.

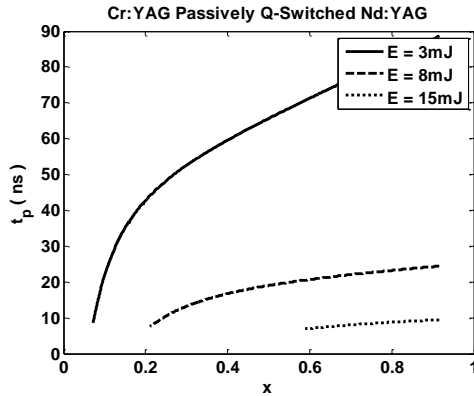


Figure 3.17 The FWHM pulse width t_p as a function of x when $E = 3mJ$, $8mJ$ and $15mJ$ (namely E_a are 0.2, 0.5 and 1) for a Nd:YAG laser system

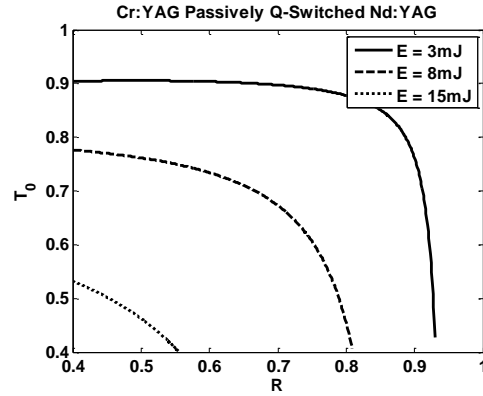


Figure 3.18 The coupling initial transmission T_0 of the output reflectivity R which to keep $E = 3mJ$, $8mJ$ and $15mJ$ (namely E_a are 0.2, 0.5 and 1) for a Nd:YAG laser system

Table 3.10 The pair of $R(x)$ and $T_0(z_a)$ to achieve the shortest t_p when $E = 3mJ$, $8mJ$ and $15mJ$ (namely E_a are 0.2, 0.5 and 1) for the Nd:YAG laser system

$E (E_a)$	$3mJ (E_a = 0.2)$	$8mJ (E_a = 0.5)$	$15mJ (E_a = 1)$
$R (x = \ln(\frac{1}{R}))$	0.93 ($x = 0.06$)	0.81 ($x = 0.21$)	0.56 ($x = 0.59$)
$T_0 (z_a = -2\ln(T_0))$	0.43 ($z_a = 1.70$)	0.41 ($z_a = 1.80$)	0.40 ($z_a = 1.83$)
$t_p (ns)$	8.5	7.6	6.9

The normalized photon density distributions (ϕ) plotted against the pulse time for different output energies for the case when t_p is the shortest are plotted in Fig. 3.19. The shapes of the curves for the Nd:Glass laser system and the Nd:YAG laser system are similar.

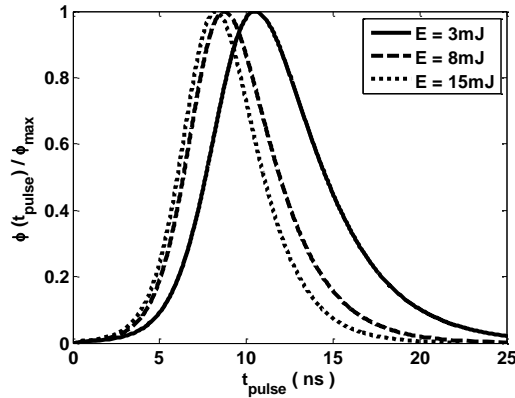


Figure 3.19 The normalized photon density distributions $\phi(t_{pulse})$ $E = 3mJ$, $8mJ$ and $15mJ$ (namely E_a are 0.2, 0.5 and 1) for a Nd:YAG laser system

3.5 Conclusions

A general model (*Model I*) based on the laser rate equations for the design of an optical resonator that controls the pulse width and maintains the pre-selected output energy is developed in this chapter. *Model I* has two suppositions which are: 1) the build-up time of the Q -switched laser pulse is quite short compared with the pumping and relaxation times of the laser medium, which means that in the laser pulse stage the pump rate, the relaxation part of the gain medium and absorber, are negligible in the laser rate equations; 2) the repetition rate of the laser system is quite slow compared with the relaxation time of an absorber, and most atoms of the absorber's excited state will return to the ground level before the beginning of each lasing cycle, which leads to the result that the initial

population density of the ground level at the beginning of Q -switching is nearly equal to the total population density of an absorber. The second assumption shows the pumping cycle in *Model I* will not affect the output of a laser system. Hence, for a passively Q -switched laser system which satisfies the two suppositions of *Model I*, the output parameters are only determined by the working state in the lasing cycle. Therefore, the study of *Model I* focuses on the lasing cycle.

The mathematical expressions for the initial conditions of lasing, the final inversion population density of the gain medium, the instantaneous inversion population density at the output power's peak point, the photon density in laser resonator, the instantaneous inversion population density of the gain medium, and the instantaneous population density of an absorber at the ground level are presented by solving the simplified laser rate equations. According to Eq. 1.2, the output parameters of a passively Q -switched laser system, such as the total output energy, the peak power and the approximate FWHM pulse width can be calculated as well. The key parameters defined in Chapter 2 are employed in *Model I* to simplify the mathematical expressions, and show their effect on the output parameters.

The simulation steps are given to get the initial transmission, the initial conditions and the FWHM pulse width when the output reflectivity and the output energy are pre-determined. The factors affecting the pulse width are shown by the key parameters as α , γ_s' , x , z_a and E_a . The following conclusions can be drawn:

- 1) when the absorber material (γ_s') is decided,
 - a) to maintain the output energy, a higher output reflectivity R has a smaller coupling initial transmission T_0 ;
 - b) as the material parameter α and the output energy are determined, a higher output reflectivity R and its corresponding T_0 result in a shorter pulse width;

c) once the material parameter α and the output reflectivity R are decided, if the output energy is high, the pulse width is short;

d) as the output energy parameter E_a is required to have higher value, the material parameter α is bigger, the number of the usable pairs of R and T_0 are greater;

2) as the output energy parameter E_a is very high and the proper output reflectivity R is too low, selecting the materials for the gain medium and absorber to get a bigger α and a smaller γ_s ' is the method to get a proper pair of R and T_0 to build a feasible laser system.

The simulation results of a Cr:YAG passively Q -switched Nd:Glass laser system [Xiao and Bass, 1998] for different values of the output energy parameter give the pairs of output reflectivity and absorber initial transmission to maintain the output energy parameter. The effect of the output reflectivity and absorber initial transmission pair on the FWHM pulse duration is shown as well. The simulation results agree well with the analysis in Section 3.3.

The effect of the gain medium on the FWHM pulse duration is demonstrated by using a same size Nd:YAG material in place of the Nd:Glass material in the laser cavity, and is represented by the parameter α in the simulation. Although the values of the output energy parameter are the same as for the Nd:Glass laser, the output energy of the Nd:YAG laser is smaller than the Nd:Glass laser because of the different material properties. The simulation results prove the discussions concerning the parameter α in Section 3.3 that the smaller α will reduce the available range of the output reflectivity and its coupling absorber initial transmission.

Chapter 4

A Model for a Passively Q -Switched Laser System with a Long Build-up Time

4.1 Introduction

Chapter 4 studies the FWHM pulse width with two assumptions: 1) the effect of the pump power at the lasing stage has to be considered in the modelling because of the longer build-up time of the Q -switched laser pulse; and 2) the repetition rate of the laser system is slow compared with the relaxation time of the absorber's upper level, hence, the initial population density of an absorber's ground level at the beginning of each Q -switch is nearly equal to the total population density of the absorber. This case is named *Model II*.

According to the first assumption shown in the previous paragraph, the pump power is an influencing factor affecting the output parameters of the laser system (such as the FWHM pulse width, the output energy, and the peak power) at the lasing stage in *Model II*. Hence, the pump rate in the laser rate equations cannot be ignored as in *Model I* at the lasing stage. When the pump rate is considered in the laser rate equations, the mathematical expressions of several variables cannot be obtained, as in *Model I*, for example, the distribution of the average photon density in the laser cavity, the power of the laser, the distribution of the inversion population density of the gain medium. Here, the Runge-Kutta method is employed to solve the laser rate equations to obtain the numerical results for the distributions of the average photon density in the laser resonator, the inversion population density of the gain medium, and the population density of an absorber at its ground level.

When a laser system satisfies the second condition for *Model II*, the initial condition of the laser system is nearly same for each of the Q -switched cycles, and the laser system will reach its stable state after the first few pumping and lasing cycles. Here, the stable state of a laser system is defined as the state when the output parameters of each pumping and lasing cycle, such as the FWHM pulse width, the output energy and the peak power, converge on stable values. When a laser system reaches its stable state after the first few working cycles,

this laser is named as working at the *quick-stable* working state. The selection range of a coupling pair, that is: an output coupler and an absorber, to keep the output energy at its pre-determined level, is limited by the pump power.

The simulation results for controlling the FWHM pulse duration by selecting the appropriate pair of output reflectivity and absorber initial transmission in *Model II* are represented by using a continuously pumped Cr:YAG passively Q -switched Yb:YAG laser. Here, the output energy parameter E_a is maintained at the pre-decided value. The effect of the pump power is demonstrated by the comparison of the data obtained in *Model I* and *Model II*. To study the effect of the gain medium, the Yb:YAG material is replaced by Nd:YAG, while the output energy parameter E_a is kept as same as the Yb:YAG laser's.

4.2 Laser rate equations

The coupled rate equations have been used to model a passively Q -switched laser in many investigations. When the pump power is considered in *Model II*, introducing the excited state of the absorber (ESA), the rate equations are as follows:

$$\frac{d\phi}{dt} = \frac{\phi}{t_r} [2\sigma n l - 2\sigma_{gs} n_{gs} l_s - 2\sigma_{es} n_{es} l_s - \ln\left(\frac{1}{R}\right) - L] \quad (4.1a)$$

$$\frac{dn}{dt} = -\gamma \sigma c \phi n + W_p (n_{tot} - n) - \frac{n}{\tau_{21}} \quad (4.1b)$$

$$\frac{dn_{gs}}{dt} = -\gamma_s \sigma_{gs} c \phi n_{gs} + \frac{n_{s0} - n_{gs}}{\tau_s} \quad (4.1c)$$

$$n_{gs} + n_{es} = n_{s0} \quad (4.1d)$$

where, ϕ is the photon density in the laser cavity, n is the instantaneous population inversion density of the gain medium, n_{gs} and n_{es} are the instantaneous population densities of the absorber ground and excited state respectively, σ is the laser stimulated emission cross-section, σ_{gs} and σ_{es} are the

absorber ground and excited state absorption cross-sections respectively, γ and γ_s are the inversion reduction factors of the gain medium and absorber respectively, R is the reflectivity of the output mirror, L is the remaining two way dissipative (none useful) optical loss, l and l_s are the lengths of the gain and absorbing media respectively, $t_r = \frac{2l'}{c}$ is the round-trip transit time of light in the resonator of optical length l' , W_p is the volumetric pump rate into the upper level and is proportional to the continuous pump power, n_{tot} is the doping concentration of the gain medium, n_{s0} is the absorber total population density, τ_{21} and τ_s are the spontaneous emission lifetimes of the upper level of the gain medium and the absorber, respectively.

At the pumping stage, the photon density in the cavity is assumed to be $\phi \approx 0$.

Hence, at the pumping stage the rate equations are:

$$\frac{dn}{dt} = W_p (n_{tot} - n) - \frac{n}{\tau_{21}} \quad (4.2a)$$

$$\frac{dn_{gs}}{dt} = \frac{n_{s0} - n_{gs}}{\tau_s} \quad (4.2b)$$

For the continuously pumped laser with a repetition rate f , integrating Eq. 4.2 (a) yields the initial inversion density of the current Q -switch n_i

$$n_i = \frac{1}{W_p \tau_{21} + 1} \{ W_p \tau_{21} n_{tot} - [W_p \tau_{21} n_{tot} - (W_p \tau_{21} + 1) n_f] e^{-\frac{1}{\tau_{21} f}} \} \quad (4.3)$$

where, n_f is the final inversion density of the gain medium at the end of the previous pulse stage.

At the pulse stage, the situation is more complicated than the case ignoring the pumping rate W_p . The instantaneous distributions of the photon density, the inversion population density of the gain medium and the population density of the absorber's ground state cannot be given directly by the mathematical

representations. But the initial inversion condition for the Q -switch can still be presented by setting the right hand side of Eq. 4.1 (a) to zero. When a laser system works at the *quick-stable* state, the initial transmission of an absorber at each pumping and lasing cycle is nearly same as the value for the first working cycle. Hence, it can be assumed that $n_{gsi} \approx n_{s0}$. Therefore, the initial condition of a laser system with a quick-stable state is written as:

$$2\sigma l n_i = 2\sigma_{gs} l_s n_{s0} + \ln\left(\frac{1}{R}\right) + L \quad (4.4a)$$

or

$$n_i = \frac{2\sigma_{gs} l_s n_{s0} + \ln\left(\frac{1}{R}\right) + L}{2\sigma l} \quad (4.4b)$$

This expression is the same as that used in *Model I* in which the pump power parameter W_p is ignored in the laser rate equations at the lasing stage.

When the power reaches its peak point, $\frac{d\phi}{dn} = 0$. Hence, the instantaneous inversion density of the gain medium n_t is

$$2\sigma l n_t = 2\sigma_{gs} l_s n_{gst} + 2\sigma_{es} l_s n_{est} + \ln\left(\frac{1}{R}\right) + L \quad (4.5a)$$

where, n_{gst} and n_{est} are the instantaneous population densities of the absorber ground and excited state at this moment in time, respectively. At this moment, most of the atoms at the absorber's ground level are pumped to the excited level. Hence, compared with the population at the excited level, it can be assumed $n_{gst} \approx 0$, and now n_t is rewritten as

$$2\sigma l n_t \approx 2\sigma_{es} l_s n_{s0} + \ln\left(\frac{1}{R}\right) + L. \quad (4.5b)$$

The expressions for the output energy E , the peak power P_{\max} and the approximate pulse width t_p of the passively Q -switched laser are the same as those in Chapter 3:

$$E = \frac{h\nu A}{2\sigma\gamma} \ln\left(\frac{1}{R}\right) \ln\left(\frac{n_i}{n_f}\right) \quad (4.6a)$$

$$P_{\max} = \frac{h\nu A l'}{t_r} \ln\left(\frac{1}{R}\right) \phi_{\max} \quad (4.6b)$$

$$t_p = \frac{E}{P_{\max}} \quad (4.6c)$$

where, A is the cross-sectional area of the laser beam, h is the Plank's constant, ν is the frequency of the laser field.

The output energy parameter E_a and the peak power parameter P_a are defined as same as in Chapter 3:

$$E_a = \ln\left(\frac{1}{R}\right) \ln\left(\frac{n_i}{n_f}\right) \quad (4.7a)$$

$$P_a = c\gamma\sigma \ln\left(\frac{1}{R}\right) \phi_{\max} . \quad (4.7b)$$

Now Eq. 4.6 is rewritten as:

$$E = \frac{h\nu A}{2\gamma\sigma} E_a \quad (4.8a)$$

$$P_{\max} = \frac{h\nu A}{2\gamma\sigma} P_a \quad (4.8b)$$

$$t_p = \frac{E_a}{P_a} \quad (4.8c)$$

4.3 The effect of the pump power on the output parameters

The general mathematical representations of the average photon density in the laser cavity, the inversion population density of the laser gain medium, and the population density of the absorber in the ground level, cannot be represented directly in *Model II*. Hence, the investigations of the output reflectivity and absorber initial transmission pairs focus on generalizing the relationships

between the FWHM pulse duration and the related variables by the numerical results of a practical laser system.

A laser diode (LD) continuously pumped Cr:YAG passively Q-switched Yb:YAG laser [Li, 2006] is used to show the output parameters of the laser system for different pump powers by solving the laser rate equations. The data for this laser system and materials are listed in the following Tables (Appendix B demonstrates more detailed material properties).

Table 4.1 Material properties of Yb:YAG

Parameters	Yb:YAG
Dopping concentration	$13.8 \times 10^{20} \text{ cm}^{-3}$
Pump wavelength	940nm
Laser wavelength	1030nm
Absorption bandwidth	19nm
Emission bandwidth	9nm
Upper-state lifetime (τ_{21})	951 μ s
Emission cross section (σ)	$2.0 \times 10^{-20} \text{ cm}^2$
Absorption cross section	$0.8 \times 10^{-20} \text{ cm}^2$
Saturation intensity	28kW / cm^2
Refractive index	1.823
Effect of level degeneracies (γ)	2
Size of the material	10 \times 10 \times 1mm (thickness)

Table 4.2 Material properties of Cr:YAG

Parameters	Cr:YAG
Ground state absorption cross-section (σ_{gs})	$7 \times 10^{-18} \text{ cm}^2$
Excited state absorption cross-section (σ_{es})	$2 \times 10^{-18} \text{ cm}^2$
Upper-state lifetime (τ_s)	4.1 μ s

Effect of level degeneracies (γ_s)	1
Thickness	0.3nm
Initial transmission (T_0)	94%

Table 4.3 Parameters of the laser cavity

Parameters	
Length of cavity	6cm
Reflectivity of the output coupler (R)	95%

According to the analysis of *Model I*, the output parameters of a passively Q -switched laser system are fixed and will not change with the pump power. However, the experimental results present different results [Li, 2006].

Figs. 4.1 and 4.2 show the FWHM pulse width of the laser system t_p and its corresponding output energy parameter E_a as a function of different pump rates W_p for two models, *Model I* (the pump rate is ignored in the laser rate equations at the lasing stage), and *Model II* (the pump rate is considered in the laser rate equations at the lasing stage).

It is shown in the figures that when the pump rate is considered in the laser rate equations, the values of t_p and E_a are not fixed. Fig. 4.1 shows, using *Model II*, that the pulse width t_p monotonically decreases as the pump rate W_p increases from $100s^{-1}cm^{-3}$ to $1500s^{-1}cm^{-3}$. On the contrary, the corresponding output energy parameter E_a in *Model II* increases monotonically as W_p increases over the same interval, which is plotted in Fig. 4.2. For example, as observed from Fig. 4.1, the simulation data for t_p of this passively Q -switched Yb:YAG laser system using *Model II* are 19.1ns, 18.5ns and 18ns for the case when the pump rate $W_p = 100s^{-1}cm^{-3}$, $200s^{-1}cm^{-3}$ and $300s^{-1}cm^{-3}$ respectively. Fig. 4.2 represents the corresponding values of E_a are 0.0572, 0.058 and 0.0585, respectively.

Comparing the plots of two models, the simulation results show that for a low pump rate the plots of t_p and E_a obtained by *Model II* approach the values obtained using the simplified model (*Model I*, without considering the pump rate in the laser rate equations), which means *Model II* can be simplified to *Model I* at a relatively low pump rate. However, the differences between the two cases increase with increasing pump rate. t_p is shortened when the pump rate increases, and on the contrary, E_a is larger with a higher pump rate. The experimental values provided by [Li, 2006] agree well with the simulation results when the model includes the pump rate at the lasing stage. The comparison of the theoretical and the experimental results is shown in Table 4.4. The agreement of the theoretical and experimental results means the pump rate must be considered in the model when the laser system is pumped at a higher pump power.

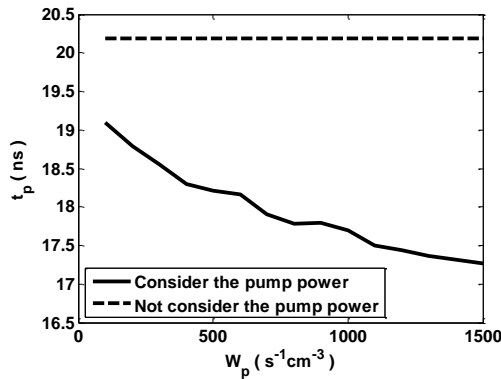


Figure 4.1 The FWHM pulse width t_p as a function of different pump rates W_p for two models, considering W_p , or not

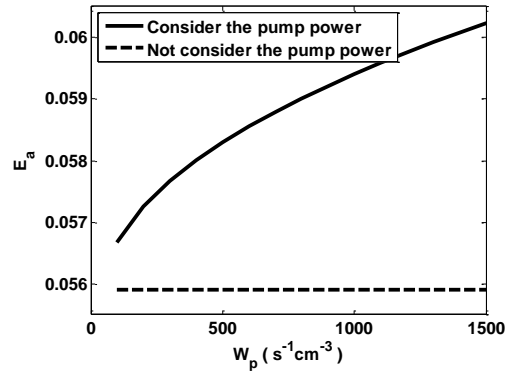


Figure 4.2 The output energy E_a as a function of different pump rates W_p for two models, considering W_p , or not

Table 4.4 The theoretical and the experimental results

The theoretical data		The experimental data	
Pump rate W_p ($s^{-1}cm^{-3}$)	t_p (ns)	Absorbed pump power (W)	t_p (ns)
100	19.1	0.35	17

700	17.9	0.43	16
1500	17.3	0.51	15.6

To show the magnitude of the pump power visually, a variable named as threshold pump rate is defined as

$$W_{p_th} = n_i / (n_{tot} \tau_{21}) \tag{4.10}$$

The pump rate W_p must be greater than the threshold pump rate W_{p_th} , otherwise, the pump power cannot provide enough atoms to the upper level in the spontaneous time of the laser gain medium, and the laser will not lase. A variable N_{Wp} is defined as the ratio of the current pump rate W_p and the threshold pump rate W_{p_th}

$$N_{Wp} = W_p / W_{p_th} \tag{4.11}$$

The value of N_{Wp} is applied to show the magnitude of the pump power compared with the threshold pump power.

For the convenience of observation, the values of t_p , and its corresponding parameter E_a as a function of N_{Wp} for two cases are plotted in Figs. 4.3 and 4.4.

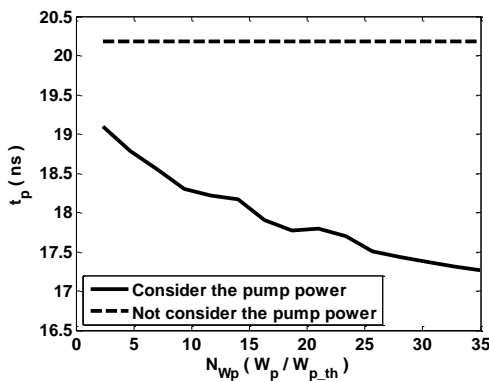


Figure 4.3 The parameter t_p as a function of N_{Wp} for two cases, considering W_p in the rate equations, or not

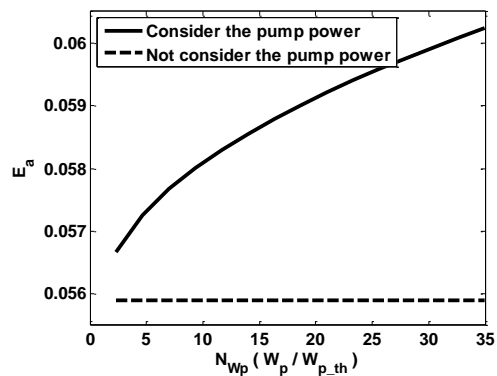


Figure 4.4 The parameter E_a as a function of N_{Wp} for two cases, considering W_p in the rate equations, or not

It can be observed in Figs. 4.3 and 4.4 that the effects of pump rate on the output parameters t_p and E_a are reducing with its increase. As an example, when N_{W_p} increases to 16, t_p is shortened from 19.1 to 17.9ns. But when N_{W_p} increases from 16 to 35, t_p only reduces from 17.9 to 17.3ns. This observed result shows the action and reaction of the pulse width and the pump power. The lower pump rate with a longer pulse width can affect the output parameters t_p and E_a more than the case with the higher pump rate and a shorter pulse width. Hence, both the pump rate W_p and the pulse width t_p have to be considered in the contribution of the pump rate in the model.

4.4 The simulation and computing steps

When the materials of the gain medium and the absorber are decided, the laser cavity is designed, and the output energy parameter E_a is pre-determined, to get the corresponding FWHM pulse width t_p of a laser system of an appropriate pair of output reflectivity and absorber initial transmission, the simulation steps are as follows:

- 1) The reflectivity of the output energy R is decided;
- 2) The probable value of the absorber initial transmission T_0 , as the coupling parameter of R which is determined in Step 1) is selected from an array valued from 0.1 to 0.99, this initial transmission is assumed to maintain the pre-determined output energy with the selected output reflectivity R ;
- 3) Once the output reflectivity R and its probable coupling initial transmission T_0 are determined, the initial inversion population density of the gain medium n_i can be calculated from Eq. 4.3;
- 4) The distributions of ϕ , n and n_{gs} as a function of pulse time are evaluated by using the Runge-Kutta method to solve the rate equations (Eq. 4.1);
- 5) The values of n_f and ϕ_{\max} are shown by the numerical results;

- 6) Using Eq. 4.7 (a), the corresponding E_a of the decided R and its probable T_0 can be obtained;
- 7) Comparing the obtained value of E_a and the value of E_a required by the system,
 - a) If it is nearly same (the error is required to be smaller than 1×10^{-6}), this T_0 is what the laser system required, and the simulation goes to the next step (Step 8);
 - b) If it is not, the computation goes back to Step 2, and selects the next data of the current T_0 in the array, then repeats Steps 2-7 until the proper value of T_0 is obtained;
- 8) Calculating P_a by Eq. 4.7 (b), then introducing the result into Eq. 4.8 (c) yields the FWHM pulse width t_p .

The programming flowchart is illustrated in Fig. 4.5. Here, $E_{a_required}$ is the required output energy parameter E_a which is pre-determined by the designer; $E_{a_current}$ is the output energy obtained using the selected R and its probable coupling T_0 .

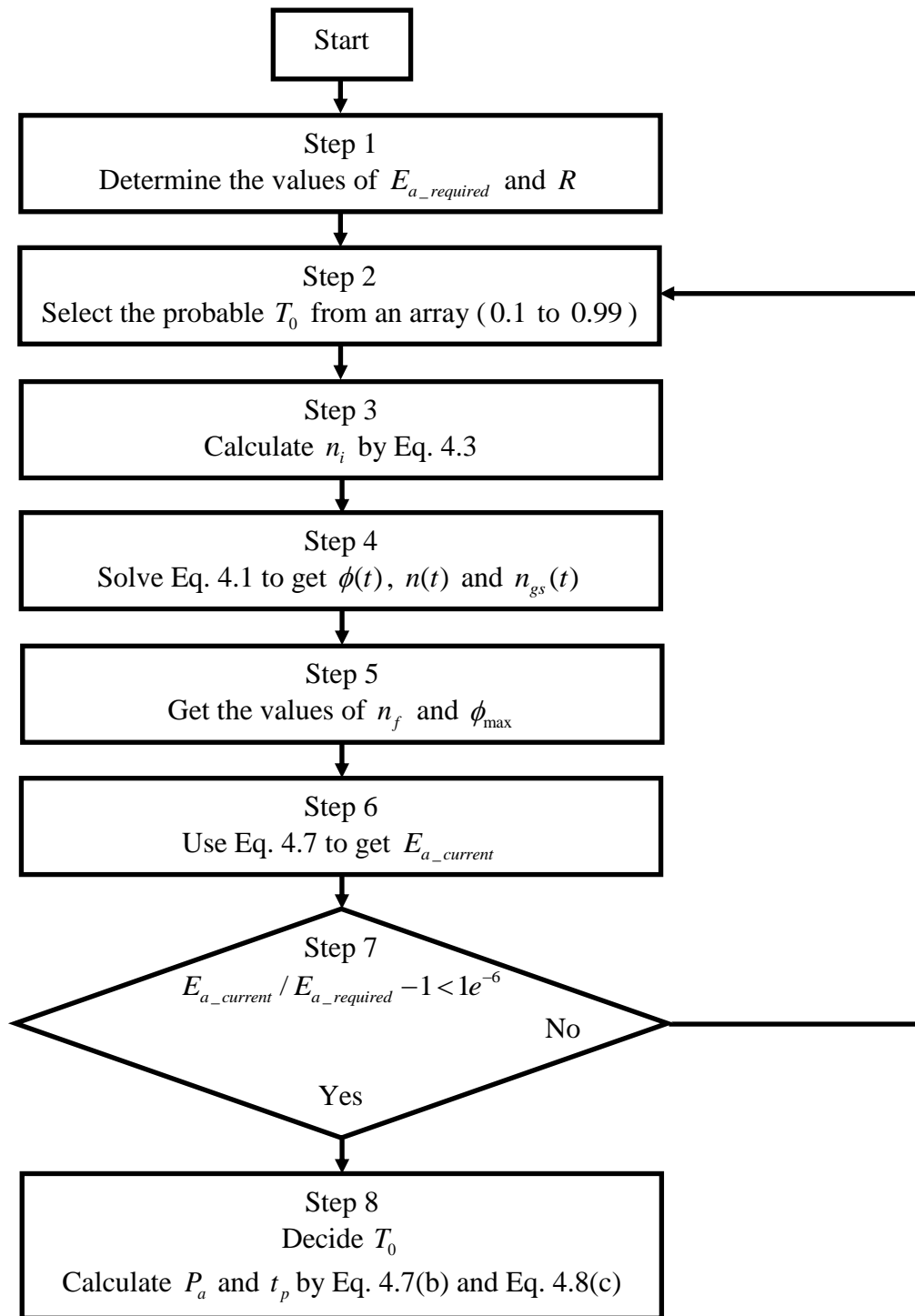


Figure 4.5 The programming flowchart to get the required R 's coupling T_0 and the FWHM pulse width t_p when E_a is known

4.5 The effect of the pump rate

A continuously pumped Cr:YAG passively Q -switched Yb:YAG laser used in Section 4.3 is employed to show simulation results. Here, the value of the output energy E_a should be kept at the required values. The parameters of the materials and the laser system are the same as shown in Tables 4.1 - 4.3. The reflectivity of the output coupler and the initial transmission of the coupling absorber are calculated by using the models, both *Model I* and *Model II*.

Figs. 4.6 - 4.9 show the coupling parameter T_0 required with the selected R to satisfy $E_a = 0.08, 0.1, 0.3$ and 0.5 , with their corresponding parameters: the FWHM pulse width t_p , the peak power P_a and N_{W_p} (the ratio of W_p and $W_{p_{th}}$) when the pump rates of the laser system W_p are $1 \times 10^3 s^{-1} cm^{-3}$, $1.2 \times 10^3 s^{-1} cm^{-3}$ and $1.6 \times 10^3 s^{-1} cm^{-3}$, respectively. Here, the laser system is assumed to work at the *quick-stable* state. The simulation results for *Model I* are plotted in Figs. 4.6 - 4.9 as well.

Figs. 4.6 (a) - 4.9 (a) plot the coupling parameter T_0 against R for the two models, *Model I* and *Model II*. The parameter T_0 decreases monotonically as R increases, which is the same as that discussed in Chapter 3. The value of T_0 for a selected R obtained using *Model II* is nearly equal to the value obtained from *Model I*. It means that when a laser system works in the *quick-stable* state, the effect of pump rate on the selection of a coupling absorber for a selected output coupler R to achieve the pre-determined output energy can be ignored. To simplify the calculation, the coupling T_0 of a determined output coupler in *Model II* can use the data of T_0 obtained using *Model I* directly.

However, with the pump rate's increase, the available range of R with its coupling T_0 to achieve the pre-determined output energy and maintain the laser

system's working state to be the *quick-stable* state is limited, especially for the case when the output energy required is relatively small and the pump rate is high compared with the threshold pump rate. In Fig. 4.6 (a), when $E_a = 0.08$ and the laser system is pumped at $1.6 \times 10^3 s^{-1} cm^{-3}$, employing an output coupler with higher reflectivity and its coupling T_0 can maintain the *quick-stable* working state while keeping the required output energy parameter. According to Fig. 4.6 (d), the range of N_{wp} is from 25 to 33 for this case.

Figs. 4.6 (b) - 4.9 (b) plot the FWHM pulse width t_p as a function of the reflectivity of the output coupler R and different values of pump rate W_p . Several conclusions are similar to the discussions in Chapter 3: 1) the value of t_p is shorter with a higher output reflectivity for the same required output energy E_a ; and 2) when the output coupler is decided, t_p has a smaller value when the output energy E_a is required to be higher.

However, the values of the FWHM pulse width t_p for some output reflectivity R using *Model II* are greatly different from those from *Model I*, especially for the case when the output reflectivity is low. As shown in Fig. 4.6 (b), when $E_a = 0.08$ and $R = 50\%$, t_p is $32ns$ for *Model II* when the laser system is pumped by W_p is $1 \times 10^3 s^{-1} cm^{-3}$; the value of t_p is $42ns$ using *Model I*. Here, the biggest difference between the two cases is nearly $10ns$, while the curve for the case when W_p is $1.2 \times 10^3 s^{-1} cm^{-3}$ approaches the plot for the case that W_p is $1 \times 10^3 s^{-1} cm^{-3}$ in *Model II*. It is also observed in Fig. 4.6 (b) that the difference between *Model I* and *Model II* reduces as R increases. The same phenomenon is shown in Figs. 4.7 (b) - 4.9 (b) as the output energy parameter is 0.1, 0.3 and 0.5, though it is not so obvious for the case when E_a is 0.5.

Figs. 4.11 (b) - 4.14 (b) show that the curves of the FWHM pulse width obtained using other high pump rates ($1.2 \times 10^3 s^{-1} cm^{-3}$ and $1.6 \times 10^3 s^{-1} cm^{-3}$) using *Model II* are very close to the curve obtained using a pump rate of $1 \times 10^3 s^{-1} cm^{-3}$ (the difference even can be ignored in the figures), which results in the differences between the curves for different pump rates, using *Model II*, being much smaller than the difference between the data obtained from different models (*Model I* and *Model II*). If the figures are magnified, it can be observed that the FWHM pulse width from the higher pump rate is shorter than one from the lower pump rate.

The conclusions that can be obtained from Figs. 4.6 (b) - 4.9 (b) are: 1) as the output reflectivity is low, the corresponding FWHM pulse width t_p is big for both *Model I* and *Model II*, but the differences in the values of t_p for a selected R , between the two models are huge; 2) as the output energy is decided, for t_p , the difference between the two models is reduced by using a high output reflectivity; 3) for a relative high output energy, the difference for t_p between the two models is diminished even when the output reflectivity is low; and 4) when the output reflectivity is decided, in *Model II* the FWHM pulse width obtained using a higher pump rate is shorter than the one obtained using a low pump rate.

For this passively Q -switched Yb:YAG laser, when t_p obtained using *Model I* is bigger than $15ns$, the value of the FWHM pulse width t_p has to be calculated using *Model II*. When $t_p < 15ns$, *Model II* can be simplified to *Model I*.

Figs. 4.6 (c) - 4.9 (c) plot the peak power parameter P_a against R for the different pump rates and different output energy parameter. The differences between *Model I* and *Model II* are especially large when both the reflectivity of an output coupler and the output energy are lower.

Figs. 4.6 (d) - 4.9 (d) plot the ratio of the current pump rate and the threshold pump rate N_{wp} against R . It is noted that: 1) for a same output reflectivity, the threshold pump rate W_{p_th} needs to be a high value to support a high output energy parameter E_a , and 2) for a pre-determined E_a , the threshold pump rate W_{p_th} increases with output reflectivity R at first, then reaches its peak point, after that it decreases. The operating mechanics of the passive Q -switch results in the high threshold pump rate for a high output energy parameter. To provide more energy output, there should be more energy stored in the gain medium, before absorber bleaching, which requires a high pump power when the initial loss of the laser cavity is high as in this case. The variation of the absorber initial transmission T_0 with increasing R , is a gentle decrease at first, then a sharp decrease, resulting in the increase-peak-decrease process of the threshold pump rate.

Fig. 4.6 (d) shows that the laser system can only maintain the *quick-stable* state with a higher R as W_p is $1.6 \times 10^3 s^{-1} cm^{-3}$ (N_{wp} is higher than 25 at this point). This shows that it is easy for a laser system with a higher output reflectivity to stay in the *quick-stable* state.

As shown in Figs. 4.6 - 4.9, when a pair of R and T_0 can satisfy a laser system working in the *quick-stable* state, the following points of *Model II* are the same as for *Model I*, given in Chapter 3: 1) to keep the value of a pre-determined E_a , the coupling T_0 for a selected R decreases with R 's increase; 2) for a selected E_a , the laser system with a higher R has a shorter FWHM pulse width t_p ; 3) for a pre-determined R , a laser system which is required to have a higher output energy E_a will have a shorter FWHM pulse width t_p , but the coupling absorber has a lower initial transmission T_0 .

However, when the pump rate is relatively high and the output energy is low, the available range of R is limited more by the pump rate. Normally, a higher output reflectivity has a wider range of pump rates.

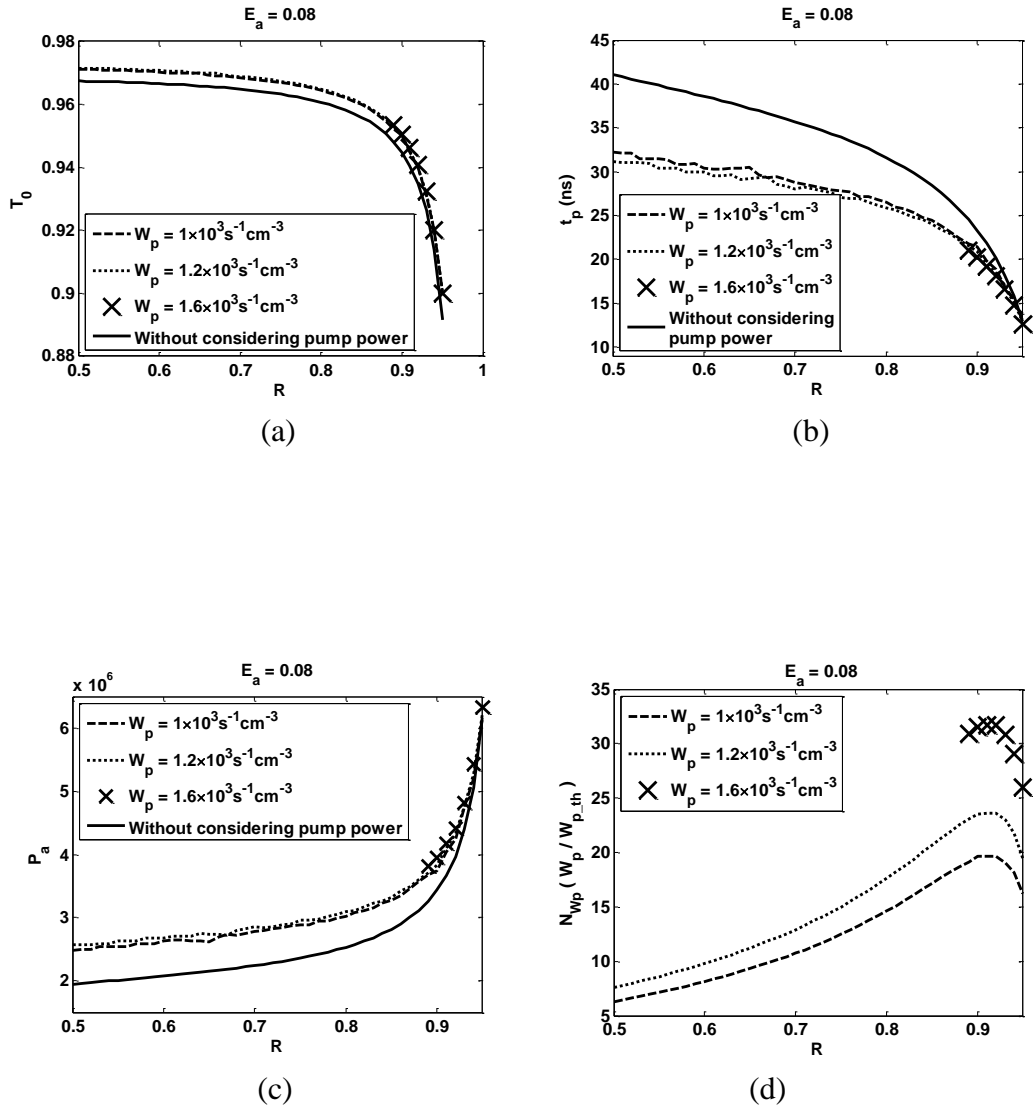


Figure 4.6 The coupling parameter T_0 (a) of R to keep $E_a = 0.08$, with t_p (b), P_a (c) and N_{Wp} (d) when $W_p = 1 \times 10^3 \text{ s}^{-1} \text{ cm}^{-3}$, $1.2 \times 10^3 \text{ s}^{-1} \text{ cm}^{-3}$ and $1.6 \times 10^3 \text{ s}^{-1} \text{ cm}^{-3}$

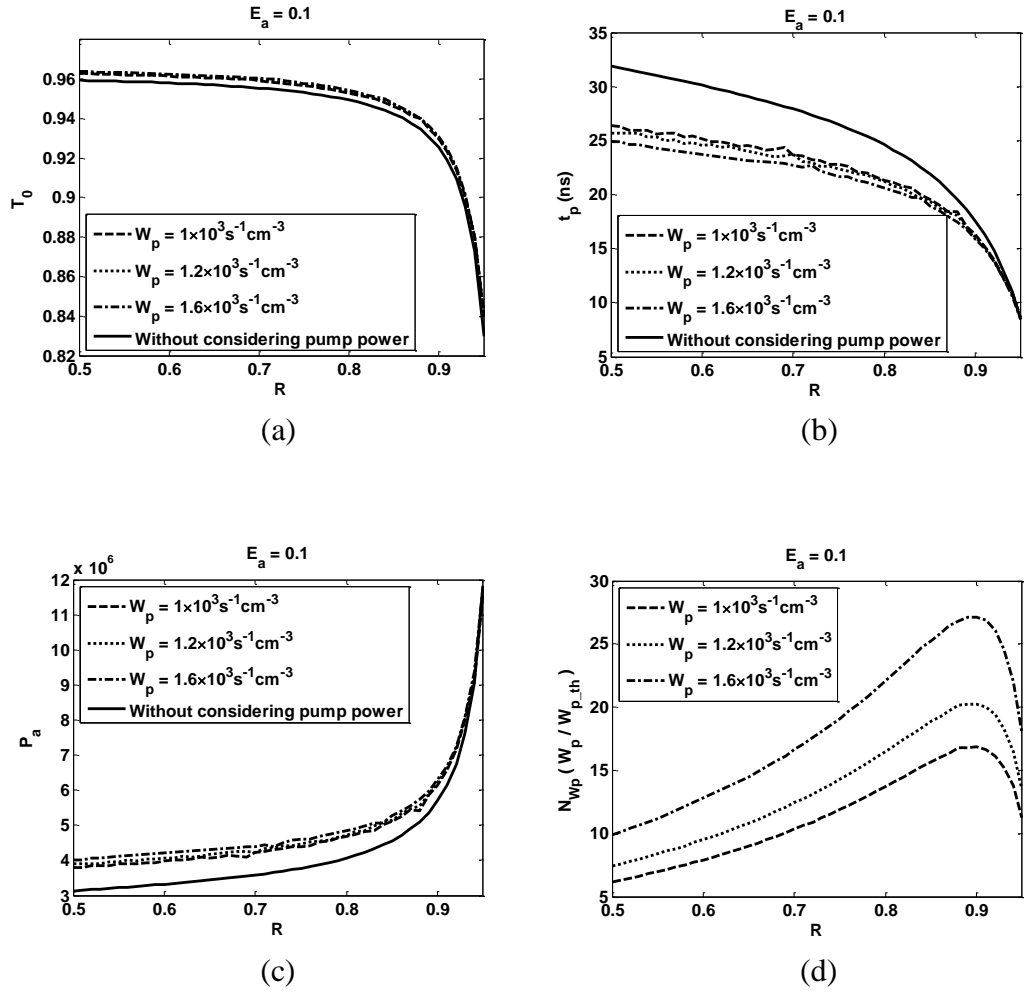
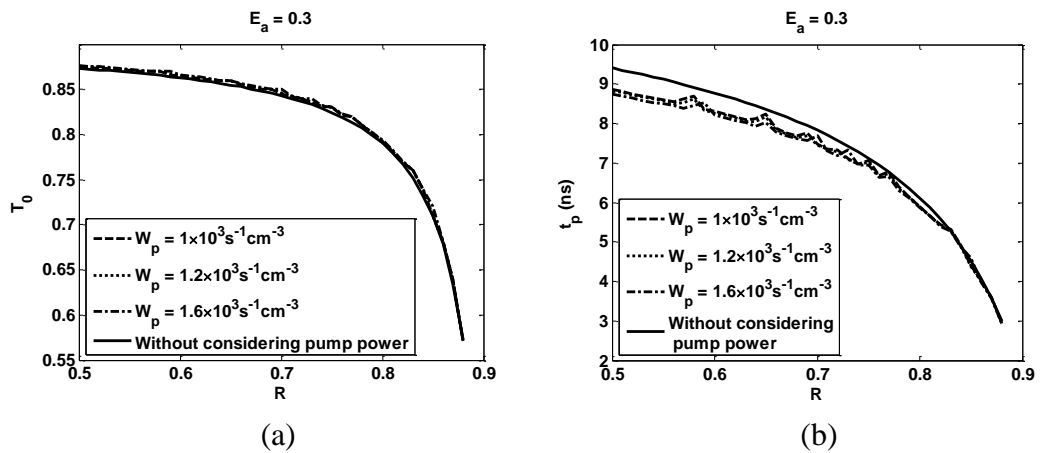


Figure 4.7 The coupling parameter T_0 (a) of R to keep $E_a = 0.1$, with t_p (b), P_a (c) and N_{wp} (d) as $W_p = 1 \times 10^3 \text{ s}^{-1} \text{ cm}^{-3}$, $1.2 \times 10^3 \text{ s}^{-1} \text{ cm}^{-3}$ and $1.6 \times 10^3 \text{ s}^{-1} \text{ cm}^{-3}$



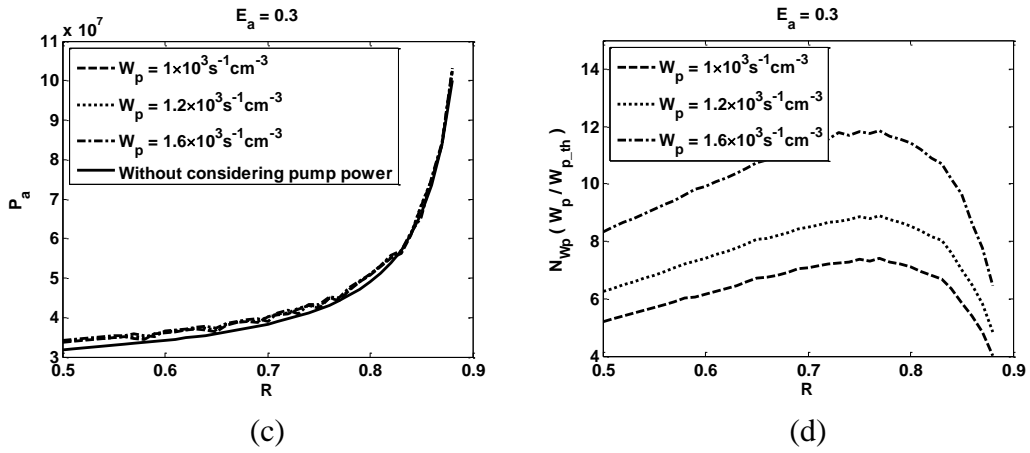


Figure 4.8 The coupling parameter T_0 (a) of R to keep $E_a = 0.3$, with t_p (b), P_a (c) and N_{Wp} (d) as $W_p = 1 \times 10^3 \text{ s}^{-1} \text{ cm}^{-3}$, $1.2 \times 10^3 \text{ s}^{-1} \text{ cm}^{-3}$ and $1.6 \times 10^3 \text{ s}^{-1} \text{ cm}^{-3}$

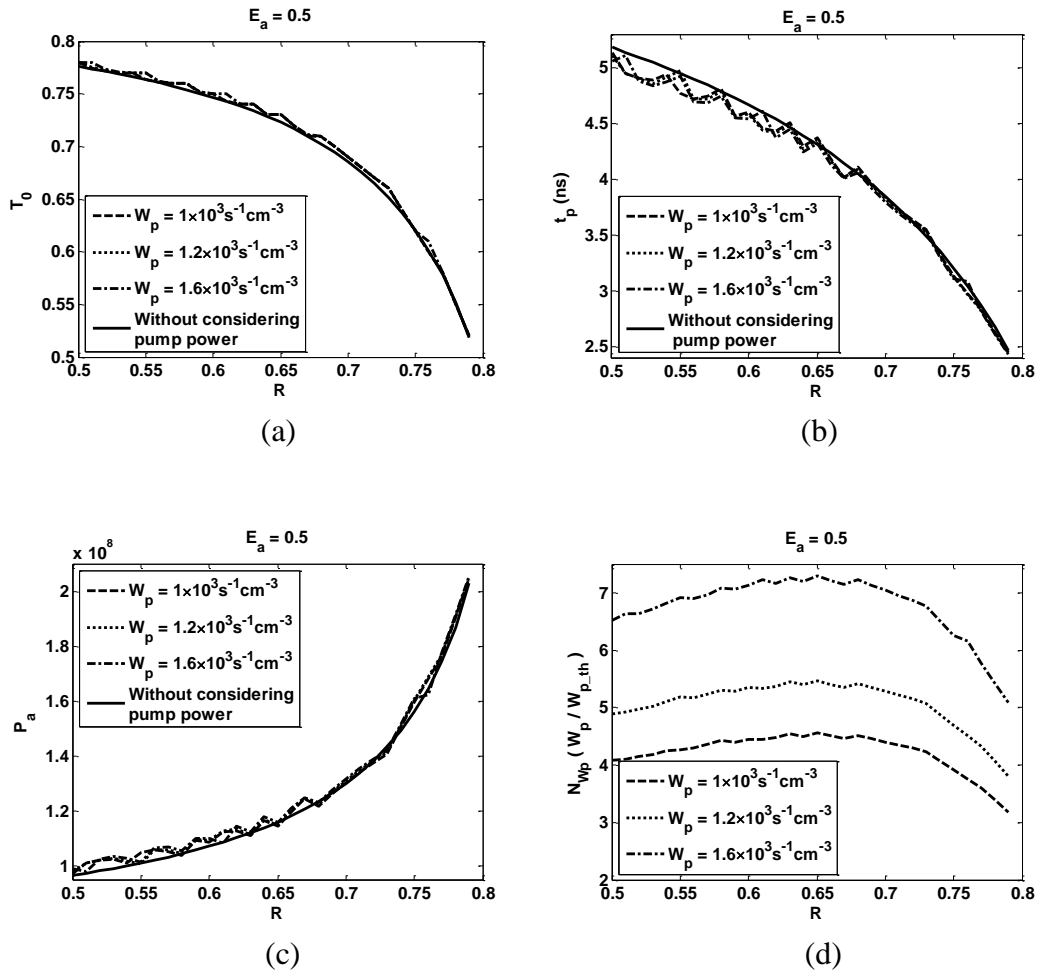
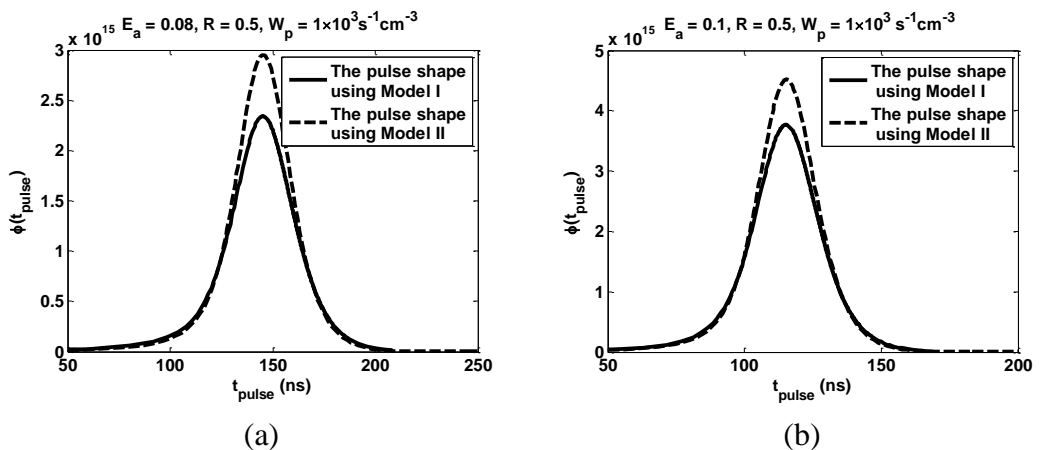


Figure 4.9 The coupling parameter T_0 (a) of R to keep $E_a = 0.5$, with t_p (b), P_a (c) and N_{Wp} (d) as $W_p = 1 \times 10^3 \text{ s}^{-1} \text{ cm}^{-3}$, $1.2 \times 10^3 \text{ s}^{-1} \text{ cm}^{-3}$ and $1.6 \times 10^3 \text{ s}^{-1} \text{ cm}^{-3}$

As shown in Figs. 4.6 - 4.9, when the output reflectivity R is selected to be at the minimum value in the figure, the data of the FWHM pulse duration t_p from *Model II* has the greatest difference from the simulation results using *Model I*. Hence, as R is at the smallest available value, the data of the laser output parameters demonstrate the effect of the pump rate most obviously. Here, the distributions of the average photon density in the laser cavity are plotted against the pulse time $\phi(t_{pulse})$ for different values of the output energy parameter ($E_a = 0.08, 0.1, 0.3$ and 0.5) when the output reflectivity R is 50% and $W_p = 1 \times 10^3 \text{ s}^{-1} \text{ cm}^{-3}$ are plotted in Fig. 4.10. In the figures, the curves of $\phi(t_{pulse})$ using both *Model I* and *Model II* are plotted to demonstrate the effect of the pump rate on $\phi(t_{pulse})$. It has been noted that the values of the FWHM pulse duration for different pump rates for a selected output reflectivity R are close to each other.

Fig. 4.10 shows that the maximum average photon density in the laser cavity using *Model II* is larger than that from *Model I*. The maximum value of the average photon density from both *Model I* and *Model II* monotonically increases with increasing output energy parameter, which leads to the corresponding FWHM pulse width being shortened. For different output energy parameter, the shapes of the laser pulse from *Model I* and *Model II* are similar, and the difference between the pulse shapes from *Model I* and *Model II* reduces when the output energy parameter has a relatively high value.



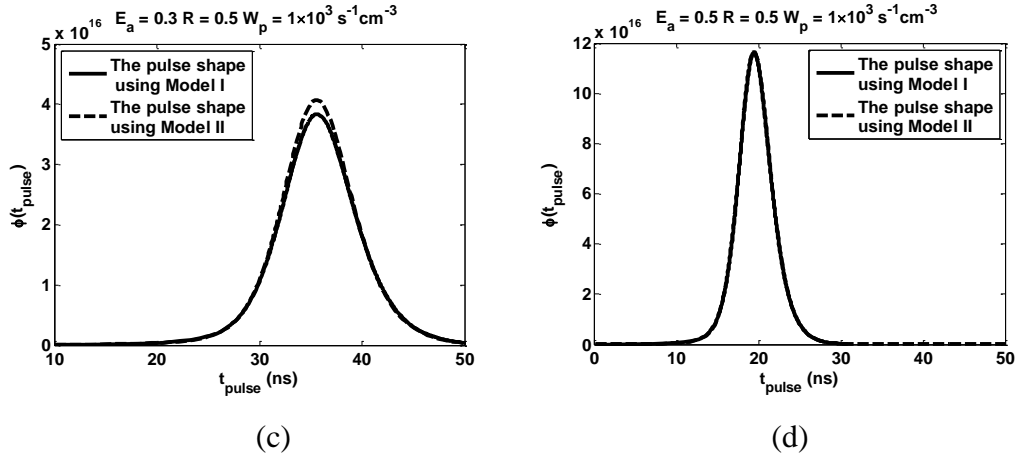


Figure 4.10 The distributions of the average photon density in the laser cavity during the pulse time using *Model I* and *Model II* as $R = 50\%$ and $W_p = 1 \times 10^3 \text{ s}^{-1} \text{ cm}^{-3}$ for different values of E_a , (a) $E_a = 0.08$, (b) $E_a = 0.1$, (c) $E_a = 0.3$, and (d) $E_a = 0.5$

To show the interaction of the pump rate and the FWHM pulse width t_p , Figs. 4.11 - 4.14 show the cases that when the laser system is pumped by the pump rates which are higher than the pump rates used in Figs. 4.6 - 4.9, the parameters T_0 , t_p , P_a and N_{wp} are plotted as a function of R and different values of the output energy parameter E_a . Here, the pump rate $W_p = 2 \times 10^3 \text{ s}^{-1} \text{ cm}^{-3}$, $4 \times 10^3 \text{ s}^{-1} \text{ cm}^{-3}$ and $8 \times 10^3 \text{ s}^{-1} \text{ cm}^{-3}$, are used respectively. However, as E_a is required to be 0.08 and 0.1, the laser system pumped by a pump rate $8 \times 10^3 \text{ s}^{-1} \text{ cm}^{-3}$ doesn't achieve the *quick-stable* working state when R changes from 50% to 95%. Hence, Figs. 4.11 and 4.12 only show the results obtained for $W_p = 2 \times 10^3 \text{ s}^{-1} \text{ cm}^{-3}$ and $4 \times 10^3 \text{ s}^{-1} \text{ cm}^{-3}$, respectively. Observing Figs. 4.11 - 4.14, the same conclusion can be drawn as in Figs. 4.6 - 4.9 that is for this continuously pump Cr:YAG passively Q -switched Yb:YAG laser, when the FWHM pulse width t_p obtained using *Model I* is shorter than 15ns, the differences between *Model I* and *Model II* can be neglected. A proper pair of R and T_0 which give a shorter FWHM pulse width t_p and maintain a pre-

determined output energy E_a can use the results obtained in *Model I*. When t_p is much longer than $15ns$, the pump rate must be considered in the model.

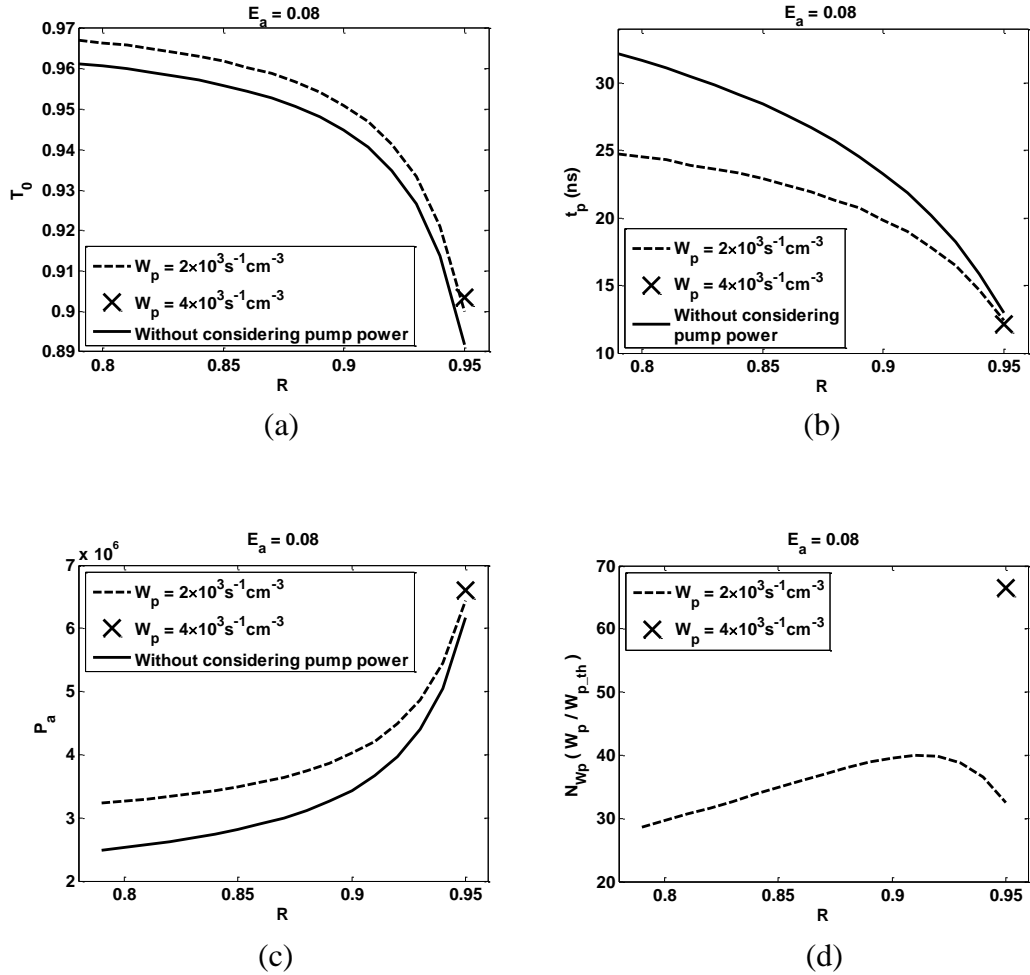
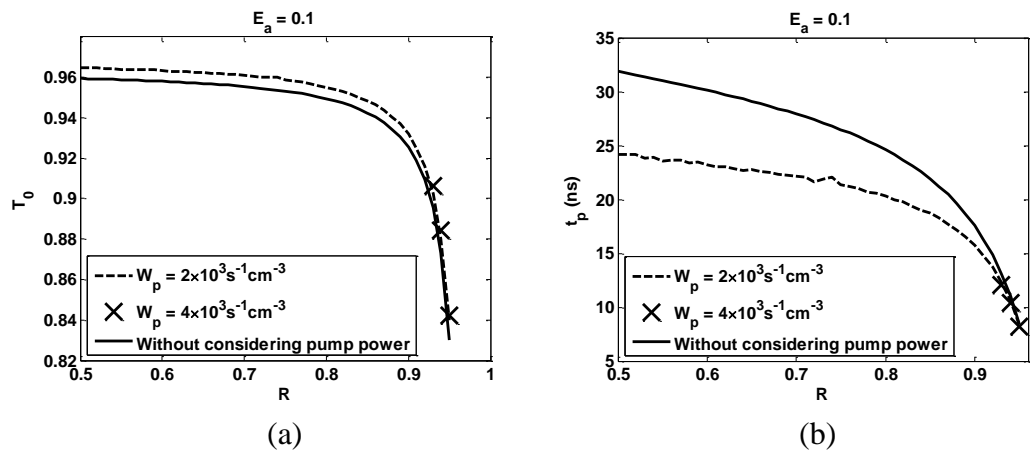


Figure 4.11 The coupling parameter T_0 (a) of R to keep $E_a = 0.08$, with t_p (b), P_a (c) and N_{wp} (d) as $W_p = 2 \times 10^3 \text{ s}^{-1} \text{ cm}^{-3}$ and $4 \times 10^3 \text{ s}^{-1} \text{ cm}^{-3}$



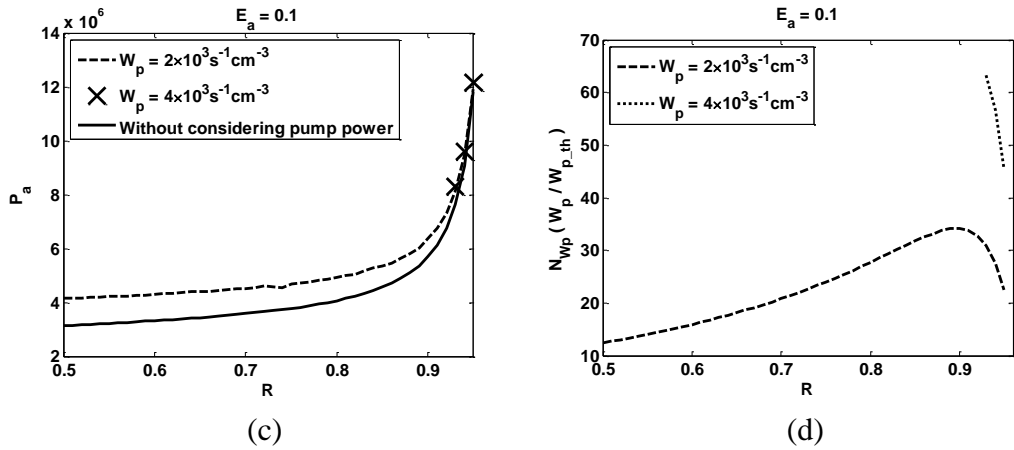


Figure 4.12 The coupling parameter T_0 (a) of R to keep $E_a = 0.1$, with t_p (b), P_a (c) and N_{wp} (d) as $W_p = 2 \times 10^3 s^{-1} cm^{-3}$ and $4 \times 10^3 s^{-1} cm^{-3}$

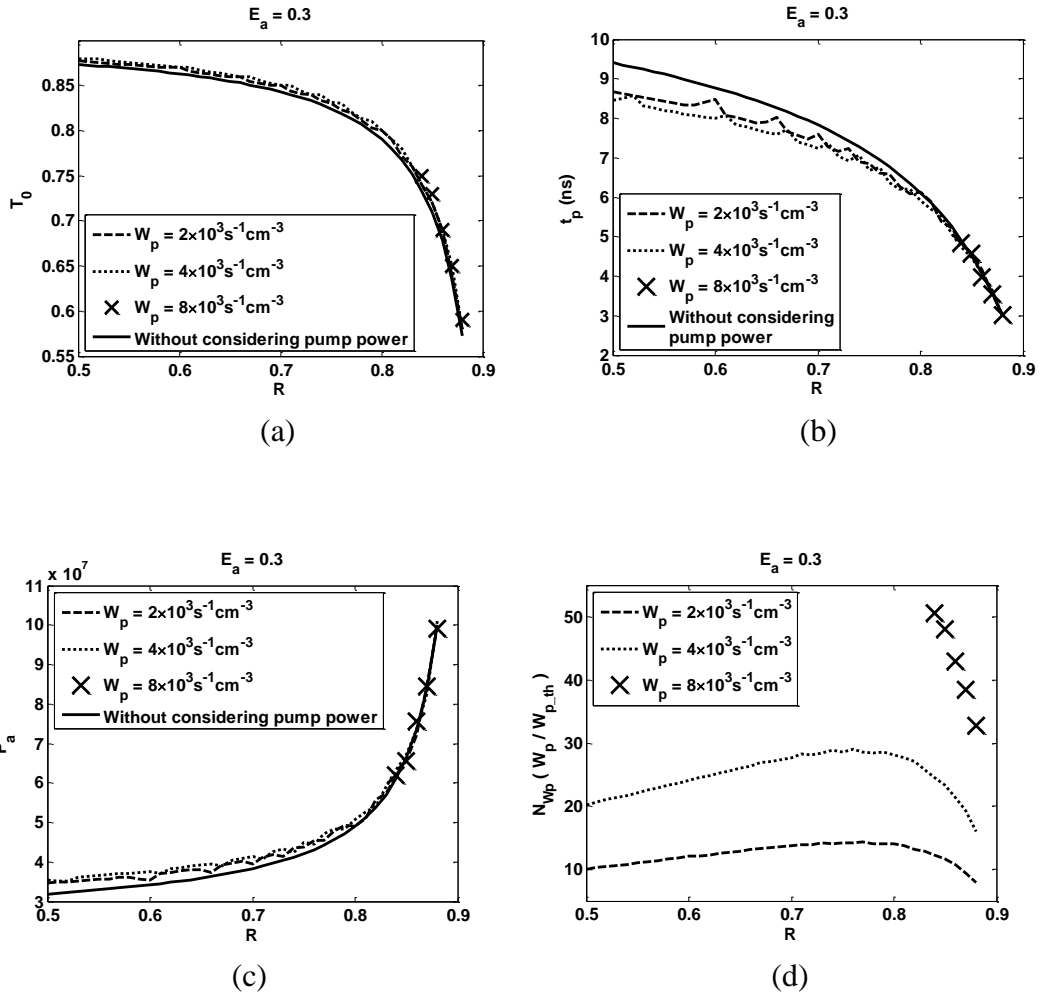


Figure 4.13 The coupling parameter T_0 (a) of R to keep $E_a = 0.3$, with t_p (b), P_a (c) and N_{wp} (d) as $W_p = 2 \times 10^3 s^{-1} cm^{-3}$, $4 \times 10^3 s^{-1} cm^{-3}$ and $8 \times 10^3 s^{-1} cm^{-3}$

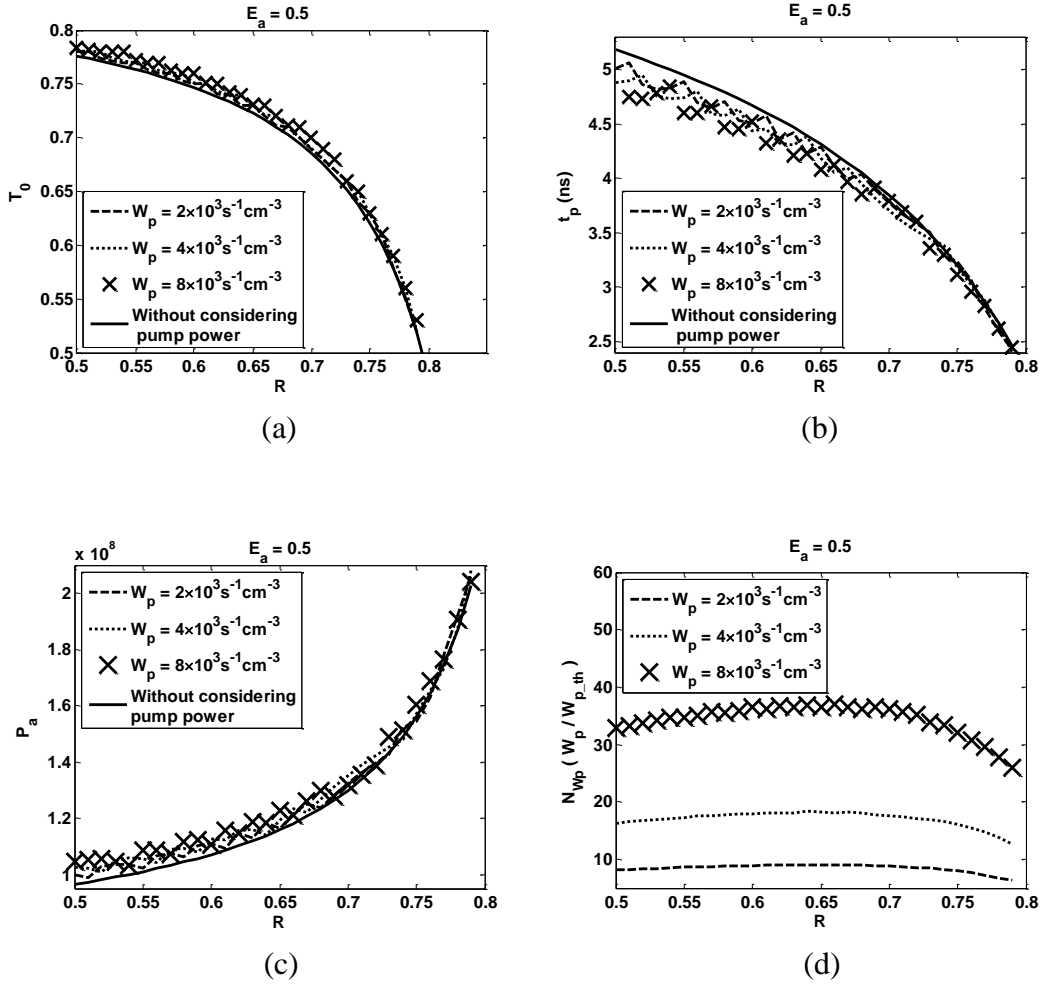


Figure 4.14 The coupling parameter T_0 (a) of R to keep $E_a = 0.5$, with t_p (b), P_a (c) and N_{wp} (d) as $W_p = 2 \times 10^3 \text{ s}^{-1} \text{ cm}^{-3}$, $4 \times 10^3 \text{ s}^{-1} \text{ cm}^{-3}$ and $8 \times 10^3 \text{ s}^{-1} \text{ cm}^{-3}$

The pulse shapes of Figs. 4.11 - 4.14, as the output reflectivity is at the minimum value and $W_p = 2 \times 10^3 \text{ s}^{-1} \text{ cm}^{-3}$, are plotted in Fig. 4.15, where the curves are from both *Model I* and *Model II*. As shown in Fig. 4.11, when the output energy parameter is set to be 0.08, the output reflectivity has to be bigger than 79% to maintain the laser system to be in the *quick-stable* state. Hence, Fig. 4.15 (a) plots the pulse shape for $R = 79\%$ and $E_a = 0.08$, and the pulse shapes for $R = 50\%$ for the cases when $E_a = 0.1, 0.3$, and 0.5 are shown in Figs. 4.15 (b) - (d).

Fig. 4.15 (a) shows that the pump rate limits the available range of the output reflectivity which keeps the laser system working in the *quick-stable* state. Comparing Fig. 4.15 (b) with Fig. 4.10 (b), the maximum value of the average photon density in the laser cavity is much higher for $W_p = 2 \times 10^3 \text{ s}^{-1} \text{ cm}^{-3}$ than for $W_p = 1 \times 10^3 \text{ s}^{-1} \text{ cm}^{-3}$. It demonstrates that the maximum average photon density increases as the pump rate increases for the same output reflectivity and same output energy when the laser system is in the quick-stable state. Figs. 4.15 (c) and (d) have the same simulation results as Fig. 4.15 (b).

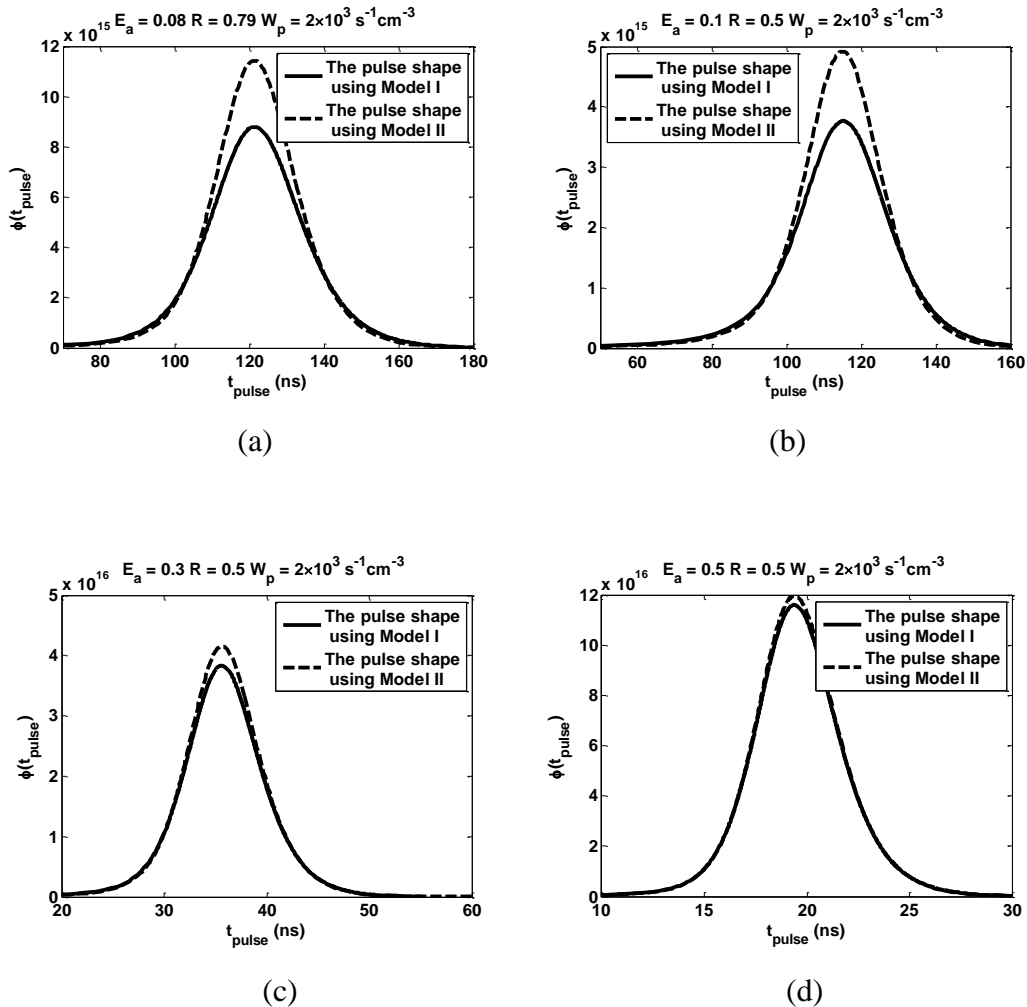


Figure 4.15 The distributions of the average photon density in the laser cavity during the pulse time using *Model I* and *Model II* as R is at the minimum value in Figs. 4.11 - 4.14 and $W_p = 2 \times 10^3 \text{ s}^{-1} \text{ cm}^{-3}$ for different values of E_a , (a) $E_a = 0.08$, (b) $E_a = 0.1$, (c) $E_a = 0.3$, and (d) $E_a = 0.5$

4.6 The pump rate and the gain medium

To analyze the effect of the gain medium material on the output parameters (such as the FWHM pulse width t_p) and the selection of output reflectivity and initial transmission pair for *Model II*, the Yb:YAG material is replaced by a Nd:YAG crystal keeping all other parameters the same. In Table 4.5, all of the parameters of the Nd:YAG material are listed.

Table 4.5 Material properties of Nd:YAG

Parameters	Nd:YAG
Laser wavelength	1060nm
Upper-state lifetime (τ_{21})	230 μ s
Emission cross section (σ)	$2.8 \times 10^{-19} \text{ cm}^2$
Refractive index	1.82
Effect of level degeneracies (γ)	1

Figs. 4.16 - 4.19 plot the parameters T_0 , t_p , P_a and N_{wp} as a function of R for different pump rates W_p , when the gain medium is Nd:YAG, and the laser system has different output energies (E_a is 0.08, 0.1, 0.3 and 0.5, respectively). To show the effect of the pump rate, the simulation results obtained using both *Model I* and *Model II* are plotted in the figures.

Compared with Figs. 4.6 - 4.9 and 4.11 - 4.14, it is noted that the following points for the Nd:YAG material laser system are the same as those for the Yb:YAG material laser system:

- 1) when the pump rate is low and the build-up time of Q -switching is long, the pump rate must be considered in the model since the difference between the FWHM pulse width from *Model I* and *Model II* cannot be ignored;
- 2) the interaction between the pump rate and the FWHM pulse width for the Nd:YAG laser is the same as for the Yb:YAG laser shown in Section 4.5; the

interaction is that when the FWHM pulse width is longer (namely that the build-up time of the Q-switch is long), the pump rate affects the output parameters of the laser system more, and the high pump rate will shorten the FWHM pulse width, but the shorter FWHM pulse width will reduce the effect of the pump rate on the output parameters of the laser system;

3) the coupling initial transmission of a selected output reflectivity decreases with the output reflectivity increase in both *Model I* and *Model II*; the values of the initial transmission in *Model II* approach those using *Model I*, and as the output reflectivity is decided, the differences between the initial transmissions using *Model I* and *Model II* diminish with the output energy parameter increase;

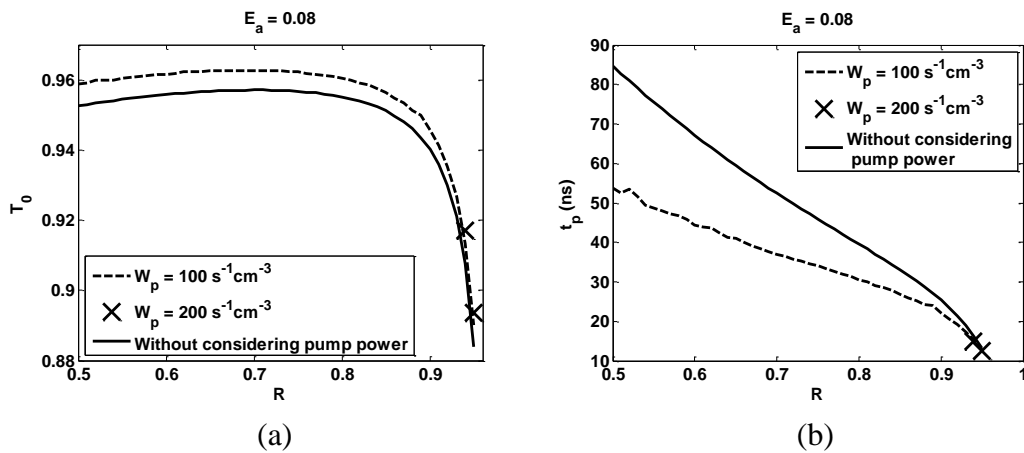
4) when the output reflectivity R is close to its highest value, the differences for the FWHM pulse width between *Model I* and *Model II* are negligible; or when FWHM pulse width is smaller than $15ns$, the differences between two models are negligible;

5) the high pump rate results in the short FWHM pulse width as the output reflectivity and the output energy are decided, but when the output reflectivity is low, the differences between different pump rates are negligible compared with the difference between *Model I* and *Model II*.

However, there are still several differences resulting from the different gain material. When the material of the absorber doesn't change, the differences between the two gain mediums can be represented by a parameter α which is demonstrated in Chapter 3. When the gain medium is Yb:YAG, α is 175; compared with α equals 25 for Nd:YAG. In Chapter 3, it is shown that 1) as the output energy parameter and the output reflectivity are pre-determined, the corresponding FWHM pulse width of the laser system having a bigger α is shorter than the laser system with a smaller α ; and 2) as the output energy parameter is pre-decided, the FWHM pulse widths for any value of α approach each other as the highest available output reflectivity is used. Here, there are the same conclusions that were obtained when the simulation results are from *Model II*. For a same output coupler and a same output energy parameter, the FWHM

pulse width t_p given by Yb:YAG laser is shorter than that produced by Nd:YAG laser. For example, when $E_a = 0.08$ and $R = 50\%$, t_p for the Nd:YAG laser pumped by $W_p = 100s^{-1}cm^{-3}$ is $53ns$ while $t_p = 32ns$ for the Yb:YAG laser system pumped by $W_p = 1000s^{-1}cm^{-3}$; it is noted that when the output reflectivity and the output energy parameter are decided, the maximum difference between the FWHM pulse durations for the Nd:YAG laser system using different pump rates are much smaller than between the Nd:YAG laser system and the Yb:YAG laser system, hence the simulation result from one pump rate is enough to represent the performance of the laser system. When $E_a = 0.08$ and $R = 95\%$, both of the coupling FWHM pulse widths for the Yb:YAG laser and the Nd:YAG laser are close to $12ns$.

Comparing with a Yb:YAG laser, the available range of R to keep a Nd:YAG laser system working in the *quick-stable state* decreases. As shown in Fig. 4.16 (d), when the output energy is required to be 0.08 and the pump rate is $200s^{-1}cm^{-3}$ (the biggest value of N_{wp} is 12), the available range of R is from 90% to 95%. But for the Yb:YAG laser, when the maximum value of N_{wp} is around 25, R can still be selected from 50% to 95%.



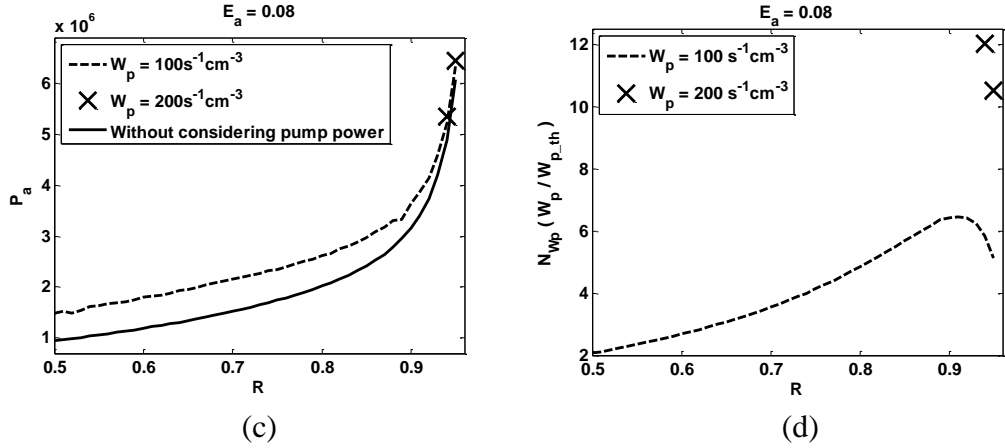


Figure 4.16 For a Nd:YAG laser system, the coupling parameter T_0 (a) of R to keep $E_a = 0.08$, with t_p (b), P_a (c) and N_{wp} (d) as $W_p = 100s^{-1}cm^{-3}$ and $200s^{-1}cm^{-3}$

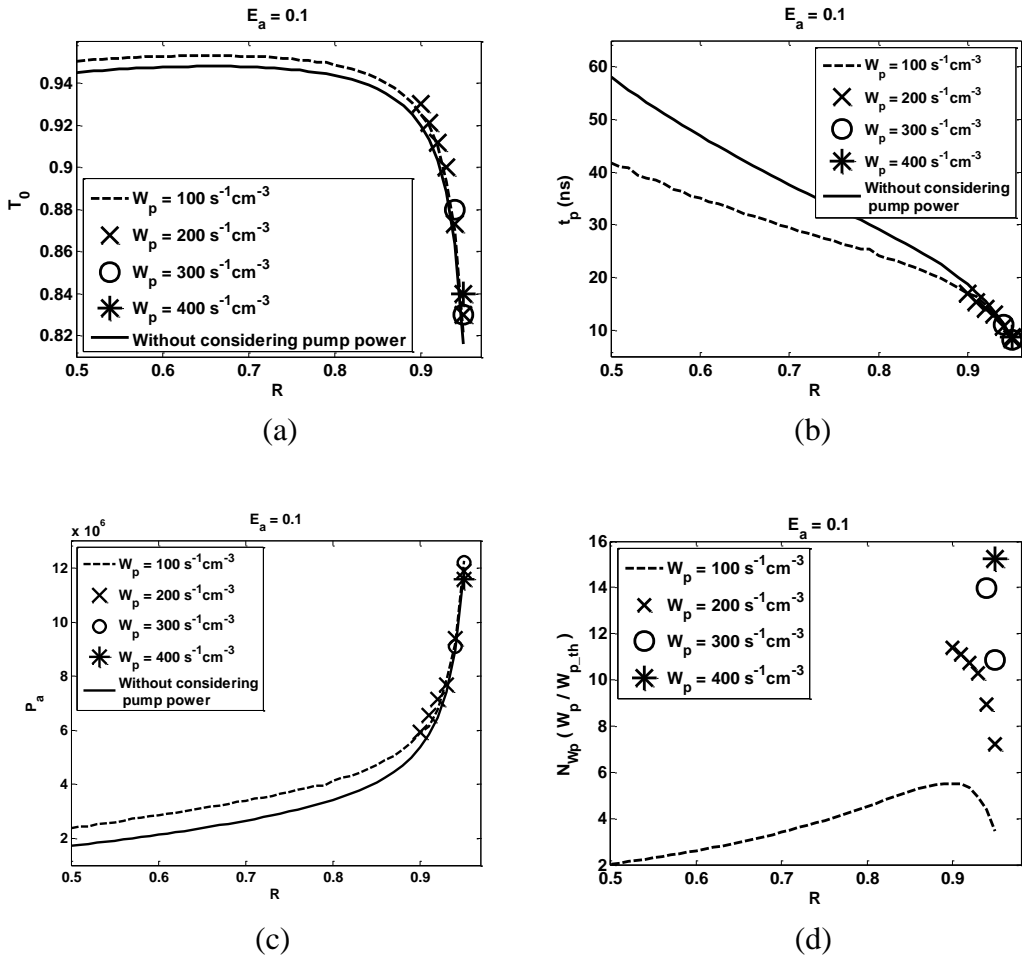


Figure 4.17 For a Nd:YAG laser system, the coupling parameter T_0 (a) of R to keep $E_a = 0.1$, with t_p (b), P_a (c) and N_{wp} (d) as $W_p = 100s^{-1}cm^{-3}$, $200s^{-1}cm^{-3}$, $300s^{-1}cm^{-3}$ and $400s^{-1}cm^{-3}$

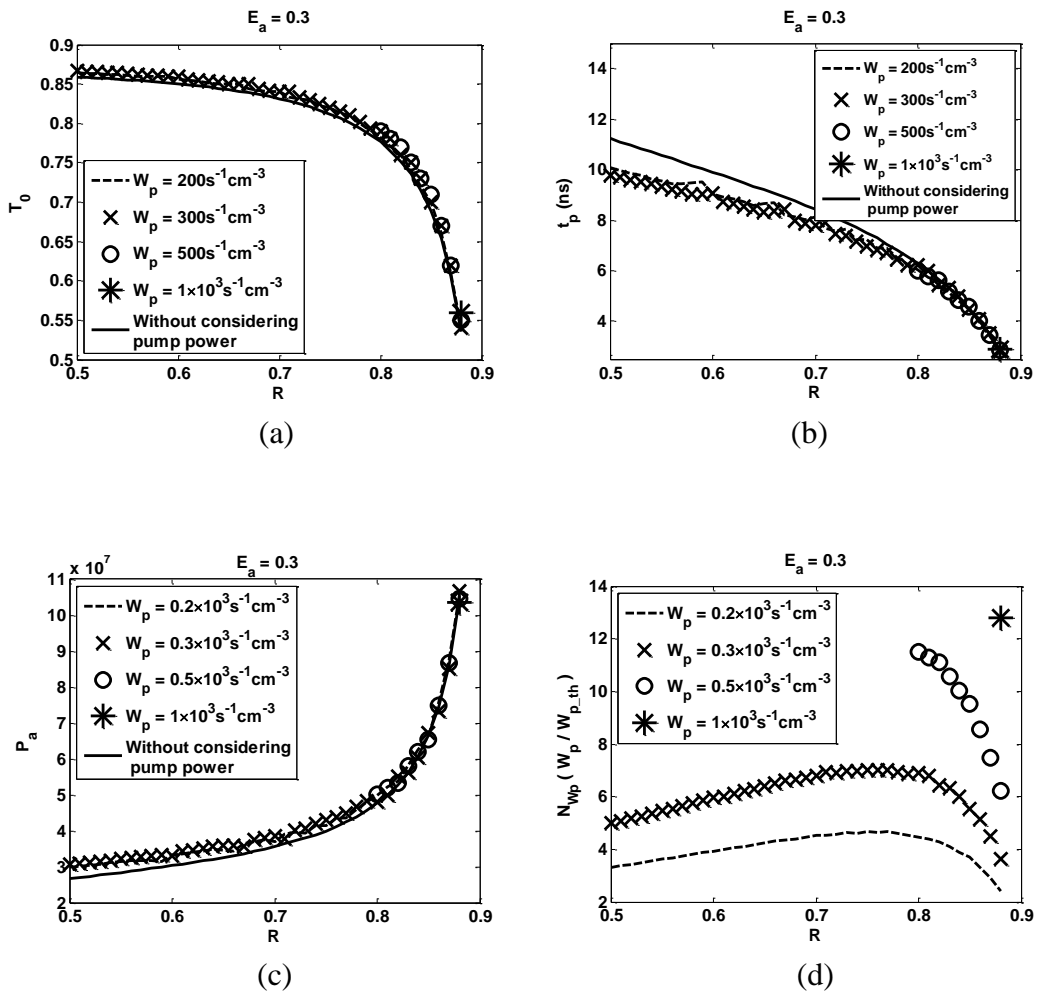
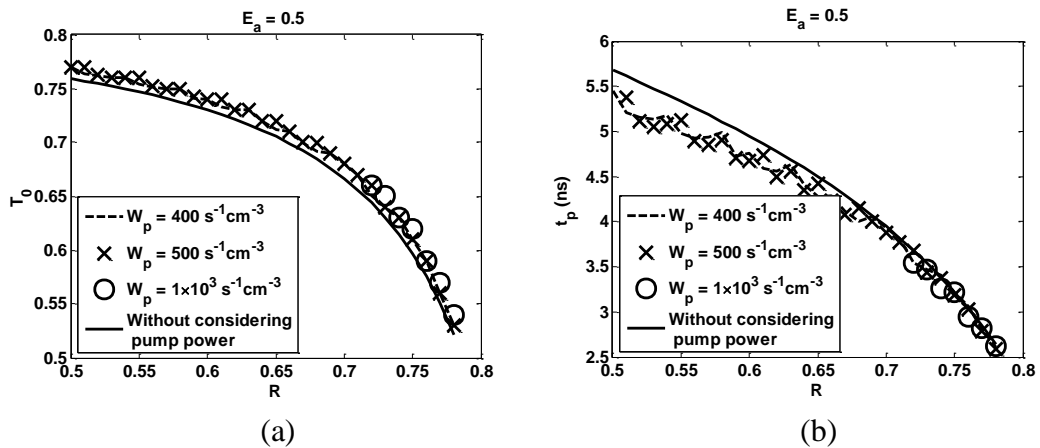


Figure 4.18 For a Nd:YAG laser system, the coupling parameter T_0 (a) of R to keep $E_a = 0.3$, with t_p (b), P_a (c) and N_{wp} (d) as $W_p = 200 \text{ s}^{-1} \text{ cm}^{-3}$, $300 \text{ s}^{-1} \text{ cm}^{-3}$, $500 \text{ s}^{-1} \text{ cm}^{-3}$ and $1000 \text{ s}^{-1} \text{ cm}^{-3}$



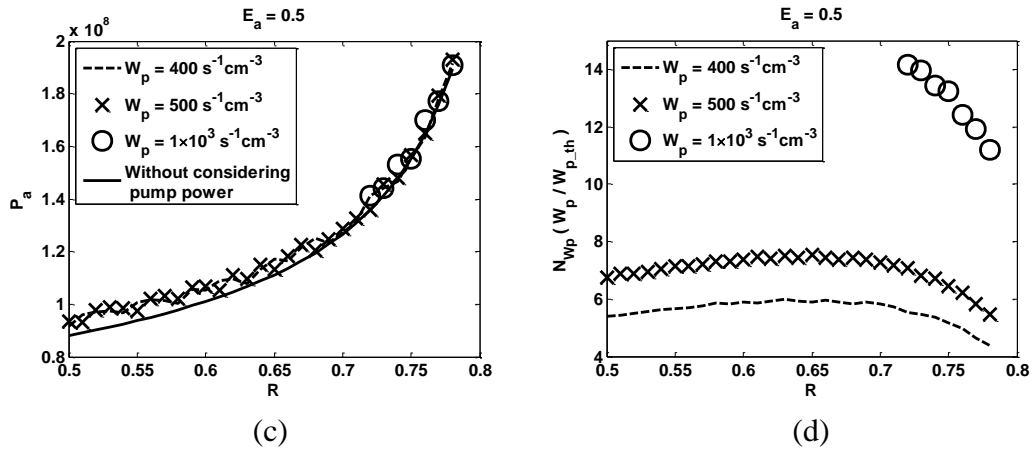
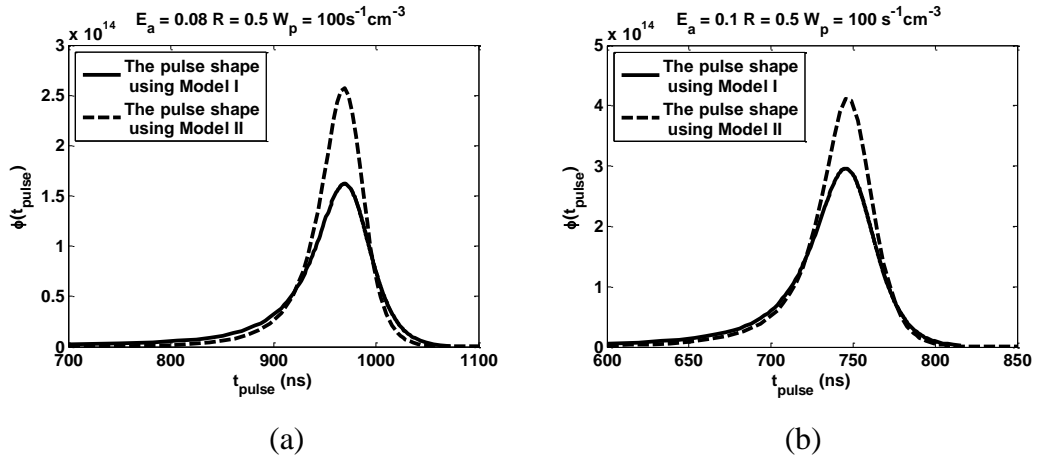


Figure 4.19 For a Nd:YAG laser system, the coupling parameter T_0 (a) of R to keep $E_a = 0.5$, with t_p (b), P_a (c) and N_{wp} (d) as $W_p = 400s^{-1}cm^{-3}$, $500s^{-1}cm^{-3}$ and $1000s^{-1}cm^{-3}$

The output pulse shapes of the laser system pumped by different pump rates when $R = 50\%$ and $E_a = 0.08, 0.1, 0.3$ and 0.5 are plotted in Fig. 4.20.



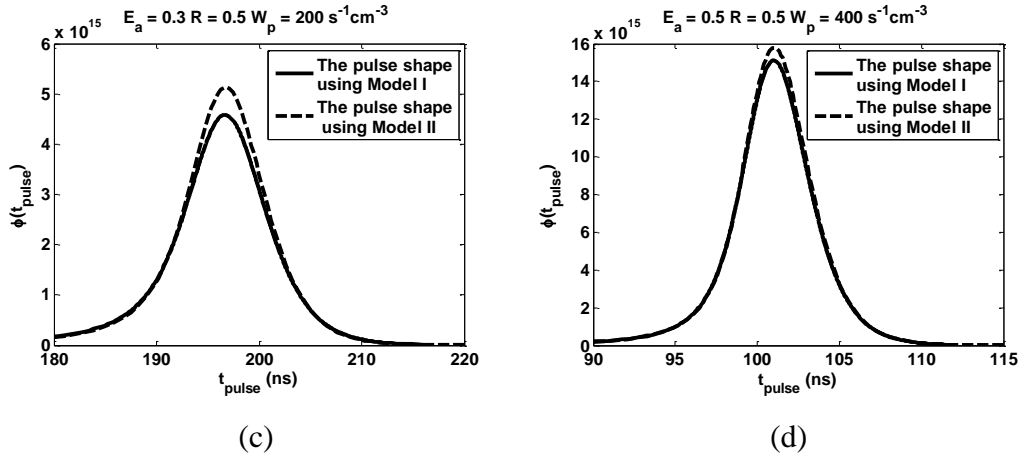


Figure 4.20 The distributions of the average photon density in the laser cavity during the pulse time using *Model I* and *Model II* as $R = 50\%$ for different pump rate and different E_a , (a) $E_a = 0.08$ and $W_p = 100 \text{ s}^{-1} \text{ cm}^{-3}$, (b) $E_a = 0.1$ and $W_p = 100 \text{ s}^{-1} \text{ cm}^{-3}$, (c) $E_a = 0.3$ and $W_p = 200 \text{ s}^{-1} \text{ cm}^{-3}$, (d) $E_a = 0.5$ and $W_p = 400 \text{ s}^{-1} \text{ cm}^{-3}$

4.6 Conclusions

In this chapter, *Model II* is set up to predict the FWHM pulse width for the situations where the build-up time of Q -switching is long, and the repetition rate of the laser system is low enough for the atoms in the excited state of an absorber to return to the ground level for the beginning of the next Q -switched pulse. In *Model II*, the output of a laser system becomes stable after the first few pumping and lasing cycles; this situation is named the *quick-stable* condition. The pump rate must be included in the lasing stage of *Model II*, which results from the long build-up time of the Q -switching. Hence, the mathematical representations of several parameters, such as the average photon density in the laser cavity, the inversion population density of the gain medium, and the population density at the absorber's ground level, cannot be derived from the laser rate equations. In this case, the characteristics of the passively Q -switched laser system are studied using the numerical results which are produced by applying the Runge-Kutta numerical method to solve the laser rate equations. In this chapter, the selection

of output coupler and absorber initial transmission pair and the output parameters of a continuously pumped Cr:YAG passively Q -switched Yb:YAG laser is studied. To show the effect of the gain medium, the Nd:YAG laser material is compared with the Yb:YAG laser.

By generalizing the simulation results of the Yb:YAG laser and the Nd:YAG laser, it is found that in *Model II* the values of R and its coupling T_0 to keep the required output energy for different pump rates are close to the data using *Model I*. It means the proper pair of R and T_0 can be obtained directly by the simplified model (*Model I*).

The changes of the FWHM pulse width when changing the output coupler or the output energy in *Model II* are similar to those predicted by *Model I*. However, the FWHM pulse width using *Model II* is significantly different from the value predicted using *Model I* when the output reflectivity is small. In *Model II*, the pulse width is affected by the pump rate, the high pump rate results in the shorter FWHM pulse width for a selected output reflectivity, but the variance is not huge. When t_p obtained using the simplified model (*Model I*) is greater than $15ns$, the difference between *Model I* and *Model II* is significant. To obtain a more accurate value of t_p , the model must include the pump rate. When the pulse width is less than $15ns$, the differences between two models are small.

The available range of R to keep the output of a laser system stable after the first few working cycles is determined by the magnitude of the pump rate. Normally, a laser system with a higher pump rate has a smaller available range of R . If an output coupler with higher reflectivity is employed, the output of a laser system even pumped by a higher pump rate still can be kept stable after the first few working cycles. A laser system with a gain medium leading to a higher α normally can deliver a stable output at the beginning of its operation with a higher pump rate than one having a lower α .

Chapter 5

**A Model for a Passively Q -Switched
Laser Considering the Recovery Time of
the Absorber**

5.1 Introduction

Model III is employed to show the effect of the absorber's recovery time on selecting an output coupler and absorber pair to control the pulse width when the pump rate is considered in the laser rate equations, and the output energy of the laser is pre-determined. This model handles the situations when: 1) the effect of the pump power is included in the laser rate equations during the lasing stage whatever the value of the build-up time of the Q -switched laser pulse is; and 2) the time interval between the end of the previous Q -switching and the beginning of the next Q -switching is relatively short compared with the spontaneous emission lifetimes of the upper level of the absorber. In this case, a fraction of the atoms excited to the absorber's upper level remains in the upper level, and the value of the initial transmission by the beginning of the next Q -switching is varied. Hence, the effect of the time interval (also called the recovery time of an absorber) is introduced into the model as one of the mechanisms affecting the output of the laser system.

A laser system has two working states: the pumping stage and the lasing stage. The two situations which *Model III* has to satisfy determine both the pumping stage and the lasing stage which decides the output of the laser system. In *Model III*, the study of the lasing stage is achieved by solving the laser rate equations using the Runge-Kutta method, and the operational performance of the pumping stage can be studied by the mathematical representations which are obtained by simplifying the laser rate equations.

Different pump powers were used to pump the laser system when selecting the output reflectivity and initial transmission pair to keep the pre-determined output energy and observe the data of the corresponding FWHM pulse duration. Simulation results of *Model III* are presented for a continuously pumped Cr:YAG passively Q -switched Yb:YAG laser. The effect of the recovery time of an absorber is shown by the comparison with the data obtained using *Model I*

(which doesn't consider the pump power and the recovery time of the absorber in the laser rate equations). Results using the Nd:YAG material in place of the Yb:YAG material in the laser system are used to show the effect of the gain medium. Concluding the simulation results of the Yb:YAG laser system and the Nd:YAG laser yields the general results concerning the influence of the recovery time of an absorber on the absorber initial transmission and the output parameters of a laser system.

5.2 Theoretical analysis

The laser rate equations are employed to set up *Model III* as in the previous chapters. Introducing the pump power and the excited state of an absorber, the expressions for the laser rate equations are the same as in Chapter 4:

$$\frac{d\phi}{dt} = \frac{\phi}{t_r} [2\sigma nl - 2\sigma_{gs} n_{gs} l_s - 2\sigma_{es} n_{es} l_s - \ln(\frac{1}{R}) - L] \quad (5.1a)$$

$$\frac{dn}{dt} = -\gamma\sigma c\phi n + W_p(n_{tot} - n) - \frac{n}{\tau_{21}} \quad (5.1b)$$

$$\frac{dn_{gs}}{dt} = -\gamma_s \sigma_{gs} c\phi n_{gs} + \frac{n_{s0} - n_{gs}}{\tau_s} \quad (5.1c)$$

$$n_{gs} + n_{es} = n_{s0} \quad (5.1d)$$

the definitions of all the parameters in Eq. 5.1 are the same as in Chapter 4.

According to the operating principle of a continuously pumped passively Q -switched laser system, the laser operation can be divided into two stages, the pumping stage and the lasing stage (Q -switch stage). The study in Chapter 4 focuses on a laser system delivering a quick-stable state (*Model II*). When working in the quick-stable state, most of the absorber's atoms excited to the excited state can return to the ground level at the beginning of each lasing stage, which results in the value of the initial transmission of absorber and the initial inversion population density of the gain medium at each lasing stage being nearly

the same as those in the first lasing stage. Hence, in *Model II* the pump rate only affects the laser output and the selection of proper output reflectivity and initial transmission at the lasing stage, the pumping stage isn't studied.

However, when the repetition rate of a laser system is quick enough, a large number of absorber's atoms excited to the excited state cannot return to the ground level during the pump time. This results in the initial transmission of an absorber at the beginning of the next working cycle not being the same as that in the previous cycle. The initial inversion population density of the gain medium will change as well. Because the initial inversion population density of the gain medium has a change, the laser system's output of each working cycle is different in this case. The working state of the laser system is unstable. Certainly, with the dynamic changes of both instantaneous initial transmission and initial conditions for each working cycle, the action and reaction between the initial transmission and initial conditions will reach equilibrium. Then the input parameters of the laser system at the beginning of each lasing stage are nearly the same, and the output of the laser system is the same as well, hence, the laser system is considered to be working in a stable state. Compared with *Model II*, the laser system in *Model III* spends much longer reaching the stable working state, the initial transmission and the initial inversion population density of the gain medium at the stable state are not the same as those at the beginning of the first working cycle. In Chapter 4, it is shown in Figs. 4.6 - 4.9 and 4.11 - 4.14 for the Yb:YAG laser that when the pump rate is relatively high and the output reflectivity is low, there are no output reflectivity and initial transmission pairs that will permit the laser system to work in the quick-stable state. Now, *Model III* can be employed to study the output of a laser system for this case.

In *Model III*, the time duration between the end of the previous pulse and the beginning of the current Q -switch affects the initial conditions of the gain medium, and for the absorber it is called the recovery time $t_{recovery}$. According to the analysis in the previous paragraph, the initial transmission will have different

values for the unstable working cycle. However, only two values are meaningful for the designer. One is the value presented before operation which is decided by the material and the doping percentage. This value is fixed and can be given by the producer. The other is the operating value of the absorber presented in the stable working state. It should be different from the initial given value and affected by the pump rate and the recovery time of the absorber. Hence, the value of the absorber initial transmission given by the producer is named as *the product initial transmission* of an absorber. The value of the initial transmission in the stable working state is called *the working initial transmission* of an absorber.

The previous analysis demonstrates the importance of the pumping stage in *Model III*. Now, at the pumping stage, the rate equations are:

$$\frac{dn}{dt} = W_p(n_{tot} - n) - \frac{n}{\tau_{21}} \quad (5.2a)$$

$$\frac{dn_{gs}}{dt} = \frac{n_{s0} - n_{gs}}{\tau_s} . \quad (5.2b)$$

For a continuously pumped laser with a pulse repetition rate f , the initial inversion density of the Q -switch n_i and the initial population density of the absorber's ground state n_{gsi} at the beginning of the Q -switch operation can be obtained by integrating Eq. 5.2, hence:

$$n_i = \frac{1}{W_p \tau_{21} + 1} \{ W_p \tau_{21} n_{tot} - [W_p \tau_{21} n_{tot} - (W_p \tau_{21} + 1) n_f] e^{-1/\tau_{21} f} \} \quad (5.3a)$$

and

$$n_{gsi} = n_{s0} - (n_{s0} - n_{gsf}) e^{-t_{recovery}/\tau_s} \quad (5.3b)$$

where, n_f is the final inversion population density of the previous Q -switch, n_{gsf} is the final population density of the absorber ground state at the end of the previous Q -switch; $t_{recovery}$ is the recovery time of the absorber. The recovery time of the absorber can be assumed to be nearly equal to the pump time, namely:

$t_{recovery} \approx 1/f$. Compared with n_{s0} , n_{gsf} is small enough to be ignored in Eq. 5.3

(b). Hence, Eq. 5.3 is rewritten as:

$$n_i = \frac{1}{W_p \tau_{21} + 1} \{ W_p \tau_{21} n_{tot} - [W_p \tau_{21} n_{tot} - (W_p \tau_{21} + 1) n_f] e^{-1/\tau_{21} f} \} \quad (5.4a)$$

and

$$n_{gsi} \approx n_{s0} (1 - e^{-1/f \tau_s}) . \quad (5.4b)$$

By Eq. 5.4 (b), when the recovery time $t_{recovery}$ is long enough compared with τ_s , most of atoms stimulated to the absorber excited state can return spontaneously to the ground state. Hence, as shown in *Model I* and *Model II*, it is assumed that $n_{gsi} \approx n_{s0}$. But when a laser system has a high repetition rate f , $t_{recovery}$ is too short for the atoms in the excited level to go back to the ground state, and n_{gsi} should be calculated by Eq. 5.4 (b).

At the pulse stage (lasing stage or Q -switch stage), $\phi \geq 0$. Setting the right hand of Eq. 5.1 (a) to zero yields the initial condition of the Q -switch is,

$$\begin{aligned} 2\sigma l n_i &= 2\sigma_{gs} l_s n_{gsi} + 2\sigma_{es} l_s n_{esi} + \ln\left(\frac{1}{R}\right) + L \\ &= 2\sigma_{gs} l_s n_{gsi} + 2\sigma_{es} l_s (n_{s0} - n_{gsi}) + \ln\left(\frac{1}{R}\right) + L \\ &= 2(\sigma_{gs} - \sigma_{es}) l_s n_{gsi} + 2\sigma_{es} l_s n_{s0} + \ln\left(\frac{1}{R}\right) + L \end{aligned} \quad (5.5a)$$

or

$$n_i = \frac{2(\sigma_{gs} - \sigma_{es}) l_s n_{gsi} + 2\sigma_{es} l_s n_{s0} + \ln\left(\frac{1}{R}\right) + L}{2\sigma l} \quad (5.5b)$$

where, n_{esi} is the initial population density of an absorber in the excited level at the beginning of the Q -switch.

Eq. 5.5 shows the initial inversion population of the Q -switch n_i is determined by both of the absorber's initial population densities of the ground state n_{gsi} and the excited state n_{esi} .

When the power reaches its peak point $\frac{d\phi}{dn} = 0$. Hence, the instantaneous inversion density of the gain medium n_t can be calculated from the following

$$2\sigma l n_t = 2\sigma_{gs} l_s n_{gst} + 2\sigma_{es} l_s n_{est} + \ln\left(\frac{1}{R}\right) + L \quad (5.6)$$

where, n_{gst} and n_{est} are the instantaneous population densities of the absorber ground and excited state at this moment, respectively. When the system begins lasing, the atoms in the absorber ground state are stimulated quickly to the excited state. Therefore, compared with the number of atoms in the excited state, $n_{gst} \approx 0$, and yields

$$2\sigma l n_t \approx 2\sigma_{es} l_s n_{s0} + \ln\left(\frac{1}{R}\right) + L \quad (5.7)$$

Introducing the variables E_a and P_a as done in the previous chapters, the expressions for the output energy E , the peak power P_{\max} and the FWHM pulse duration t_p of a passively Q -switched laser are:

$$E = \frac{h\nu A}{2\sigma\gamma} \ln\left(\frac{1}{R}\right) \ln\left(\frac{n_t}{n_f}\right) = \frac{h\nu A}{2\sigma\gamma} E_a \quad (5.8a)$$

$$P_{\max} = \frac{h\nu A l'}{t_r} \ln\left(\frac{1}{R}\right) \phi_{\max} = \frac{h\nu A}{2\gamma\sigma} P_a \quad (5.8b)$$

$$t_p = \frac{E}{P_{\max}} = \frac{E_a}{P_a} \quad (5.8c)$$

where, A is the cross sectional area of the laser beam, h is Plank's constant, ν is the frequency of the laser EM field.

5.3 The simulation results showing the effect of recovery time

A laser diode (LD) continuously pumped Cr:YAG passively Q -switched Yb:YAG laser [Li, 2006] is used to show the effect of the recovery time of an absorber on the output of a laser system. The data for this laser system and materials are the same as the ones listed in Tables 4.1 - 4.3 of Chapter 4. The range of pump rate pumping the laser system is from $50s^{-1}cm^{-3}$ to $4000s^{-1}cm^{-3}$.

Fig. 5.1 plots the following parameters: the peak power parameter P_a , the output energy parameter E_a , the FWHM pulse width t_p and the working initial transmission T_{0_stable} (the initial transmission of an absorber at the stable output state) as a function of pumping rate W_p . It is found that the parameters P_a , E_a and t_p don't change monotonically along W_p . Both P_a and E_a follow an increase-peak-decrease process (which means that the variable increases along with the pump rate W_p , then reaches its maximum value, then after that it begins decreasing), and on the contrary t_p follows a decrease-valley-increase trajectory (which means that the variable has a downward slope at first, after it reaches its minimum point it becomes upward sloping). These simulation results agree well with the experimental results shown in [Li, 2006]. Here, it is assumed that both the pump rate W_p and the corresponding absorber working initial transmission at the stable output state, shown in Fig. 5.1 (d), results in the changes of the other three parameters: P_a , E_a , and t_p .

As discussed in the previous sections, when most of the atoms excited to the excited state of an absorber have time to return to the ground level, the initial transmission at the stable output state T_{0_stable} is nearly the same as the given value at the beginning of the first working cycle, then the initial condition of the Q -switching isn't influenced by the pumping stage, this case is reported in

Chapter 3 and Chapter 4, and is named the quick-stable state in Chapter 4. In Fig. 5.1 (d), when the pumping rate W_p is lower than $1600s^{-1}cm^{-3}$, the absorber initial transmission is nearly equal to the given value, namely $T_0 = 94\%$, and this Yb:YAG laser system works in the quick-stable state. However, when the pumping rate W_p is greater than $1700s^{-1}cm^{-3}$, the recovery time of the absorber is much shorter, and the population of the atoms residing at the excited state cannot be ignored, which leads to the more transparent absorber and a bigger absorber working initial transmission. As shown in Fig. 5.1 (d), the working absorber initial transmission increases monotonically along with the pump rate W_p when $W_p > 1700s^{-1}cm^{-3}$.

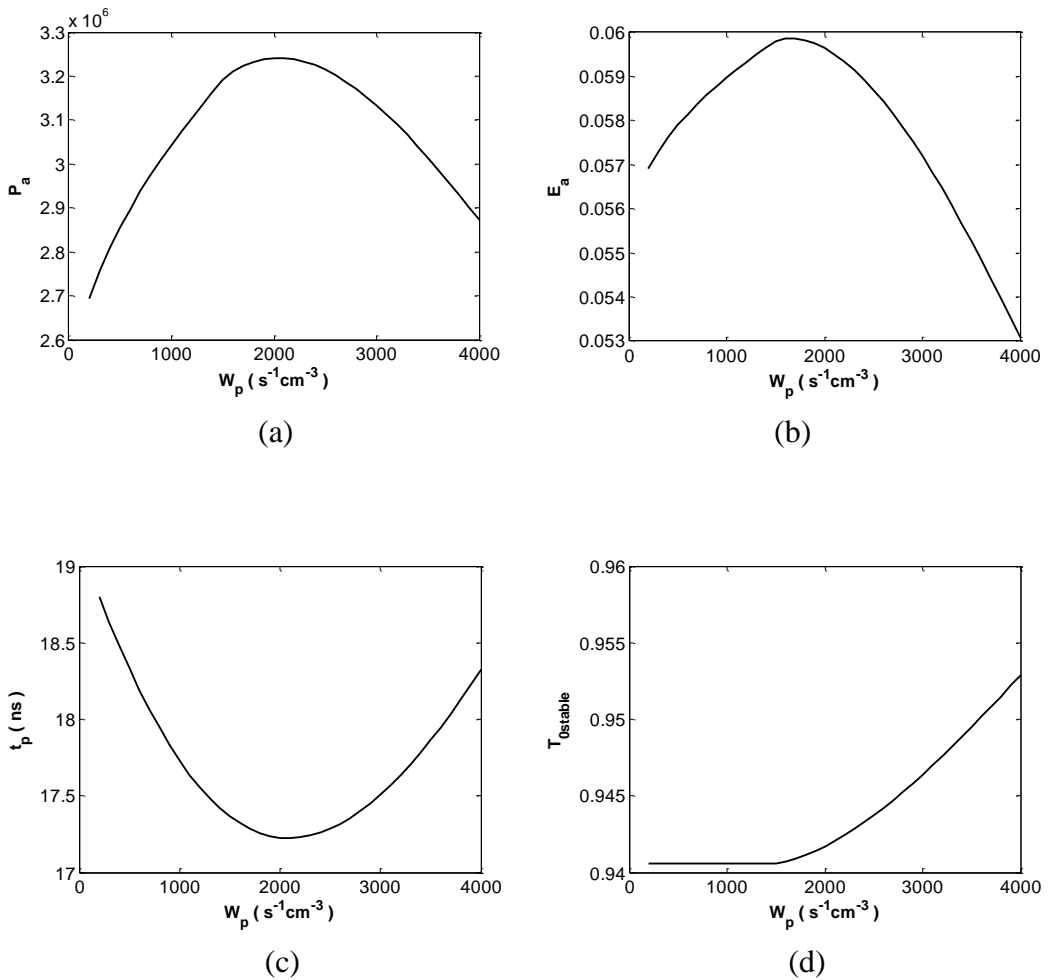


Figure 5.1 The parameters P_a (a), E_a (b), t_p (c) and the initial transmission T_0 (d) at the stable output state as a function of pumping rate W_p

To show the magnitude of the pump rate visually, the parameters P_a , E_a , t_p and T_{0_stable} as a function of the rate of the current pump rate and the threshold pump rate N_{Wp} are plotted in Fig. 5.2. It is noted that when $N_{Wp} > 40$, the recovery time of the absorber influences the output parameters of the laser system, and the Yb:YAG laser system doesn't work in the quick-stable state. The extreme points of P_a , E_a and t_p with the corresponding W_p (N_{Wp}) and T_{0_stable} are listed in Table 5.1.

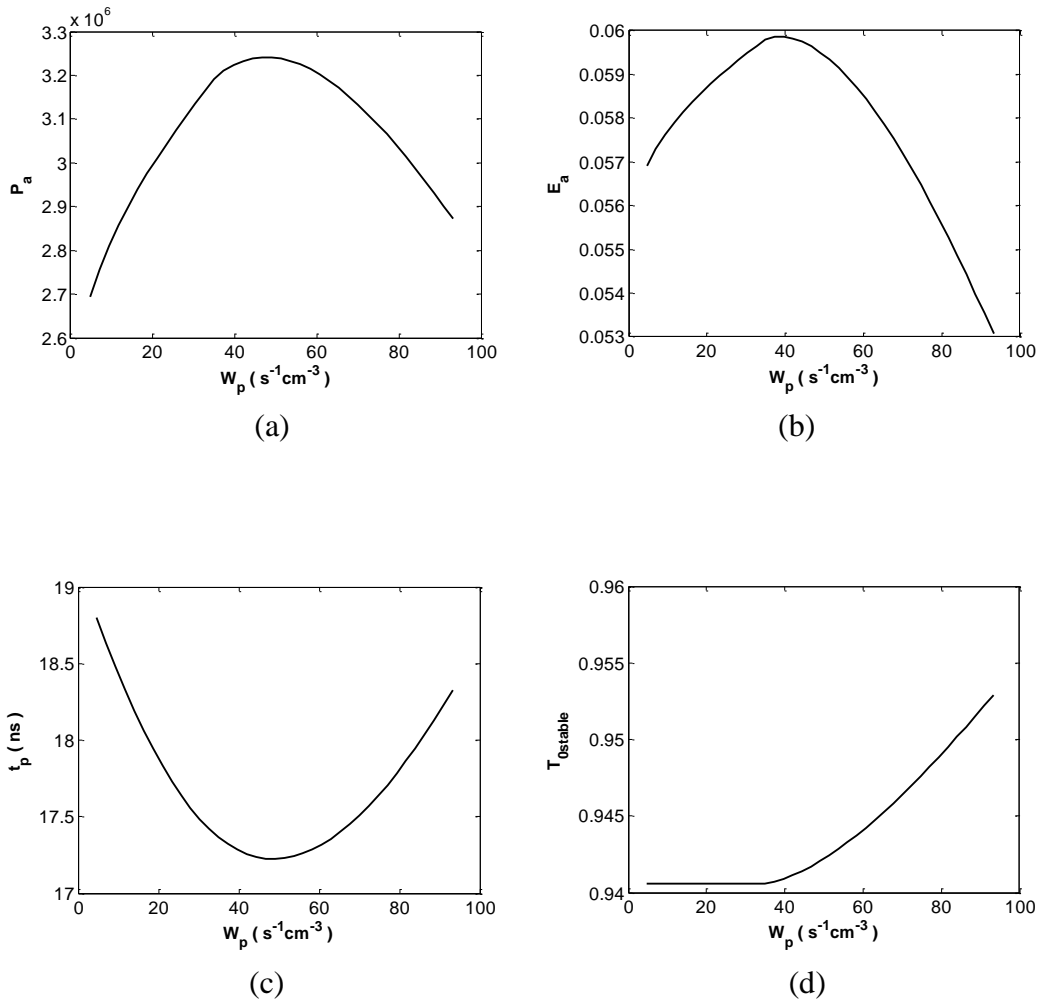


Figure 5.2 The parameters P_a (a), E_a (b), t_p (c) and the initial transmission T_0 (d) at the stable output state as a function of N_{Wp}

Table 5.1 The extreme points of P_a , E_a and t_p with the corresponding W_p and T_{0_stable}

$W_p \text{ s}^{-1}\text{cm}^{-3} (N_{Wp})$	T_{0_stable}	P_a	E_a	$t_p \text{ (ns)}$
1500 (35)	94%	3.23×10^7	0.0602	17.3
2100 (49)	94.2%	3.2×10^7	0.0595	17.2
2800 (65)	94.5%	3.16×10^7	0.0579	17.3

5.4 The simulation and computing steps

In *Model III*, to get the coupling absorber *product initial transmission* and the *working initial transmission* of a selected output coupler, the corresponding FWHM pulse width t_p of a laser system when the output energy parameter E_a and the pump rate W_p are pre-determined, and the recovery time of an absorber is considered, the simulation steps are as follows:

- 1) A value is given as the reflectivity of the output energy R ;
- 2) The probable value of the absorber initial transmission T_{0_1st} as the coupling parameter of R determined in Step 1) is selected from an array valued from 0.1 to 0.99 in the first pumping and lasing cycle;
- 3) The initial inversion population density of the gain medium n_{i_1st} for the first cycle is calculated using Eq. 5.5 (for the first cycle, $n_{esi_1st} \approx 0$);
- 4) The distributions of ϕ_{1st} , n_{1st} and n_{gs_1st} as a function of time are given by using the Runge-Kutta method to solve the rate equations (Eq. 5.1);
- 5) The values of n_{f_1st} and ϕ_{\max_1st} are shown by the numerical results;
- 6) Substituting n_{f_1st} into Eq. 5.4 and solving Eq. 5.4 and Eq. 5.5 (b) yields the values of the parameters n_{i_2nd} , n_{gsi_2nd} for the second Q-switching and f_{1st} between the end of the first Q-switching and the beginning of the second Q-switching;

- 7) Repeating Step 4) to Step 6) until in the last three cycles the values of n_{f_nth} / n_{i_nth} are nearly the same, once equilibrium is established this is termed the stable working state, and now the values of n_{gsi_stable} , n_{i_stable} , n_{f_stable} and ϕ_{\max_stable} are delivered to the next step;
- 8) Using Eq. 4.7 (a) yields the corresponding E_{a_stable} ;
- 9) Comparing the obtained value of E_{a_stable} and the value of E_a required by the system, if it is nearly the same (the error is smaller than 1×10^{-6}), T_{0_1st} is the absorber-product initial transmission that the laser system wanted, T_{0_stable} is the practical working initial transmission of an absorber for this pump rate at the stable working state, then the simulation goes to the next step (Step 10); if it is not, the computing goes back to Step 2 and repeats Steps 2 - 9 until the proper values of T_{0_1st} and T_{0_stable} are obtained to maintain the pre-determined output energy E_a ;
- 10) Calculating P_a by Eq. 4.7 (b), and introducing the result into Eq. 5.9 (c) yields the FWHM pulse width t_p .

According to the definition of the product initial transmission and the working initial transmission, the parameters T_{0_1st} and T_{0_stable} are the product specification and working initial transmission of an absorber, respectively.

The programming flowchart to get the FWHM pulse width t_p is illustrated in Fig. 5.3. Fig. 5.4 shows how to get T_{0_stable} .

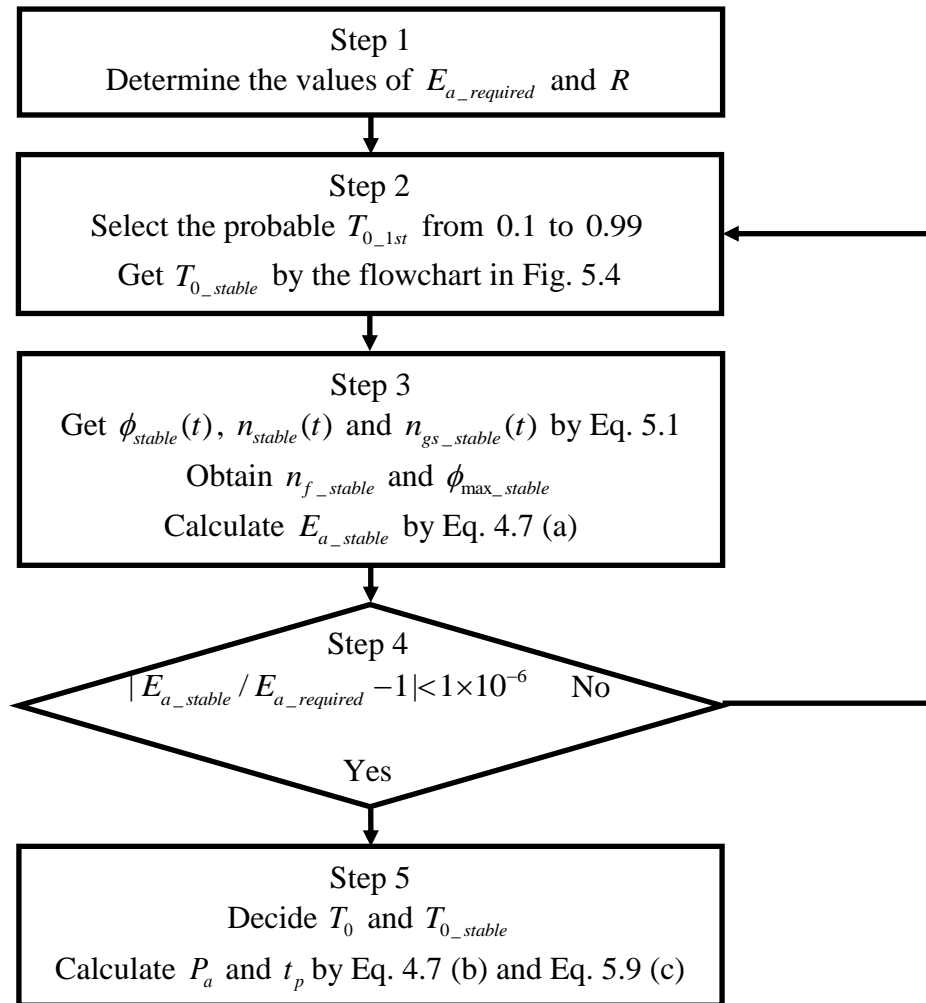


Figure 5.3 The programming flowchart to get the decided R 's coupling T_0 and the FWHM pulse width t_p when E_a and W_p are known

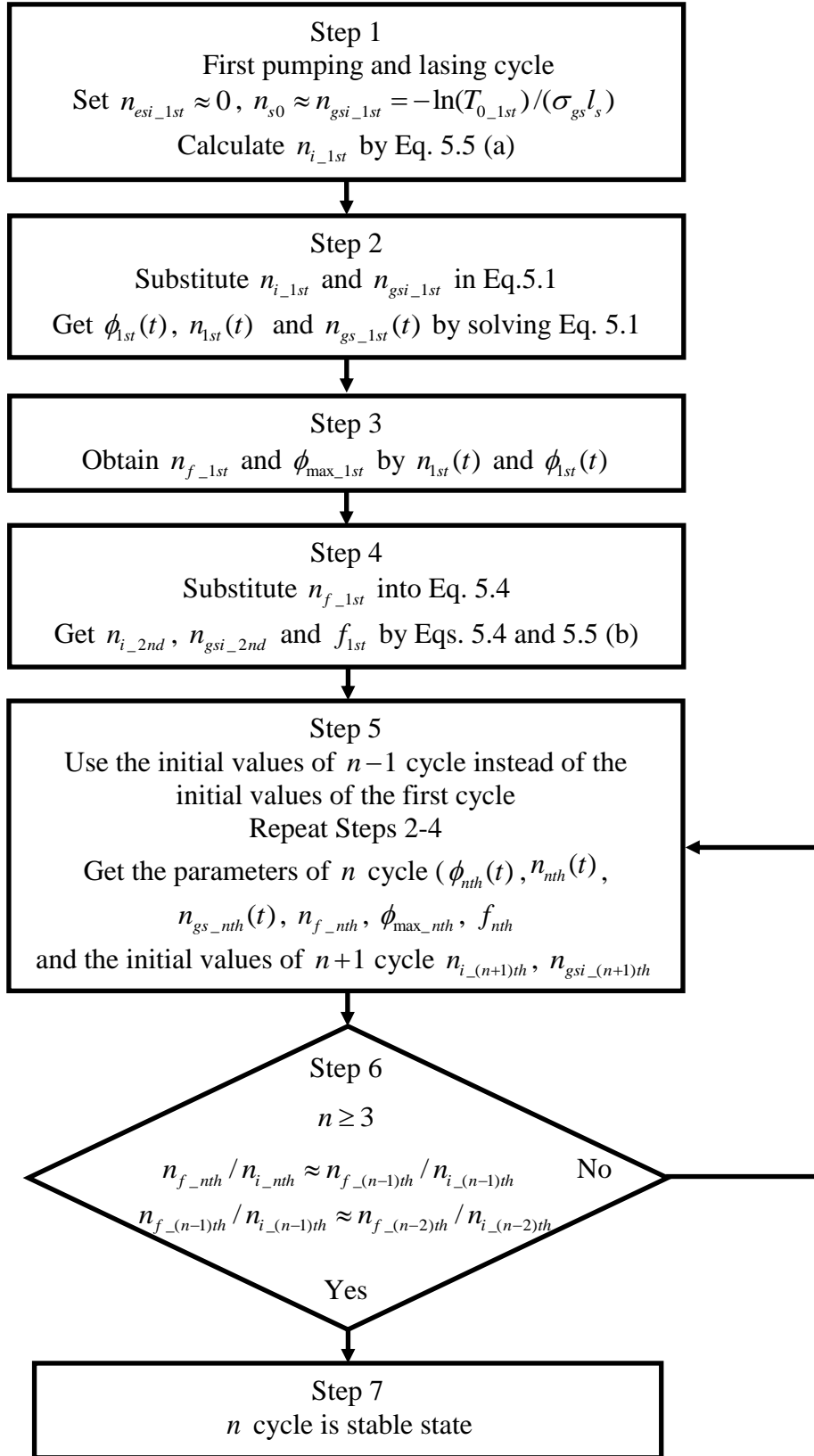


Figure 5.4 The programming flowchart to get the stable state

5.5 The simulation results of a continuously pumped Cr:YAG passively Q -switched Yb:YAG laser

A continuously pumped Cr:YAG passively Q -switched Yb:YAG laser shown in Section 5.3 is employed to illustrate the simulation results. The data for this laser system and materials are the same as the ones listed in Tables 4.1 - 4.3 of Chapter 4.

As shown in Fig. 4.10, when the output energy parameter E_a is required to be 0.08, the Cr:YAG passively Q -switched Yb:YAG laser system doesn't maintain the quick-stable state when the pump rate W_p is over $2 \times 10^3 s^{-1} cm^{-3}$ and the output reflectivity is smaller than 80%. Hence, Fig. 5.5 plots the initial transmission for the first working cycle T_{0_1st} (the product initial transmission) and at the stable state T_{0_stable} (the working initial transmission) as a function of the output coupler R and E_a (it is 0.08) for the cases that the pump rates W_p are $2 \times 10^3 s^{-1} cm^{-3}$, $4 \times 10^3 s^{-1} cm^{-3}$, $6 \times 10^3 s^{-1} cm^{-3}$ and $8 \times 10^3 s^{-1} cm^{-3}$. The pairs of R and T_0 obtained using *Model I* are plotted in Fig. 5.5 as well.

In Fig. 5.5, both the initial transmissions obtained using *Model I* and *Model III* decrease monotonically with increasing output reflectivity R . Here, the absorber initial transmissions obtained using *Model III* include the product initial transmission T_{0_1st} and the working initial transmission T_{0_stable} . It is noted that as R increases, both T_{0_1st} and T_{0_stable} approach the curve from *Model I*, which excludes the pump rate in the laser rate equations in the lasing stage, and the recovery time of the absorber in the pumping stage. As shown in the previous sections, the number of atoms in the absorber's ground level in the stable state is less than the population for the first cycle, T_{0_stable} is larger than the product-value presented for the first working cycle. The simulation results in Fig. 5.5 agree well with this analysis. As the pump rate increases, the recovery time of the absorber

is shortened which leads to more atoms residing in the upper level of the absorber, then the differences between T_{0_1st} and T_{0_stable} become more obvious. For example, as $R = 50\%$, for the case when $W_p = 4 \times 10^3 s^{-1} cm^{-3}$, T_{0_stable} is 97.6% and T_{0_1st} is 96.6%, but for the case when $W_p = 8 \times 10^3 s^{-1} cm^{-3}$, T_{0_stable} is 98% and T_{0_1st} is 95.4%.

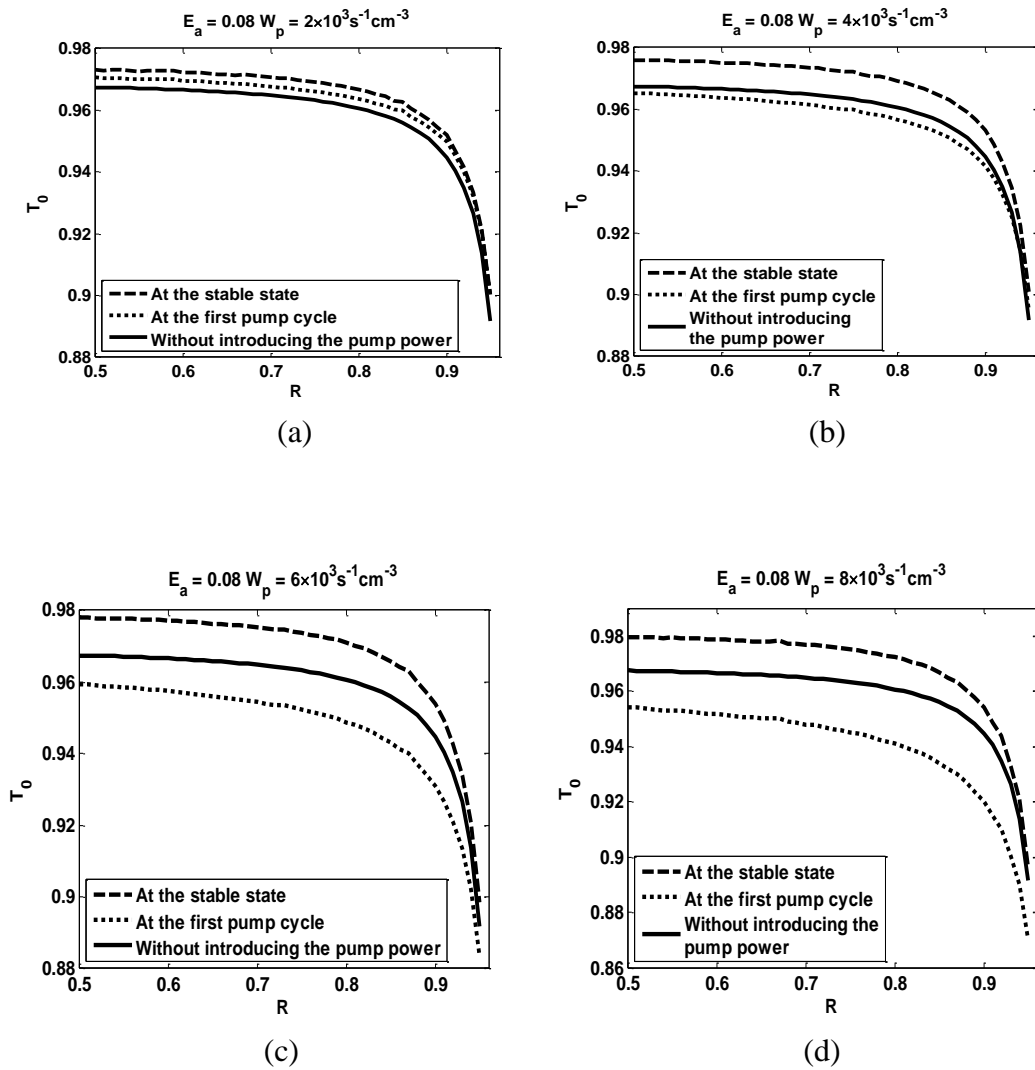


Figure 5.5 The output coupler R with its coupling initial transmissions at the first pump cycle T_{0_1st} and at the stable state T_{0_stable} for the cases when the pump rates W_p are $2 \times 10^3 s^{-1} cm^{-3}$, $4 \times 10^3 s^{-1} cm^{-3}$, $6 \times 10^3 s^{-1} cm^{-3}$ and $8 \times 10^3 s^{-1} cm^{-3}$, compared with the results obtained using *Model I*

The ratios of the current pump rate and the threshold pump rate N_{W_p} obtained for the first working cycle and the stable state when W_p is: $2 \times 10^3 s^{-1} cm^{-3}$, $4 \times 10^3 s^{-1} cm^{-3}$, $6 \times 10^3 s^{-1} cm^{-3}$ and $8 \times 10^3 s^{-1} cm^{-3}$ for *Model III* are shown in Fig. 5.6. The curve of the parameter $N_{W_p_stable}$ has an increase-peak-decrease shape, the same as $N_{W_p_1st}$. However, the data for T_{0_stable} is larger than T_{0_1st} which results in the practical N_{W_p} at the stable state being bigger than the value of N_{W_p} presented for the first working cycle. For a selected output coupler, the difference between $N_{W_p_1st}$ and $N_{W_p_stable}$ increases as pump rate W_p increases. When the pump rate W_p is selected, the difference between $N_{W_p_1st}$ and $N_{W_p_stable}$ increases as R increases, once it peaks the difference decreases.

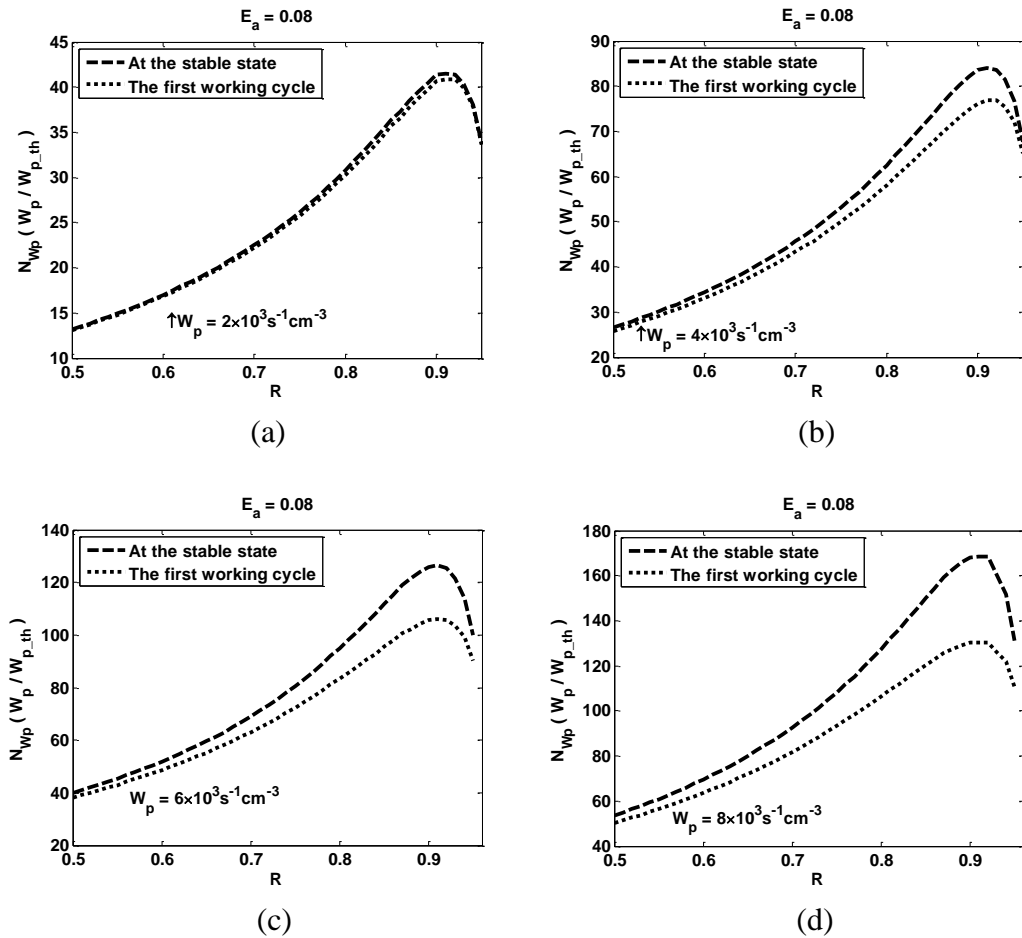


Figure 5.6 The parameter N_{W_p} as a function of R for two cases, one is for the first pump cycle, and the other is for the stable state when the pump rates W_p are $2 \times 10^3 s^{-1} cm^{-3}$, $4 \times 10^3 s^{-1} cm^{-3}$, $6 \times 10^3 s^{-1} cm^{-3}$ and $8 \times 10^3 s^{-1} cm^{-3}$.

Fig. 5.7 shows the FWHM pulse width t_p as a function of R obtained using *Model III* when the output energy parameter E_a is 0.08, and the pump rates W_p are: $2 \times 10^3 s^{-1} cm^{-3}$, $4 \times 10^3 s^{-1} cm^{-3}$, $6 \times 10^3 s^{-1} cm^{-3}$ and $8 \times 10^3 s^{-1} cm^{-3}$. For the comparison, the data for t_p obtained using *Model I* are plotted in Fig. 5.7 as well. The variation of t_p for increasing R obtained using *Model II* is the same as using *Model I*, which monotonically decreases as R increases. The value of t_p for the same output reflectivity R decreases as the pump rate increases. For example, for the output reflectivity R is 50%, the biggest value of t_p is 25ns as W_p is equal to $2 \times 10^3 s^{-1} cm^{-3}$, while it is 16ns for W_p is equal to $4 \times 10^3 s^{-1} cm^{-3}$. For the lower output reflectivity, the data of t_p obtained using *Model III* is far away from those obtained using *Model I*.

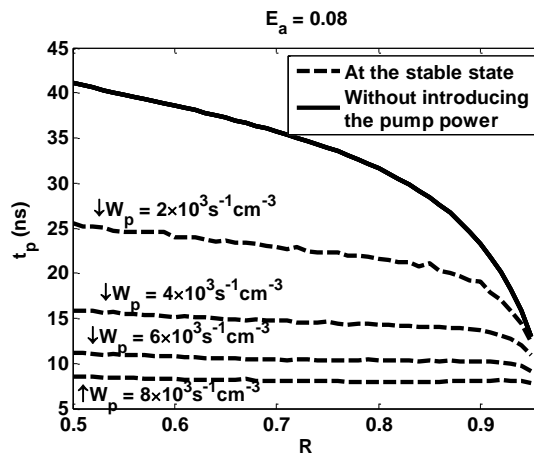
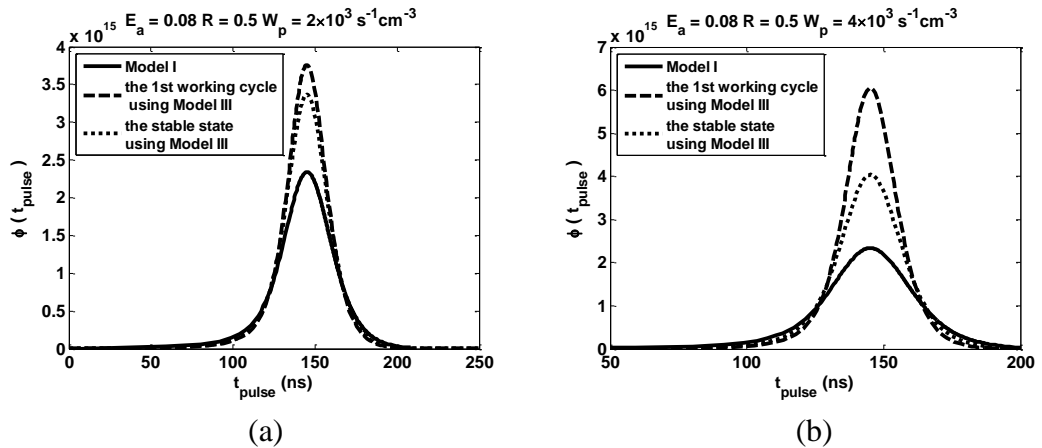


Figure 5.7 The FWHM pulse width t_p as a function of R obtained using *Model III* for different pump rate (the pump rates W_p are $2 \times 10^3 s^{-1} cm^{-3}$, $4 \times 10^3 s^{-1} cm^{-3}$, $6 \times 10^3 s^{-1} cm^{-3}$ and $8 \times 10^3 s^{-1} cm^{-3}$) are compared with the data obtained using *Model I*

The average photon density in the laser cavity during the pulse $\phi(t)$ is studied to observe the effects of the pump rate and the recovery time of the absorber on the pulse shape. The distribution of $\phi(t)$ in the first working cycle and in the stable working cycle, for the cases when the output reflectivity R is 50%, the output energy parameter E_a is 0.08 and the pump rates W_p are $2 \times 10^3 \text{ s}^{-1} \text{ cm}^{-3}$, $4 \times 10^3 \text{ s}^{-1} \text{ cm}^{-3}$, $6 \times 10^3 \text{ s}^{-1} \text{ cm}^{-3}$ and $8 \times 10^3 \text{ s}^{-1} \text{ cm}^{-3}$, are plotted in Fig. 5.8. The corresponding photon densities obtained using *Model I* are shown in Fig. 5.8 as well. In Fig. 5.8, the maximum point of $\phi(t)$ in the stable cycle is substantially different from the first working cycle when the pump rate increases. It illustrates the influence of the recovery time of the absorber on the photon density, which is that the high pump rate shortens the recovery time of the absorber, and leads to more atoms residing in the upper level of the absorber by the beginning of Q -switching. Hence, the absorber working initial transmission becomes higher compared with the product value. Fig. 5.8 also shows for different pump rates, the working values of an absorber are not same.



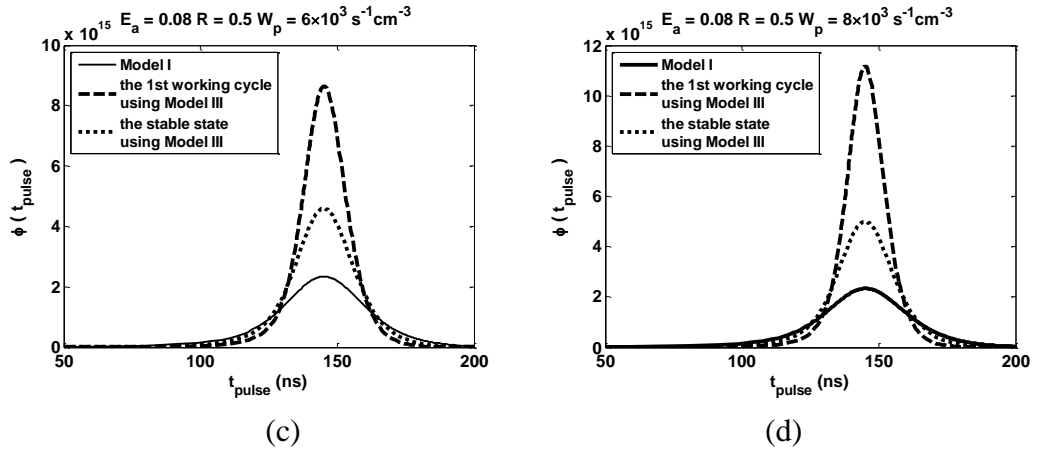


Figure 5.8 When R is 50% and E_a is 0.08, the distribution of the average photon densities in laser cavity $\phi(t)$ obtained using *Model I* and using *Model III* for the cases when W_p is (a) $2 \times 10^3 s^{-1} cm^{-3}$, (b) $4 \times 10^3 s^{-1} cm^{-3}$, (c) $6 \times 10^3 s^{-1} cm^{-3}$ and (d) $8 \times 10^3 s^{-1} cm^{-3}$.

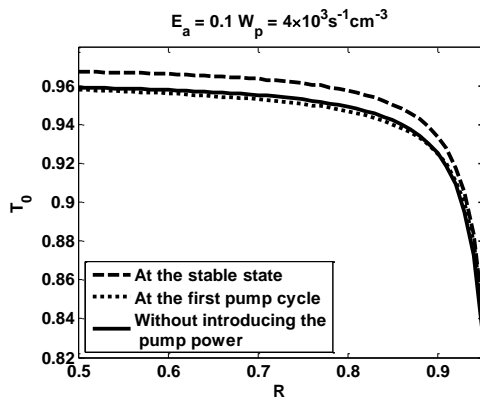
To get the general relationship, the variation of the following parameters: the initial transmission T_0 , the rate of the current pump rate and the ratio of pump rates N_{W_p} , and the FWHM pulse width t_p as a function of the output reflectivity R for different values of the output energy parameter E_a (0.1, 0.3 and 0.5) and different pump rates W_p are studied and shown in Figs. 5.9 - 5.11. Figs. 5.9 - 5.11 plot both the absorber product initial transmission T_{0_1st} and its working initial transmission for different pump rates T_{0_stable} obtained using *Model III*. The data for T_0 and the FWHM pulse width t_p obtained using *Model I* are also plotted in Figs. 5.9 - 5.11 as well. For the case when E_a is 0.1, the pump rates W_p are $4 \times 10^3 s^{-1} cm^{-3}$, $6 \times 10^3 s^{-1} cm^{-3}$, $8 \times 10^3 s^{-1} cm^{-3}$ and $10 \times 10^3 s^{-1} cm^{-3}$ in Fig. 5.9. When the output energy parameter E_a is 0.3, the laser system is pumped by $8 \times 10^3 s^{-1} cm^{-3}$, $10 \times 10^3 s^{-1} cm^{-3}$, $20 \times 10^3 s^{-1} cm^{-3}$ and $30 \times 10^3 s^{-1} cm^{-3}$ in Fig. 5.10. When E_a is 0.5, the pump rates W_p are $8 \times 10^3 s^{-1} cm^{-3}$, $10 \times 10^3 s^{-1} cm^{-3}$, $20 \times 10^3 s^{-1} cm^{-3}$ and $30 \times 10^3 s^{-1} cm^{-3}$ in Fig. 5.11.

Figs. 5.9 (a) - (d) show for a decided output reflectivity R and a pre-determined output energy parameter E_a , the value of T_{0_stable} is bigger as the laser system is pumped with a higher pump rate W_p , but its corresponding product value T_{0_1st} is smaller compared with one with a lower pump rate W_p . As R increases, the difference between T_{0_stable} and T_{0_1st} increases at first, then reaches its maximum point, after that the difference decreases. The value of T_{0_stable} approaches T_0 obtained using *Model I* as R increases. Figs. 5.10 (a) - (d) and Figs. 5.11 (a) - (d) present the same behaviour. Figs. 5.9 (a) - 5.11 (a) show for a selected output reflectivity R , the value of T_{0_stable} is reduced to get a higher output energy parameter E_a , and its T_{0_1st} is reduced as well. It means when a high output reflectivity R is selected in the laser resonator, the coupling product-value of the initial transmission of an absorber T_{0_1st} with its working value T_{0_stable} can be evaluated using the simplified model (*Model I*).

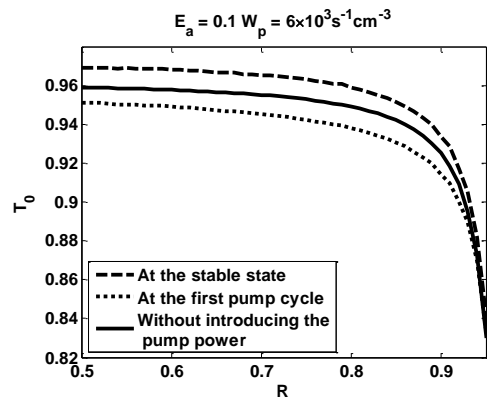
Comparing Figs. 5.9 (e) - (g) with Figs. 5.10 (e) - (g) and Figs. 5.11 (e) - (g), it is shown that to get a higher output energy, the initial inversion population density of the gain medium is required to have a higher value, and the laser system must be pumped with a higher pump power. For all the cases of E_a shown in Figs. 5.9 - 5.11, the distributions of N_{Wp_1st} and N_{Wp_stable} are similar, which at first increases with increasing output reflectivity R , then decreases after the variable reaches its peak point. The threshold pump rate W_{p_th} decided by the initial conditions of Q -switching results in the distributions of N_{Wp_1st} and N_{Wp_stable} which also represent the effects of both R and T_{0_1st} , or R and T_{0_stable} . The curve of N_{Wp_stable} approaches the plot of N_{Wp_1st} as R is close to its greatest available value.

Although the distribution of the FWHM pulse width t_p obtained using *Model III* is similar to the one obtained using *Model I* as shown in Figs. 5.9 (h) - 5.11 (h),

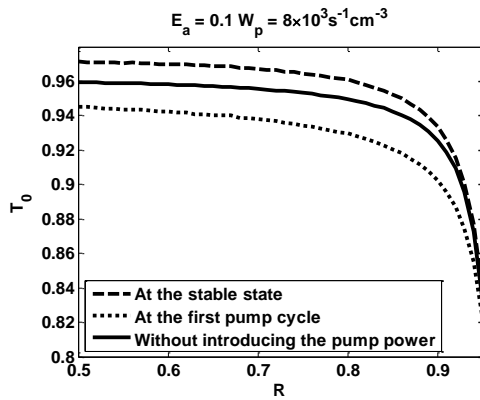
t_p decreases monotonically as R increases, the values of t_p for the two cases that is *Model I* and *Model III* are significantly different when R doesn't reach its maximum value. For example, when E_a is 0.1 and R is 90%, t_p is 13ns for the case when W_p is $4 \times 10^3 s^{-1} cm^{-3}$, however its value is 18ns using *Model I*.



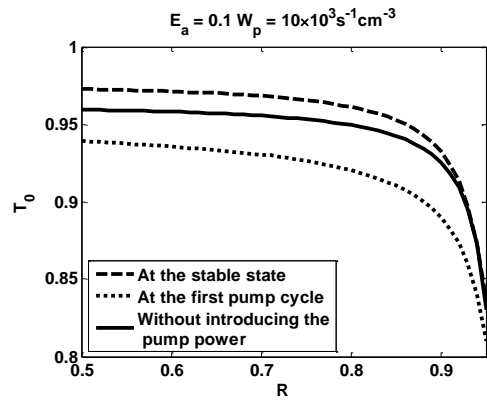
(a)



(b)



(c)



(d)

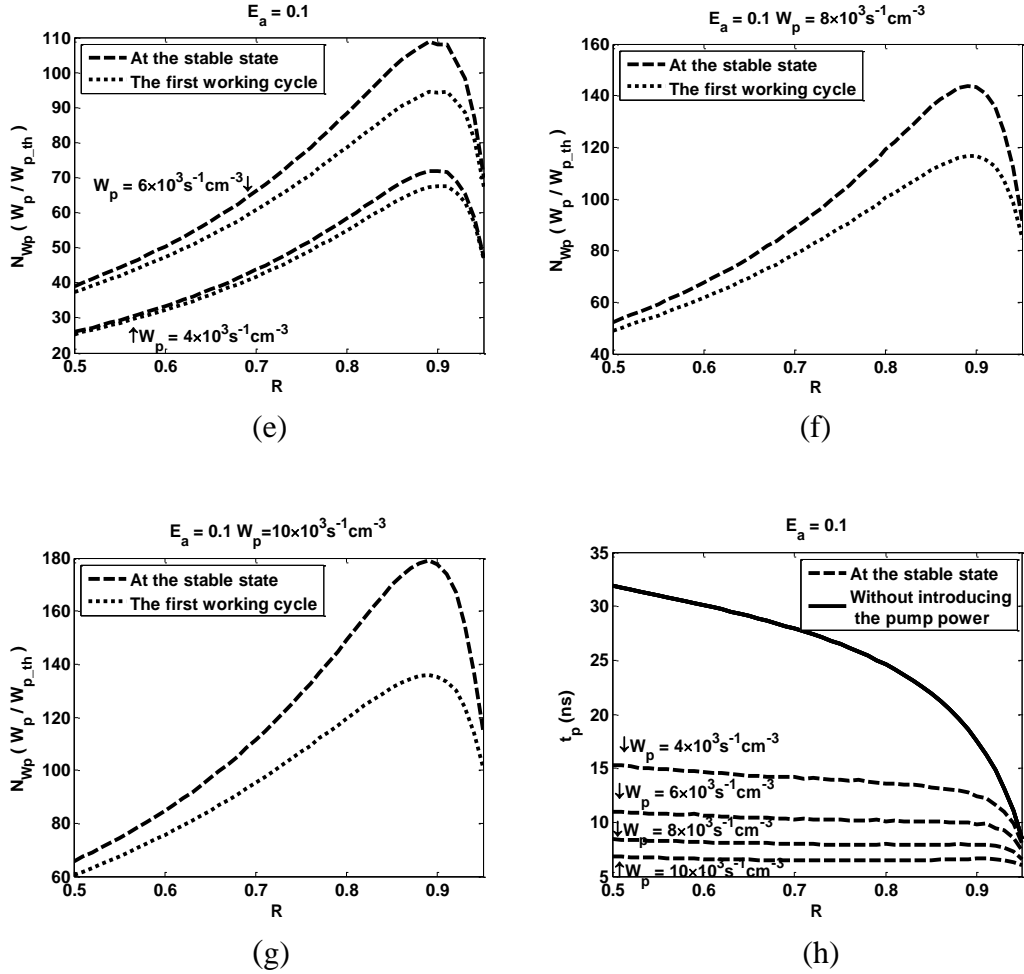
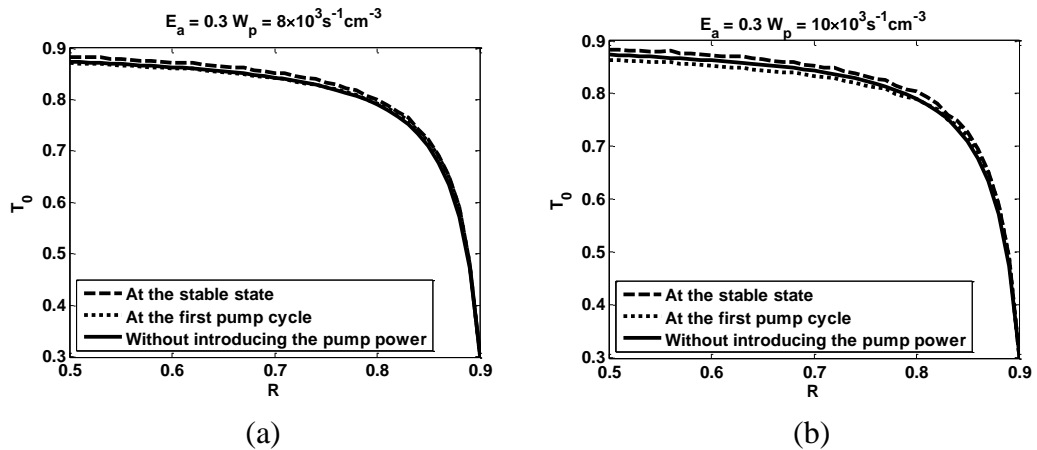


Figure 5.9 The initial transmissions at the first working cycle T_{0_1st} and at the stable state T_{0_stable} , the parameter N_{Wp} , and the FWHM pulse width t_p as a function of R and different W_p ($4 \times 10^3 s^{-1} cm^{-3}$, $6 \times 10^3 s^{-1} cm^{-3}$, $8 \times 10^3 s^{-1} cm^{-3}$ and $10 \times 10^3 s^{-1} cm^{-3}$) as E_a is 0.1 for *Model III*, the corresponding parameters obtained using *Model I* are plotted as well



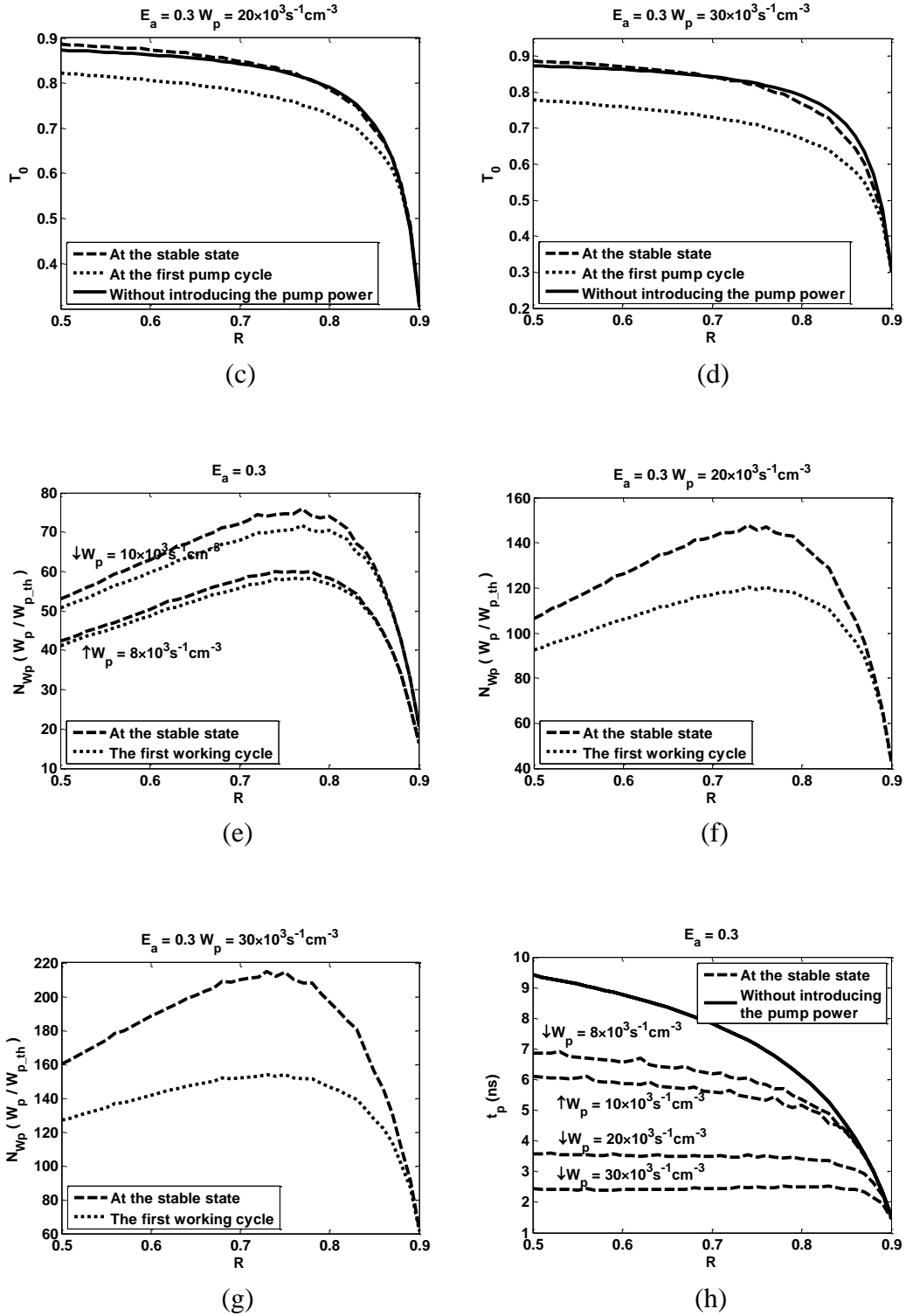
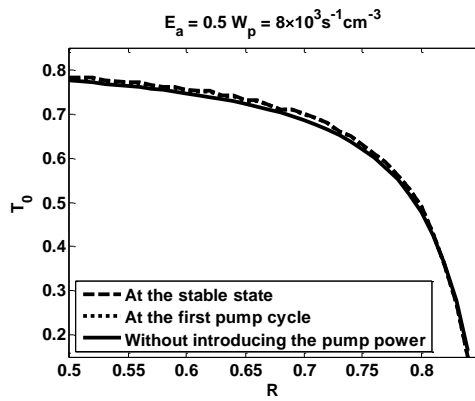
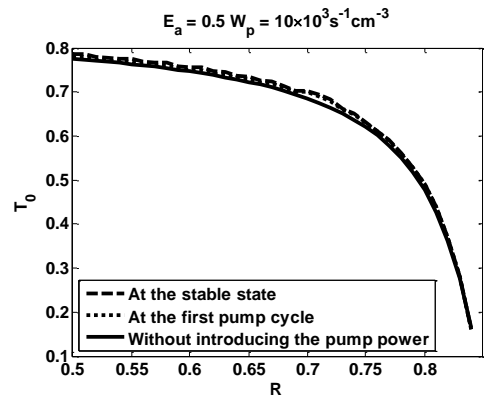


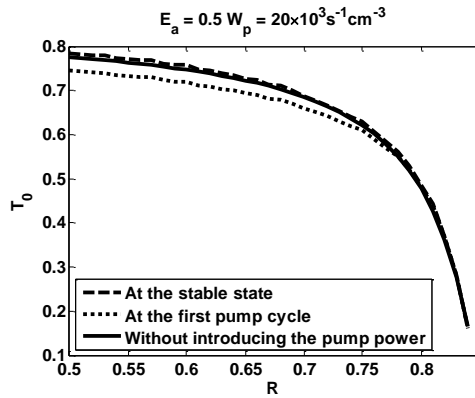
Figure 5.10 The initial transmissions at the first working cycle T_{0_1st} and at the stable state T_{0_stable} , the parameter N_{Wp} , and the FWHM pulse width t_p as a function of R for different W_p ($8 \times 10^3 \text{ s}^{-1} \text{ cm}^{-3}$, $10 \times 10^3 \text{ s}^{-1} \text{ cm}^{-3}$, $20 \times 10^3 \text{ s}^{-1} \text{ cm}^{-3}$ and $30 \times 10^3 \text{ s}^{-1} \text{ cm}^{-3}$) as E_a is 0.3 for *Model III*, the corresponding parameters obtained using *Model I* are plotted as well



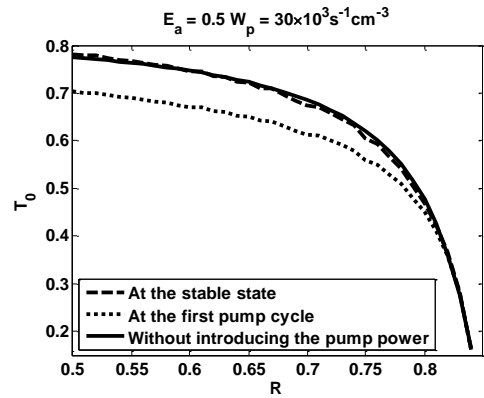
(a)



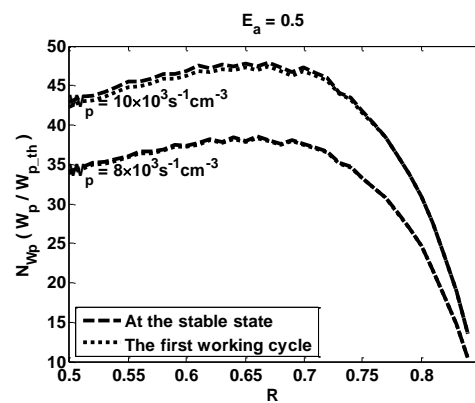
(b)



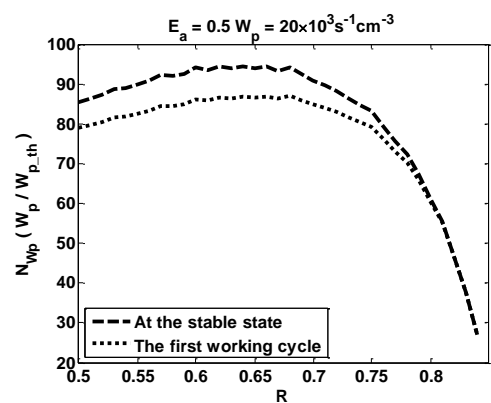
(c)



(d)



(e)



(f)

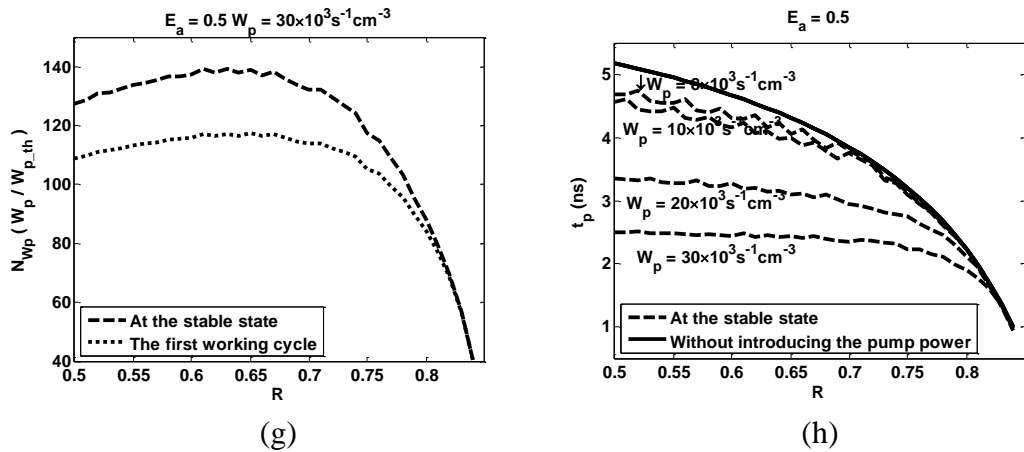


Figure 5.11 The initial transmissions at the first working cycle T_{0_1st} and at the stable state T_{0_stable} , the parameter N_{Wp} , and the FWHM pulse width t_p as a function of R and different W_p ($8 \times 10^3 s^{-1} cm^{-3}$, $10 \times 10^3 s^{-1} cm^{-3}$, $20 \times 10^3 s^{-1} cm^{-3}$ and $30 \times 10^3 s^{-1} cm^{-3}$) when E_a is 0.5 for *Model III*, the corresponding parameters obtained using *Model I* are plotted as well

The distribution of the average photon density in the laser cavity during the pulse stage $\phi(t)$, is employed to study the effects of the pump rate and the recovery time of the absorber on the pulse shape. Figs. 5.12 - 5.14 plot the distribution of $\phi(t)$ as a function of different output energy parameters E_a (0.1, 0.3 and 0.5) and different pump rates W_p when the output reflectivity R is 50%. As shown in previous sections, with *Model III* the recovery time of the absorber is shortened as the pump rate increases, and the working initial transmission of the absorber increases. Hence, the peak point of $\phi(t)$ at the stable state is smaller than for the first working cycle. The simulation results shown in Figs. 5.12 - 5.14 agree well with this conclusion. It is also noted that when the output energy parameter E_a and the output reflectivity R are pre-determined, the peak point of $\phi(t)$ increases as the pump rate increases, and the shape of $\phi(t)$ is sharp.

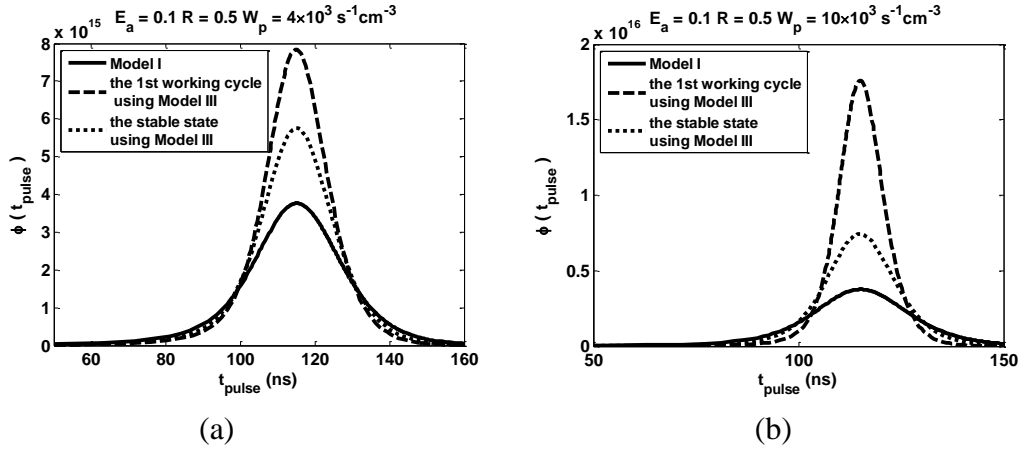


Figure 5.12 When R is 50% and E_a is 0.1, the distribution of the average photon densities in laser cavity $\phi(t)$ obtained using *Model I* and using *Model III* for the cases when W_p is (a) $4 \times 10^3 \text{ s}^{-1} \text{ cm}^{-3}$, (b) $10 \times 10^3 \text{ s}^{-1} \text{ cm}^{-3}$.

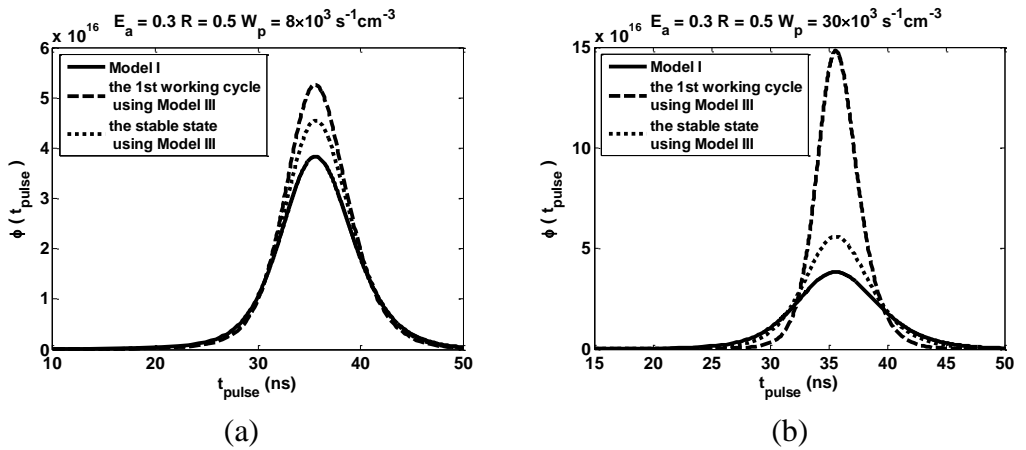


Figure 5.13 When R is 50% and E_a is 0.3, the distribution of the average photon densities in laser cavity $\phi(t)$ obtained using *Model I* and using *Model III* for the cases when W_p is (a) $8 \times 10^3 \text{ s}^{-1} \text{ cm}^{-3}$, (b) $30 \times 10^3 \text{ s}^{-1} \text{ cm}^{-3}$.

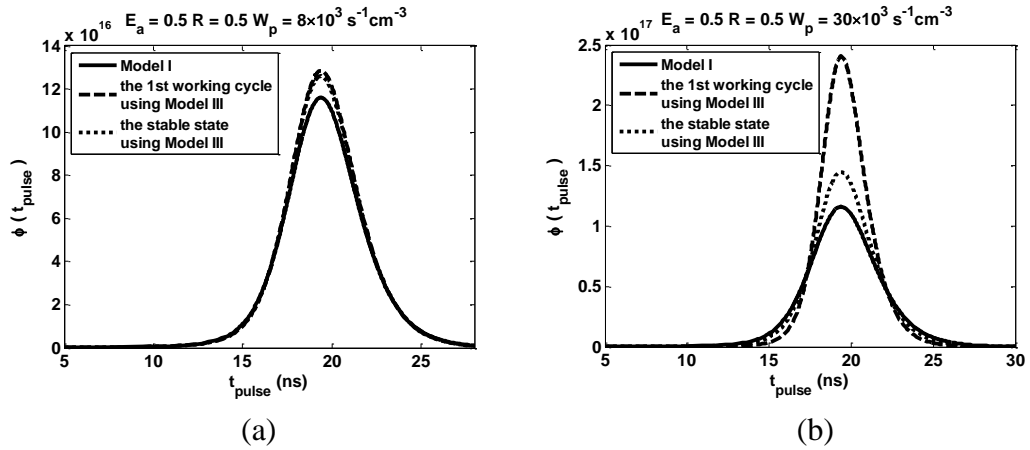


Figure 5.14 When R is 50% and E_a is 0.5, the distribution of the average photon densities in laser cavity $\phi(t)$ obtained using *Model I* and using *Model III* for the cases when W_p is (a) $8 \times 10^3 \text{ s}^{-1} \text{ cm}^{-3}$, (b) $30 \times 10^3 \text{ s}^{-1} \text{ cm}^{-3}$.

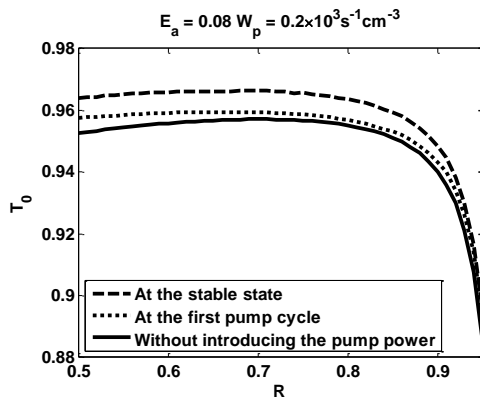
5.6 The pump rate and the gain medium

To analyze the effect of the gain medium on the FWHM pulse width t_p for *Model III*, Yb:YAG crystal is replaced by a same size of Nd:YAG crystal. The data for the Nd:YAG material are listed in Table 4.5.

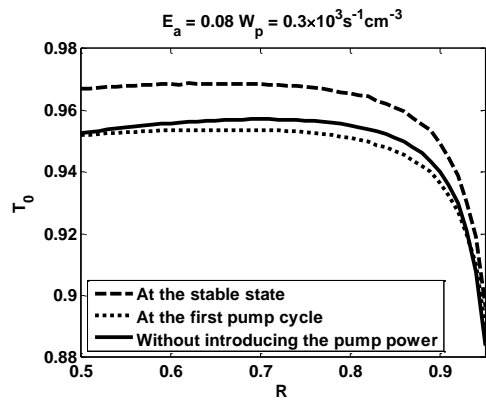
Figs. 5.15 - 5.18 plot the product-value of the initial transmission of an absorber T_{0_1st} with its working value T_{0_stable} for different pump rates; the values of E_a are 0.08, 0.1, 0.3 and 0.5. The corresponding N_{Wp_1st} and N_{Wp_stable} as a function of the output reflectivity R are plotted in Figs. 5.15 - 5.18 as well. The simulation values of the FWHM pulse width t_p are shown in the figures.

Comparing the simulation results from the Nd:YAG material with the ones for Yb:YAG, the following conclusions can be drawn: 1) the laser system with Yb:YAG as the gain medium should be pumped with a higher power than the Nd:YAG laser system for the same output coupler; 2) as the rate of pump power

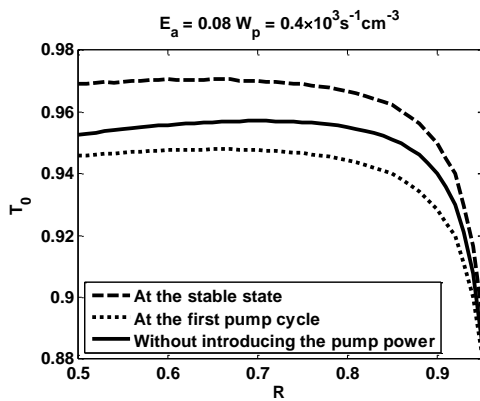
and the threshold pump power N_{wp} is same for two gain media, the recovery time of the absorber for the case when Nd:YAG is the gain medium affects the laser system more than Yb:YAG; 3) the FWHM pulse width of the Yb:YAG laser is shorter than one of Nd:YAG as the output reflectivity and the parameter N_{wp} are the same; 4) as with the Yb:YAG laser, the effect of the absorber's recovery time reduces as the output reflectivity increases; 5) similar to the Yb:YAG laser, the curves for the different pump powers approach the curves obtained using *Model I* as the output reflectivity increases.



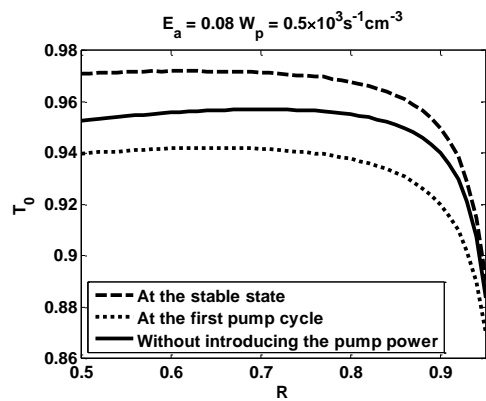
(a)



(b)



(c)



(d)

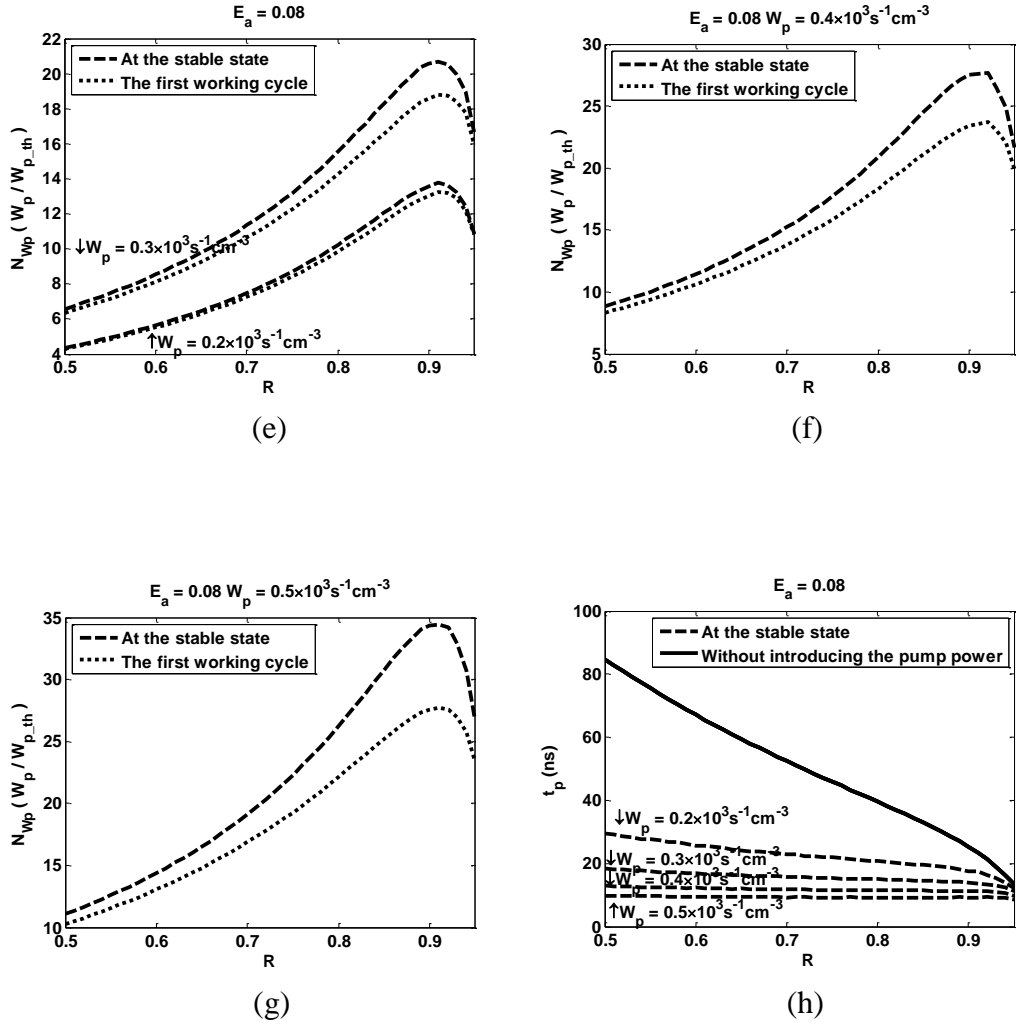
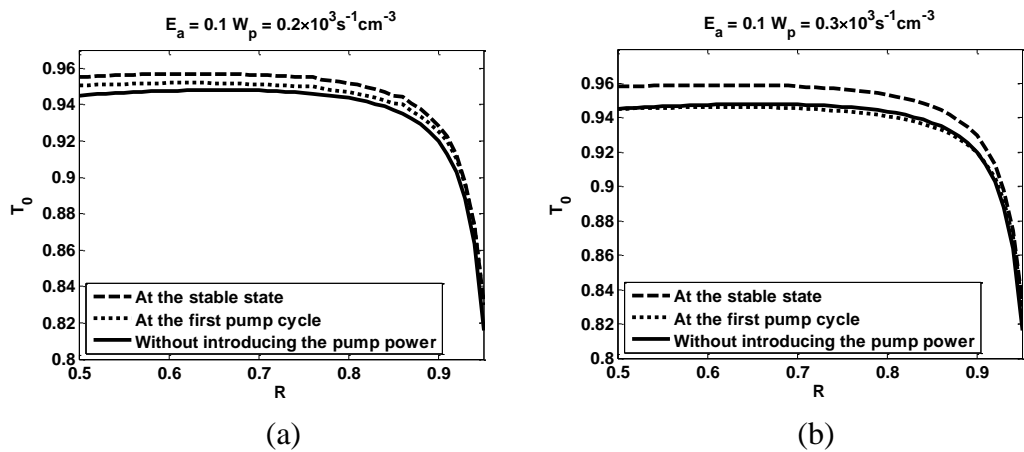


Figure 5.15 For a Nd:YAG laser system, the coupling parameter T_{0_1st} , T_{0_stable} (a) - (d) of R to keep $E_a = 0.08$, with N_{Wp_1st} and N_{Wp_stable} (e) - (g) and t_p (d) as W_p is $200s^{-1}cm^{-3}$, $300s^{-1}cm^{-3}$, $400s^{-1}cm^{-3}$ and $500s^{-1}cm^{-3}$



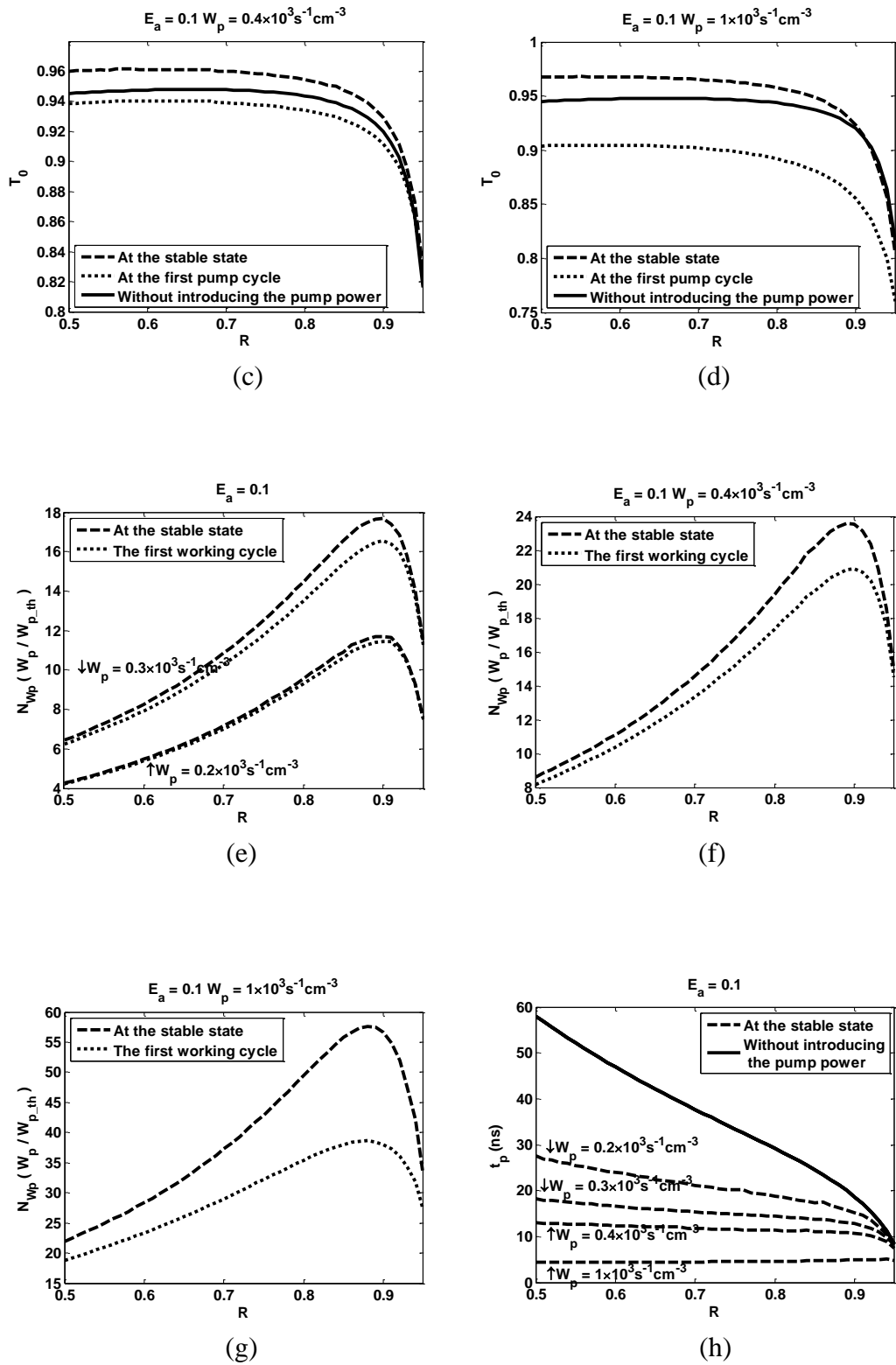
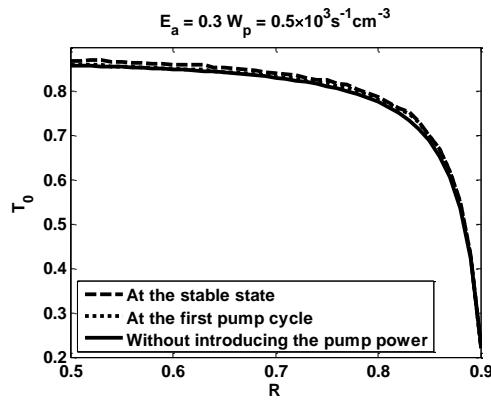
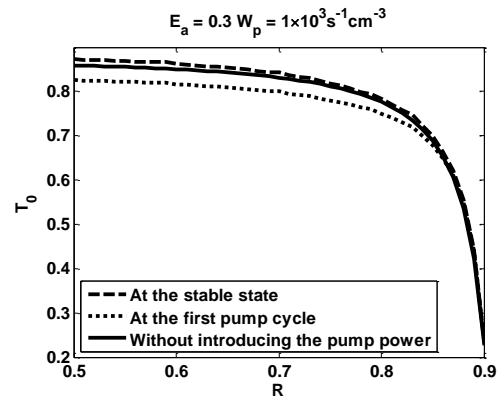


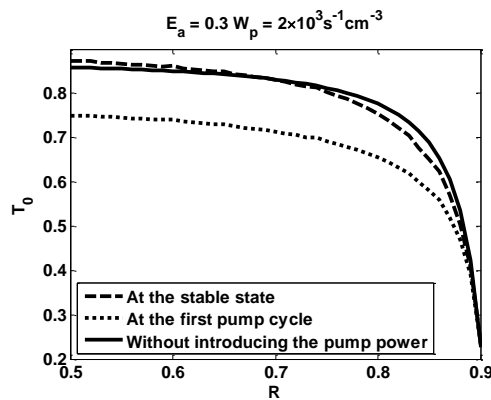
Figure 5.16 For a Nd:YAG laser system, the coupling parameter T_{0_1st} , T_{0_stable} (a) - (d) of R to keep $E_a = 0.1$, with N_{Wp_1st} and N_{Wp_stable} (e) - (g) and t_p (d) as W_p is $200 \text{ s}^{-1} \text{ cm}^{-3}$, $300 \text{ s}^{-1} \text{ cm}^{-3}$, $400 \text{ s}^{-1} \text{ cm}^{-3}$ and $1000 \text{ s}^{-1} \text{ cm}^{-3}$



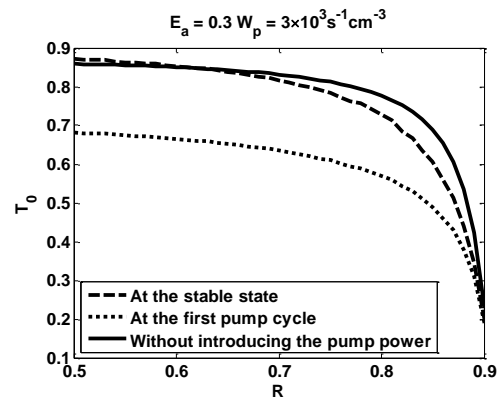
(a)



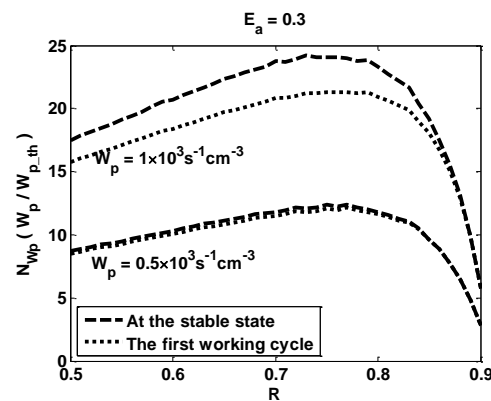
(b)



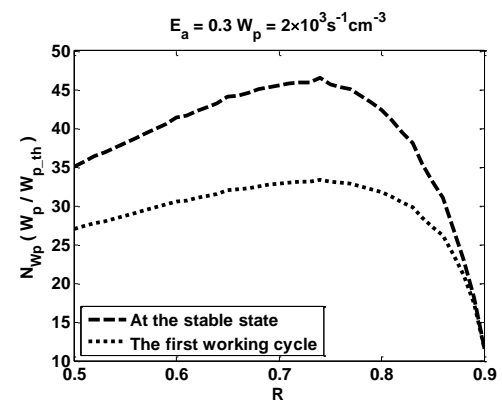
(c)



(d)



(e)



(f)

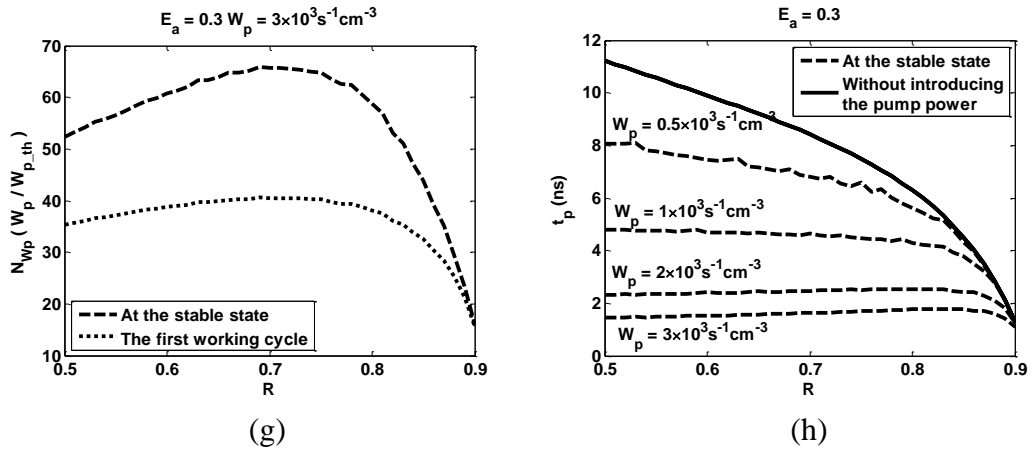
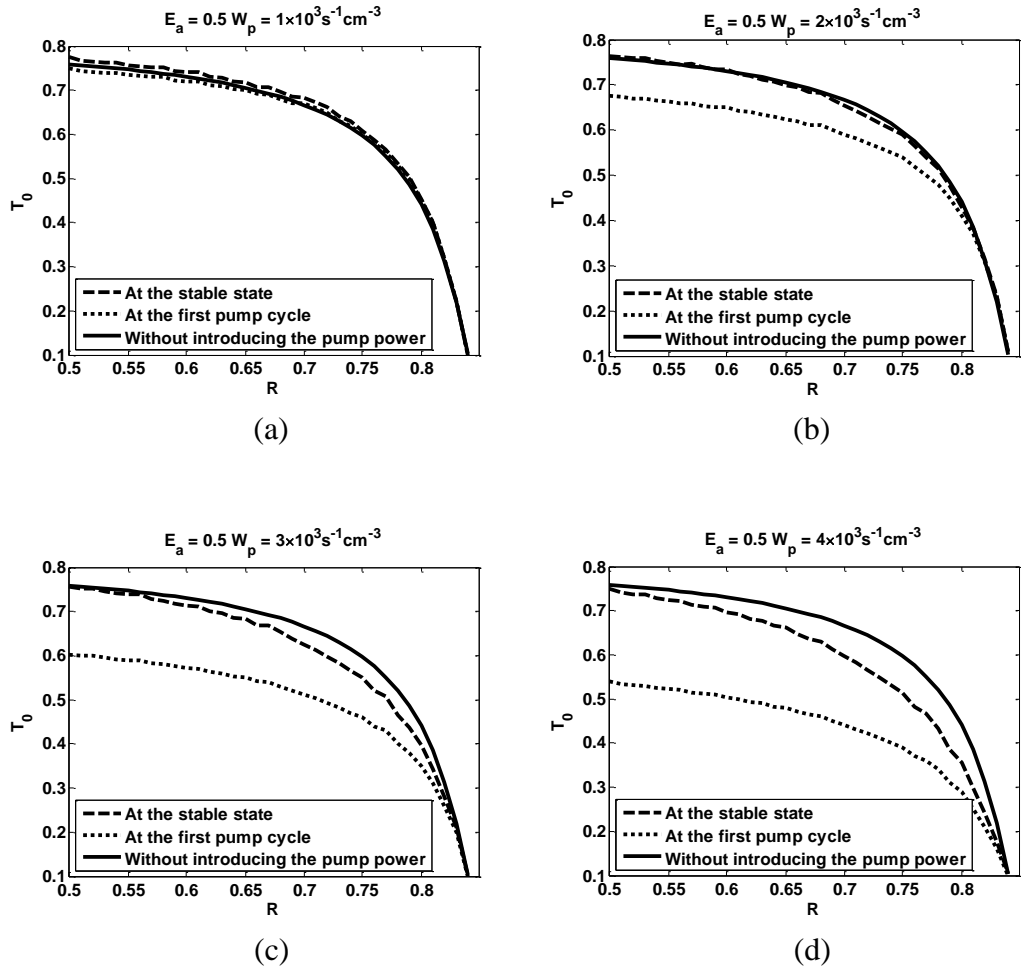


Figure 5.17 For a Nd:YAG laser system, the coupling parameter T_{0_1st} , T_{0_stable} (a) - (d) of R to keep $E_a = 0.3$, with N_{Wp_1st} and N_{Wp_stable} (e) - (g) and t_p (d) as W_p is $500 \text{ s}^{-1} \text{ cm}^{-3}$, $1000 \text{ s}^{-1} \text{ cm}^{-3}$, $2000 \text{ s}^{-1} \text{ cm}^{-3}$ and $3000 \text{ s}^{-1} \text{ cm}^{-3}$



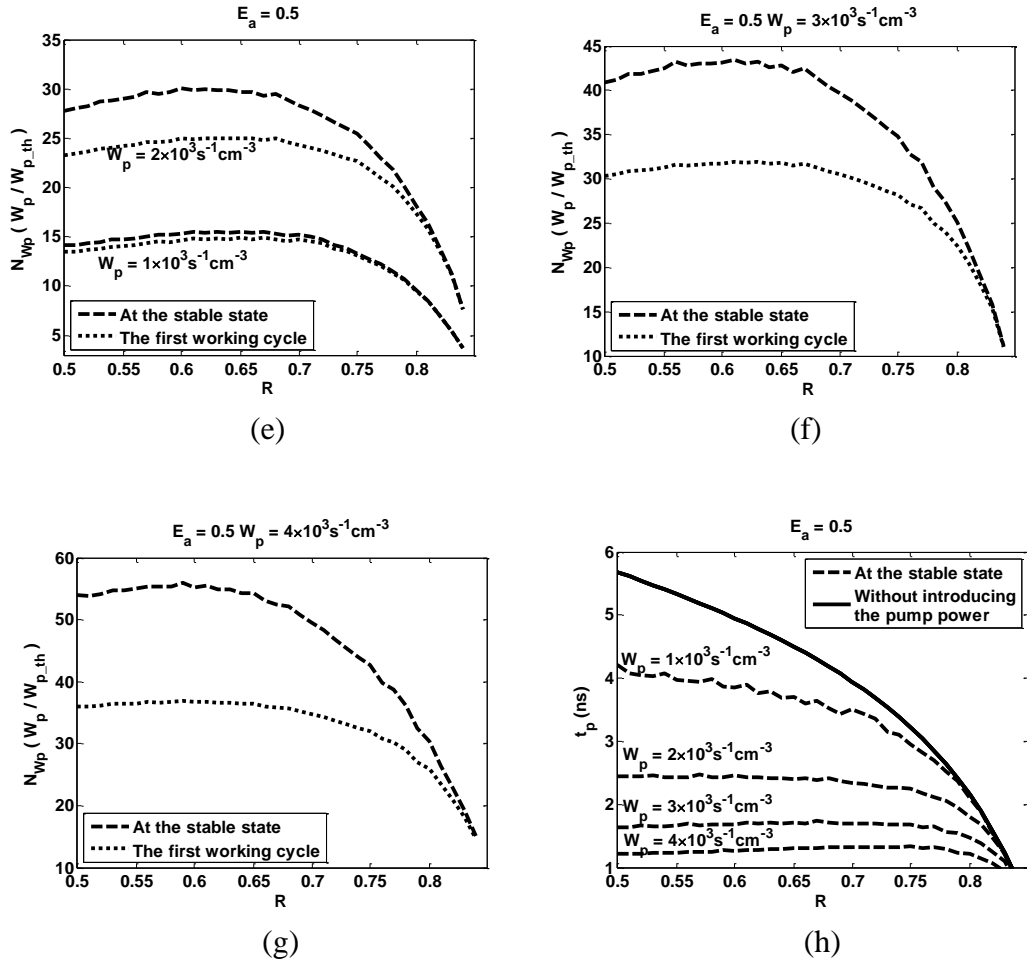


Figure 5.18 For a Nd:YAG laser system, the coupling parameter T_{0_1st} , T_{0_stable} (a) - (d) of R to keep $E_a = 0.5$, with N_{Wp_1st} and N_{Wp_stable} (e) - (g) and t_p (d) as W_p is $1000s^{-1}cm^{-3}$, $2000s^{-1}cm^{-3}$, $3000s^{-1}cm^{-3}$ and $4000s^{-1}cm^{-3}$

The distributions of the average photon density in the laser cavity during the pulse stage $\phi(t)$ for different pump rates W_p obtained using *Model I and Model III* are shown in Figs. 5.19 - 5.22. Here, the values of the output energy parameter E_a are 0.08, 0.1, 0.3 and 0.5, and the output reflectivity R is 50%. As with the Yb:YAG laser system, it is noted that when the output energy parameter E_a and the output reflectivity R are pre-determined, the peak point of $\phi(t)$ for the Nd:YAG laser shown in Figs. 5.19 - 5.22 has a smaller value at the stable working state than in the first working cycle, but it is still larger than the

one obtained using *Model I*. The peak point of $\phi(t)$ obtained using *Model III* increases as the pump rate increases.

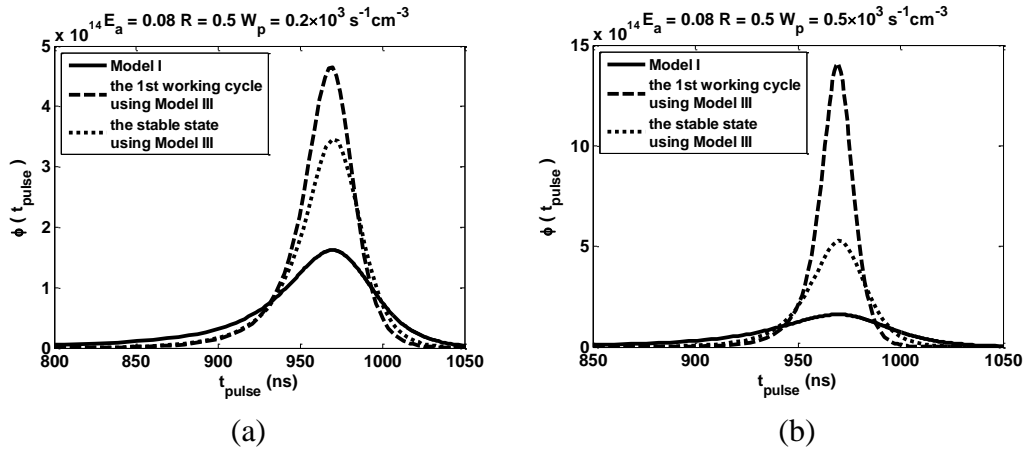


Figure 5.19 For a Nd:YAG laser system, when R is 50% and E_a is 0.08, the distribution of the average photon densities in the laser cavity $\phi(t)$ obtained using *Model I* and using *Model III* for the cases when W_p is (a) $200 \text{ s}^{-1} \text{ cm}^{-3}$, (b) $500 \text{ s}^{-1} \text{ cm}^{-3}$.

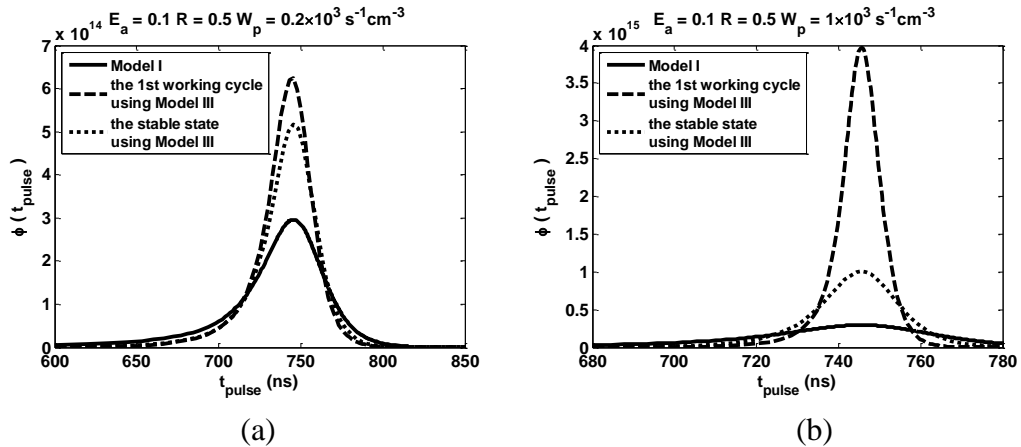


Figure 5.20 For a Nd:YAG laser system, when R is 50% and E_a is 0.1, the distribution of the average photon densities in the laser cavity $\phi(t)$ obtained using *Model I* and using *Model III* for the cases when W_p is (a) $200 \text{ s}^{-1} \text{ cm}^{-3}$, (b) $1 \times 10^3 \text{ s}^{-1} \text{ cm}^{-3}$.

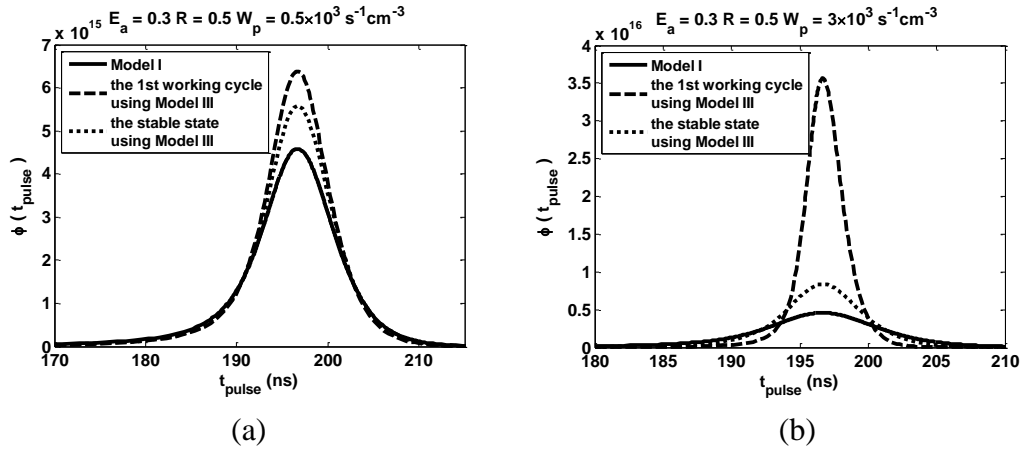


Figure 5.21 For a Nd:YAG laser system, when R is 50% and E_a is 0.3, the distribution of the average photon densities in the laser cavity $\phi(t)$ obtained using *Model I* and using *Model III* for the cases when W_p is (a) $500 \text{ s}^{-1} \text{ cm}^{-3}$, (b) $3 \times 10^3 \text{ s}^{-1} \text{ cm}^{-3}$.

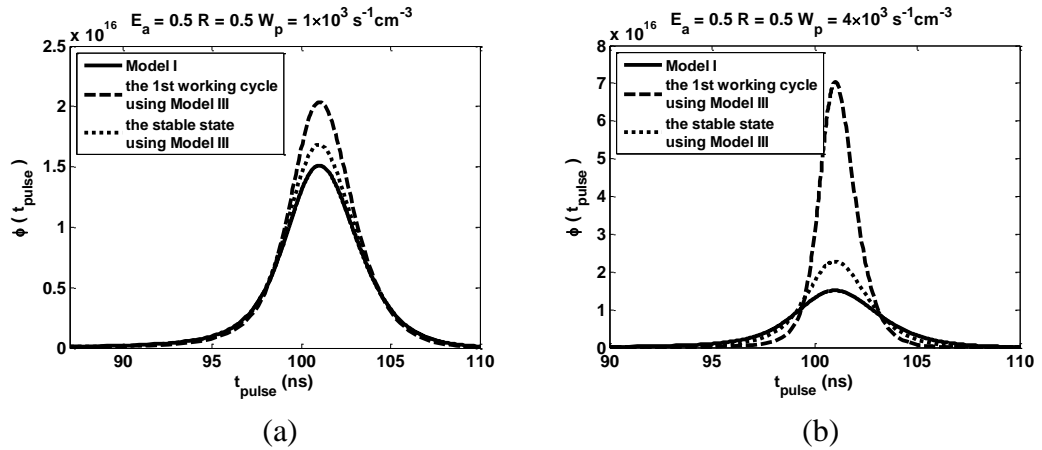


Figure 5.22 For a Nd:YAG laser system, when R is 50% and E_a is 0.5, the distribution of the average photon densities in the laser cavity $\phi(t)$ obtained using *Model I* and using *Model III* for the cases when W_p is (a) $1 \times 10^3 \text{ s}^{-1} \text{ cm}^{-3}$, (b) $4 \times 10^3 \text{ s}^{-1} \text{ cm}^{-3}$.

5.7 Conclusions

In this chapter, *Model III* is set up to study the effect of the recovery time of an absorber on the output performance of a passively Q -switched solid-state laser and the selection of the output reflectivity and initial transmission pair. In *Model III*, the Runge-Kutta method is applied to solve the laser rate equations.

The effect of the recovery time of an absorber on the population of the atoms in the absorber's excited state, when the pump power is relatively high, results in the value of the initial transmission of an absorber at the stable working state of a laser system being bigger than the performance value of an absorber at the beginning of the first working cycle. It is noted that the product-design-value of an absorber is decided by the doping percentage and the absorber material, but the working initial transmission value of an absorber results from both the product-design-value of an absorber and the pump power. Hence, for different pump power, an absorber has different working initial transmission. The difference between the working value of an absorber's initial transmission and the product-value of an absorber increases as the pump power increases. As the output energy and the pump power are held to different constant values, the differences between the working value and the performance value of the initial transmission of an absorber decrease if the output reflectivity increases.

Compared with *Model I*, the values of the FWHM pulse width obtained using *Model III* are much shorter when the output reflectivity is relatively low. The influences of both the pump rate and the recovery time of absorber leads to this result. This phenomenon is more pronounced when the parameter α is small.

The curve of the FWHM pulse width obtained using *Model III* converges on the curve obtained with *Model I* as the output reflectivity increases.

Compared with *Model II*, *Model III* has a higher practical working initial transmission which results in a longer FWHM pulse width.

Chapter 6

Conclusions and Future work

6.1 Introduction

The laser was a remarkable technical breakthrough that plays an important role in modern life. The major applications of lasers are mostly based on the output characteristics which include average and peak power, pulse width, pulse repetition rate, wavelength, and mode. A passively Q -switched solid-state laser is a common laser system used to obtain short, high-peak-power laser pulses with a high repetition rate. Such passively Q -switched lasers can be used for micro-machining, material processing, nonlinear optics etc. Passively Q -switched lasers can also produce long-pulse-duration, high-pulse-power pulses with low repetition rates, and are used for tattoo removal and the removal/reduction of hyper-pigmentation. The flexibility of passively Q -switched lasers stem from the fact that they can have particular performance characteristics to satisfy different requirements. Hence, the study of how to control the output pulse and at the same time not to affect the output energy is an important research subject for passively Q -switched solid-state lasers.

With the development of the technology and the requirements of the industry, a continuous wave (CW) diode pumping system has become a widely used pumping source for laser systems. As shown in Refs. [Langrock, 2002], [Li, 2004], [Li, 2005b], and [Mercer, 2007], the pumping power affects the laser output pulse characteristics, and cannot be ignored in the study of the laser's output parameters. In this thesis the research focuses on how the output pulse duration is affected by the output reflectivity and initial transmission pair for different boundary conditions, especially the pumping power and gain material.

6.2 Conclusions

The output properties of a passively Q -switched laser system are strongly influenced by the following factors: 1) the pump power, 2) the length of the laser

resonator, 3) the gain media and its size, 4) the material and size of the saturable absorber, 4) the output coupler, and 5) the initial transmission of the absorber.

Theoretically, the easiest and most direct way to control the FWHM pulse duration is to control the length of the laser cavity for the case when the pump power, the gain media and the absorber are already selected. However, two practical requirements restrict this method; one is that for some applications the size of the laser must be limited, the other is the cost of the products. Hence, to reduce or control the FWHM pulse duration to a required value, the most convenient and low-cost method, stemming from the factors affecting the output performance characteristics, is to select a proper pair of resonator output reflectivity and initial transmission of an absorber for the case when the laser resonator, the pump power, the gain media and the absorber are already decided. Otherwise, choosing an appropriate gain medium can reduce the size of the laser cavity and maintain the desirable output energy, which can also be used to control the FWHM pulse duration.

6.2.1 Models and their boundary conditions

To study the effect of the output reflectivity and initial transmission on the output characteristics of a passively Q -switched solid-state laser, models based on the laser rate equations have been created for different boundary conditions. Two of the main parameters affecting the models are: 1) the length of the build-up time of Q -switching; and 2) the recovery time of the absorber. The recovery time of an absorber is defined as the time duration between the end of the previous pulse and the beginning of the current Q -switch, and nearly equal to the pumping time. The models have been constructed to study factors influencing the FWHM pulse duration for the case when the output energy is set to different fixed values.

According to the operating principle of a continuously pumped passively Q -switched laser, the laser working cycle contains two stages, the pumping stage

and the pulse stage. The first factor: the length of the build-up time of Q -switching, demonstrates the effect of the pumping power on the output characteristics at the pulse stage. The second factor, the recovery time of an absorber, affects the ground level population density of the absorber at the beginning of Q -switching; this controls an absorber's initial transmission, and furthermore influences the initial conditions for Q -switching. Hence, the second influence has to be considered at the pumping stage.

Model I satisfies the following conditions: 1) the build-up time of the Q -switched laser pulse is quite short compared with the pumping and relaxation times of the laser medium; and 2) the recovery time of the absorber (nearly equals the reciprocal of the repetition rate of the laser system) is quite long compared with the relaxation time of an absorber. The first condition leads to the result that the effect of the pumping power on the output characteristics at the pulse stage can be neglected. The relatively long recovery time of the absorber allows most of the absorber's atoms excited to the excited state to return to the ground level at the beginning of each pulse stage, this results in nearly the same value of the absorber's initial transmission, and guarantees each pumping and pulse cycle of the laser has virtually the same initial conditions. It means that the recovery time of the absorber doesn't have much influence on the output characteristics; therefore, the pumping stage doesn't affect the output of the laser system. Hence, the simplified laser rate equations at the pulse stage are used to build up *Model I* and study the output performance of a passively Q -switched laser.

In *Model I*, integrating the simplified laser rate equations yields the mathematical expressions for the initial conditions of lasing and the following parameters: the final inversion population density of the gain medium, the instantaneous inversion population density at the output power's peak point, the average photon density in the laser resonator, the instantaneous inversion population density of the gain medium, and the instantaneous population density of an absorber at the ground level. As shown in Chapter 1, the output characteristics of a laser, i.e.: the

output energy, the peak power and the approximate FWHM pulse width, can be evaluated using these parameters. Hence, for a practical laser system where the properties of the laser resonator are known, the values of these parameters can be calculated, and then substituted into the expressions to obtain the laser output characteristics. This has practical value for a laser designer.

Model II studies the FWHM pulse duration for the case when the build-up time of the Q -switched laser pulse is relatively long, and the repetition rate of the laser system is slow compared with the relaxation time of the absorber's upper level. In this case, the pump power has an influence on the output characteristics at the pulse stage. The initial conditions of each working cycle of the laser system is still supposed to be the same, which is the same as *Model I*. Compared with *Model I*, the laser rate equations for *Model II* must contain the pump power. Hence, the mathematical expressions of several variables, such as the final inversion population density of the gain medium, the average photon density in the laser resonator, the instantaneous inversion population density of the gain medium, and the instantaneous population density of an absorber at the ground level, cannot be given directly. For this situation, the study of the FWHM pulse duration is by the following steps: 1) compute the numerical results of the output characteristics of several practical passively Q -switched solid-state laser systems by using the Runge-Kutta method to solve the laser rate equations, 2) generalise the simulation data to obtain the general conclusions, which are suitable for other laser systems.

Model III is built up under the assumption that the repetition rate of the laser is very rapid compared with the relaxation time of the absorber's upper level. In this case, a fraction of the atoms excited to the absorber's upper level in the previous working cycle cannot return to the ground level in time for the beginning of next Q -switching; therefore, the value of the absorber's initial transmission for the next Q -switching is changed, and the corresponding initial condition for the next Q -switching is different compared with the last Q -

switching. When the initial condition of next Q -switching is changed, the output characteristics of the laser system vary as well. For this case, the laser system is in an unstable working state because different Q -switching events have different initial conditions and output. After several working cycles, the action and reaction between the recovery time of the absorber and the initial condition of Q -switching will reach equilibrium, and the laser system will have nearly the same input parameters and almost unvaried output performance characteristics. This means that the laser system is working in a stable state. The process whereby that the laser system reaches its stable working state shows that the output characteristics of the laser system are influenced by the recovery time of the saturable absorber. Compared with *Model I* and *Model II*, the laser system satisfying the assumptions of *Model III* spends a much longer time reaching its stable working state, the initial transmission and the initial inversion population density of the gain medium at the stable state are not the same as those at the beginning of the first working cycle. Hence, in *Model III*, the study of the pumping cycle shows the working value of the absorber's initial transmission in the stable state.

As with *Model II*, generalizing the simulation results of several practical passively Q -switched laser systems yields general conclusions concerning the FWHM pulse duration. The Runge-Kutta method is used to solve the laser rate equations when considering the pumping power.

It is noted that *Model I* works well for the cases when 1) the pump power is relatively low compared with the threshold pump power, and the FWHM pulse duration of a laser system is relatively short; or 2) the pump power is high, but the FWHM pulse duration of a laser system is very short. *Model II* can solve the problems in the situation when the pump power isn't too high, and the FWHM pulse duration is relatively long. When the pump power is very high compared with the threshold pump power, *Model III* is suitable.

6.2.2 Controlling the FWHM pulse duration

For all of the models (*Model I, II and III*), the following conclusions are drawn:

- 1) When the pump power, the output energy, the laser cavity, the gain media and the absorber's material are pre-selected,
 - a) To maintain the pre-determined output energy, a high output reflectivity has a small coupling absorber initial transmission, and a small output reflectivity has a big coupling absorber initial transmission;
 - b) A shorter FWHM pulse duration can be obtained by selecting the output coupler with higher reflectivity;
- 2) When the pump power, the laser cavity, the gain media and the absorber are decided,
 - a) To maintain higher output energy, the available range of output reflectivities is reduced;
 - b) A shorter FWHM pulse duration can be produced by the laser system which has a higher output energy; for the case when the output reflectivity is selected, its coupling absorber initial transmission is smaller than one for the low output energy;
 - c) When the output reflectivity is close to its maximum value, the differences between the FWHM pulse durations for different output energies reduce;
- 3) When the laser cavity and the absorber material are decided, to maintain a higher output energy parameter E_a , the material parameter α is bigger; the available range of the output reflectivity and its coupling absorber initial transmission is greater;
- 4) If the output energy parameter E_a is very high, selecting the proper gain media and absorber to get a bigger material parameter α and a smaller γ_s' (which is decided by the absorber, and defined in Eq. 2.16) can enlarge the available range of the output reflectivity and its coupling absorber initial transmission, and provide a feasible laser system.

Comparing *Model I* with *Model II* the following conclusions can be drawn:

- a) The coupling absorber's initial transmission for a selected output reflectivity obtained by *Model II* is close to that obtained by *Model I*;
- b) The FWHM pulse duration of a selected output reflectivity using *Model II* is smaller than that predicted using *Model I*;
- c) The available range of output reflectivity is limited by the magnitude of the pump rate; a laser system with a higher pump rate has a smaller available range of output reflectivity;
- d) For a selected output reflectivity, the higher pump rate results in a shorter FWHM pulse duration, but the difference decreases when the output reflectivity is close to its highest value;

Model III is required when the repetition rate is high; the initial absorber transmission at the laser's stable working state is different compared to the value at the first working cycle. Hence, the working value and the product-design-value of an absorber's initial transmission are determined in *Model III*. The working value is bigger than the product-design-value, and controlled by both the product-design-value of the absorber and the pump power. It is found that:

- a) When the pump power is high, and the output reflectivity is low, the difference between the absorber working value and the product-design-value of an absorber's initial transmission is large;
- b) For a fixed pump power, the difference between the coupling working value and the product-design-value of an absorber's initial transmission decreases when the output reflectivity is close to its maximum value;
- c) When the output reflectivity is low, the FWHM pulse duration obtained using *Model III* are much shorter than that obtained using *Model I*;
- d) The differences between the FWHM pulse durations obtained using *Model I* and *Model III* decreases when the output reflectivity approaches its highest value;
- e) The effect of the pump power on the output performance of a laser system for the case when the laser has a small α is bigger than one with a large α .

Generally, it is noted that in spite of the magnitude of the pump power, the output pulse duration decreases with the increase of the output reflectivity, and the coupling absorber's initial transmission decreases as well. When the output reflectivity reaches its maximum value, the curves obtained using *Model II* and *Model III* approach those obtained using *Model I*. The laser system more easily generates a shorter pulse when the output energy required has a high value.

Once the output reflectivity is determined, the working initial transmission of an absorber in the stable working state increases as the pump power increases. The difference between the product-value and the actual working value of the initial transmission increases as well. At the same time, the pulse duration of the laser system is shortened.

6.2.3 Programs and their run time

All of the three models are built by Matlab. In *Model II* and *Model III*, the Runge-Kutta method, which is used to solve the laser rate equations (three differential equations), is implemented by the function "ode45". The syntax of this function is $[T, Y] = \text{ode45}(\text{odefun}, \text{tspan}, y_0)$. Here, *odefun* is a function handle that evaluates the right side of the differential equations, *tspan* is a vector specifying the interval of integration, *y0* is a vector of initial conditions, *T* is a vector of time points, and *Y* is the solution array. The default relative and absolute tolerances are $1e-3$ and $1e-6$, respectively.

For all of the models (*Model I, II* and *III*), the input variables were the properties of gain medium and absorbing material, the properties of laser resonator, the reflectivity index of output mirror, and the required output energy. The output results of program are the coupling initial transmission of absorber, the instantaneous inversion population density of gain medium, the instantaneous population density of absorber's ground level, the instantaneous average photon density in laser cavity, the peak power and the output FWHM pulse duration.

The run times of programs for the three models have great differences. When the required parameters are inputted into programs, the run time of program for *Model I* is shortest (nearly real-time), while the program's run time for *Model III* is longest (to get a group of outputs, the run time is approximately 3-4 minutes). Hence, although *Model III* is a general model which is applicable to all the pump rates, *Model I* and *Model II* have their advantages of the shorter run time of modelling.

6.3 Further work

Although the models work well in analyzing the pulse duration of the continuously pumped passively *Q*-switched solid-state laser when the output energy is pre-determined, there are still several areas of activity which would improve the laser model.

- 1) In this thesis, the spatial distribution of the intra-cavity photon density isn't considered. To obtain a more accurate and general model, the spatial distribution and the longitudinal variation of the photon density can be introduced into the model.
- 2) With low resonator output reflectivity a very high population inversion density is generated, this leads to significant amplified spontaneous emission prior to lasing. This should be considered in the model in the near future.
- 3) For a continuously pumping passively *Q*-switched laser, thermal lensing will affect the output of the laser system and can be considered in the models.
- 4) Using a pulsed pumping source is another pump style besides the continuously pumping source, and also used for the passively *Q*-switched laser system. Pulsed pumped passively *Q*-switched lasers have advantages in reducing the thermal lens effect, easy control of the repetition rate, etc., and have nearly the same applications as the continuously pumped

passively Q -switched laser systems. Normally the pulsed pumped passively Q -switched lasers are used for drilling and shock-peening of materials. Hence, the models can be modified to study the FWHM pulse duration of a pulsed pumped passively Q -switched laser system in the future.

- 5) A GUI (*graphical user interface*) can be created to help the designer to get the FWHM pulse duration in the future. It should give the values of the initial transmission of the absorber and the FWHM pulse duration after the following steps: a) key in the properties of the laser cavity, b) key in the material properties of the gain media and the absorber, c) key in the required output energy, d) key in the pump power, e) key in the output reflectivity.

Appendix A

The Lagrange Multiplier Technique

The Lagrange multiplier technique is the most frequently used method for finding the extrema (maxima and minima) of a function subject to constraints, and is a useful technique in multivariable calculus.

A real-valued function $f(x_1, x_2, \dots, x_n)$ is defined on an open set Ω in \mathbb{R}^n , and has a gradient $\nabla f(x) = (\partial f / \partial x_1, \partial f / \partial x_2, \dots, \partial f / \partial x_n)$ at each point of Ω . The necessary condition on extremum (maximum or minimum) is that the gradient ∇f is equal to zero at any local extremum

$$\nabla f(x) = 0. \tag{A.1}$$

The local extrema of $f(x_1, x_2, \dots, x_n)$ in Lagrange multiplier technique is subject to a constraint

$$g(x_1, x_2, \dots, x_n) = c. \tag{A.2}$$

Then, the Lagrangian function can be written as:

$$L(x, \lambda) = f(x) + \lambda[g(x) - c] \tag{A.3}$$

where, the new variable λ which is a constant is called the Lagrange multiplier, and $\lambda \in \mathbb{R}$.

Partially differentiate the Lagrangian function by all of the variables and set them equal to zero yields the following equations:

$$\begin{aligned}\frac{\partial L(x_1, x_2, \dots, x_n, \lambda)}{\partial x_1} &= 0 \\ \frac{\partial L(x_1, x_2, \dots, x_n, \lambda)}{\partial x_2} &= 0 \\ &\vdots \\ \frac{\partial L(x_1, x_2, \dots, x_n, \lambda)}{\partial x_n} &= 0 \\ \frac{\partial L(x_1, x_2, \dots, x_n, \lambda)}{\partial \lambda} &= 0\end{aligned}\tag{A.4}$$

Finally, the extremum is found by solving the set of the equations (Eq. A.4).

Appendix B

Material Properties

In Appendix B, the properties of the materials used in the thesis are introduced in detail.

B.1 Nd:YAG

Nd:YAG ($\text{Nd:Y}_3\text{Al}_5\text{O}_{12}$) is one of the most commonly used materials in commercial solid-state lasers. The properties of Nd:YAG are listed in Table B.1.

Table B.1 Properties of Nd:YAG at 25°C (with 1% Nd doping)

Weight % Nd	0.725
Atom % Nd	1
Nd (cm^{-3})	1.38×10^{20}
Melting point (°C)	1970
Knoop hardness	1215
Density (g/cm^3)	4.56

Rupture stress (kg/cm^2)	$1.3 - 2.6 \times 10^3$
Young's modulus ($K g/mm^{-2}$)	3.17×10^4
Thermal conductivity ($W cm^{-1} K^{-1}$)	0.14
Specific heat capacity ($J g^{-1} K^{-1}$)	0.59
Thermal expansion coefficient (K^{-1})	7.8×10^{-6} (at $\langle 111 \rangle$)
Poisson's ratio	0.25
Resistance to thermal shock ($W m^{-1}$)	790
Index of refractive	1.82 (at $1.0 \mu m$)
Radiative lifetime (${}^4F_{3/2} \rightarrow {}^4I_{11/2}$) (μs)	550
Relaxation time (${}^4I_{11/2} \rightarrow {}^4I_{9/2}$) (μs)	30
Emission wavelength (nm)	1064
Spontaneous fluorescence lifetime (μs)	230
Stimulated emission cross section (cm^2)	6.5×10^{-19}
$\partial n / \partial T$ (K^{-1})	7.3×10^{-6}

B.2 Yb:YAG

Yb:YAG is a quasi-three-level system, and is more suitable for diode-pumping than the traditional Nd-doped systems. It has become an important laser material. The properties of Yb:YAG are listed in Table B.2.

Table B.2 Properties of Yb:YAG (with 1% Yb doping)

Atom % Nd	1
Yb (cm^{-3})	1.38×10^{20}
Melting point ($^{\circ}C$)	1970
Mohs hardness	1215
Density (g/cm^3)	4.56
Thermal conductivity ($W\ cm^{-1}\ K^{-1}$)	0.14
Thermal expansion coefficient (K^{-1})	7.8×10^{-6} (at $\langle 111 \rangle$)
Index of refractive	1.82 (at $1.0\ \mu m$)
Laser transition	$^2F_{5/2} \rightarrow ^2F_{7/2}$
Fluorescence lifetime (μs)	1200
Emission wavelength (nm)	1030
Emission linewidth (nm)	9
Stimulated emission cross section (cm^2)	2.1×10^{-20}
Pump absorption band width (nm)	8
Loss Coefficient (cm^{-1})	0.003

B.3 Cr:YAG

Cr:YAG is an excellent material used as an active media for continuously diode pumped or pulsed pumped passively Q-switched solid-state laser with operating wavelength at 950 - 1100 nm. The properties of Cr:YAG are listed in Table B.3.

Table B.3 Properties of Cr:YAG

Mohs hardness	8.5
Density (g/cm^3)	4.56
Dopant level (mol%)	0.5 - 3
Thermal conductivity ($W\ cm^{-1}\ K^{-1}$)	0.12
Index of refractive	1.82 (at 1.064 μm)
Absorption band (nm)	900 - 1150
Emission band (nm)	1340 - 1580
Ground state absorption cross section (cm^2)	7×10^{-18}
Excited state absorption cross section (cm^2)	2×10^{-18}
Upper level life time (μs)	4.1
$\partial n / \partial T$ (K^{-1})	8.0×10^{-6}

References

[Agnesi, 1998] A. Agnesi, S. Dell'Acqua, E. Piccinini, G. Reali, G. Piccinno. Efficient wavelength conversion with high-power passively Q -switched diode-pumped neodymium lasers. *IEEE Journal of Quantum Electronics*, 34: 1480-1484, 1998.

[Agnesi, 2000] A. Agnesi, S. Dell'Acqua, G. Reali. Diode-pumped quasi-cw intracavity optical parametric oscillator at 1.57 μm with efficient pulse shortening. *Applied Physics B: Lasers and Optics*, 70: 751-753, 2000.

[Aldag, 2005] Henry R. Aldag and David H. Titterton. From flashlamp-pumped liquid dye lasers to diode-pumped solid-state dye lasers. *Proceedings of SPIE Photonics West (San Jose, CA)*, 5707: 194-207, January 2005.

[Alferov, 1970] Zh. I. Alferov, V. M. Andreev, D. Z. Garbuzov, Yu. V. Zhilyaev, E. P. Morozov, E. L. Portnoi, and V. G. Trofim. Effect of the heterostructure parameters on the laser threshold current and the realization of continuous generation at room temperature. *Fiz. Tekh. Poluprovodn.*, 4: 1826-1829, 1970, English translation, in *Sov. Phys. Semicond.*, 4:1573-1575, 1971.

[Andrews, 1997] M. R. Andrews, C. G. Townsend, H. J. Miesner, D. S. Durfee, D. M. Kurn, and W. Ketterle. Observation of interference between two Bose condensates. *Science*, 275: 637-641, 1997.

[Arkin, 2002] William T. Arkin. *Advances in laser and optics research, Volume 2*. Nova Publishers, 2002.

[Arnold, 1973] S. J. Arnold, and H. Rojeska. Chemical lasers: a comprehensive literature survey. *Applied Optics*, 12: 169, 1973.

- [Asaki, 1993] M. T. Asaki, C. Huang, D. Garvey, J. Zhou, H. C. Kapteyn, M. M. Murnane. Generation of 11-fs pulses from a self-mode-locked Ti:Sapphire laser. *Optics Letters*, 18: 977-979, 1993.
- [Atkinson, 1976] K. Atkinson. An automatic program for linear Fredholm integral equations of the second kind. *ACM Transactions on Mathematical Software*, 2: 154-171, 1976.
- [Atkinson, 2008] K. E. Atkinson, and L. F. Shampine. Algorithm 876: Solving Fredholm Integral Equations of the Second Kind in Matlab. *ACM Transactions on Mathematical Software*, 34 (4), 2008.
- [Backus, 1997] S. Backus, C. G. Durfee III, G. Mourou, H. C. Kapteyn, and M. M. Murnane. 0.2-TW laser system at 1 kHz. *Optics Letters*, 22: 1256-1258, 1997.
- [Bass, 2003] M. Bass, L. S. Weichman, S. Vigil, B. K. Brickeen. The temperature dependence of Nd³⁺ doped solid-state lasers. *IEEE Journal of Quantum Electronics*, 39: 741-748, 2003.
- [Basov, 1964] N. G. Basov. Semiconductor lasers. *Nobel Lecture*, December, 1964.
- [Basov, 1970] N. G. Basov, V. A. Danilychev, Y. Popov, and D. D. Khodkevich. Laser for vacuum region of the spectrum with excitation of liquid xenon by an electron beam. *Zh. Eksp. Fiz. i Tekh. Pis'ma. Red.*, 12: 473-474, 1970.
- [Baues, 1968] P. Baues. Huygens' principle in inhomogenous, isotropic media and a general integral equation applicable to optical resonators. *Opto-Electronics*, 1: 37-44, 1969.
- [Beach, 2001] R. J. Beach, S. C. Mitchell, H. E. Meissner, O. R. Meissner, W. F. Krupke, J. M. McMahon, W. J. Bennett, D. P. Shepherd. Continuous-wave and passively *Q*-switched cladding-pumped planar waveguide lasers. *Optics Letters*, 26: 881-883, 2001.
- [Bertolotti, 1983] M. Bertolotti. *Mases and lasers: A historical approach*. Adam Hilger, Ltd., Bristol 1983.
- [Bova, 2002] Ben Bova. *The story of light*. Sourcebooks Inc., 2002.

- [Boyraz, 2004] O. Boyraz and B. Jalali. Demonstration of a silicon Raman laser. *Optics Express*, 12: 5269-5273, 2004.
- [Brackmann, 2000] Ulrich Brackmann. *Laser dyes*. Lambda Physik AG, the third edition, 2000.
- [Brown, 1998] D. C. Brown. Nonlinear thermal distortion in YAG rod amplifiers. *IEEE Journal of Quantum Electronics*, 34: 2383-2382, 1998.
- [Carrasco, 2003] M. Carrasco, J. Florens and E. Renault. Estimation of the Solution of an Integral Equation of the Second Kind. (Mimeo) <http://idei.fr/display.php?a=1045>.
- [Chen, 2000a] J. Chen, H. F. Yau, H. P. Liu, T. C. Chen, F. M. Liu. Passive Q -switch and mode-locking modulators for Nd: hosted lasers. *Optics Laser Technology*, 32: 215-219, 2000.
- [Chen, 2001b] Y. F. Chen, Y. P. Lan, H. L. Chang. Analytical model for design criteria of passively Q -switched lasers. *IEEE Journal of Quantum Electronics*, 37: 462-468, 2001.
- [Chen, 2001] Y. Chen and S. W. Tsai. Simultaneous Q -Switching and mode-locking in a diode-pumped Nd :YVO₄-Cr⁴⁺ :YAG laser. *IEEE Journal of Quantum Electronics*, 37: 580-586, April 2001.
- [Chen, 2002] Y. Chen, J. Lee, H. Hsieh and S. Tsai. Analysis of passively Q -switched lasers with simultaneous modelocking. *IEEE Journal of Quantum Electronics*, 38: 312-317, March 2002.
- [Cheo, 1989] Peter K. Cheo. *Handbook of solid-state lasers*. Marcel Dekker, 1989.
- [Chiang, 2004] A. Chiang, T. Wang, Y. Lin, C. Lau, etc.. Pulsed optical parametric generation, amplification, and oscillation in monolithic periodically poled lithium niobate crystals. *IEEE Journal of Quantum Electronics*, 40: 791-799, 2004.
- [Degnan, 1995] J. J. Degnan. Optimization of passively Q -switched lasers. *IEEE Journal of Quantum Electronics*, 31: 1890-1901, 1995.

- [Dingle, 1974] R. Dingle, W. Wiegmann, and C. H. Henry. Quantum States of Confined Carriers in Very Thin $\text{Al}_x\text{Ga}_{1-x}\text{As}$ -GaAs- $\text{Al}_x\text{Ga}_{1-x}\text{As}$ Heterostructures. *Physical Review Letters*, 33: 827-830, 1974.
- [Dong, 1993] S. Dong, Q. Lu, I. Lancranjan. 220 W average output power a Q -switching Nd:YAG slab laser with a LiF:F^{2-} crystal. *Optics Laser Technology*, 25: 175-178, 1993.
- [Dong, 2001] J. Dong, P. Deng, Y. Liu, Y. Zhang, J. Xu, W. Chen and X. Xie. Passively Q -switched Yb: YAG laser with Cr^{4+} : YAG as the saturable absorber. *Applied Optics*, 40: 4303-4307, 2001.
- [Dong, 2003] J. Dong. Numerical modeling of CW-pumped repetitively passively Q -switched Yb:YAG lasers with Cr:YAG as saturable absorber. *Optics Communication*, 226: 337-344, 2003.
- [Drexhage, 1972] K. H. Drexhage, U. T. Muller-Westerhoff. New Q -switch compounds for infrared lasers. *IEEE Journal of Quantum Electronics*, QE-8: 759, 1972.
- [Erneux, 2010] Thomas Erneux, and Pierre Glorieux. *Laser dynamics*. Cambridge University Press, 2010.
- [Faist, 1994] J. Faist, F. Capasso, D. L. Sivco, C. Sirtori, A. L. Hutchinson, and A. Y. Cho. Quantum cascade laser. *Science*, 264: 553-556, 1994.
- [Fan, 2006] S. Fan, X. Zhang, Q. Wang, S. Li, S. Ding, F. Su. More precise determination of thermal lens focal length for end-pumped solid-state lasers. *Optics Communications*, 266: 620-626, 2006.
- [Fang, 2006] A. W. Fang, H. Park, R. Jones, O. Cohen, M. J. Paniccia, J. E. Bowers. A Continuous-Wave Hybrid AlGaInAs-Silicon Evanescent Laser. *IEEE Photonics Technology Letters*, 18: 1143-1145, 2006.
- [Feng, 2004] Y. Feng, J. Lu, K. Takaichi, K. Ueda, H. Yagi, T. Yanagitani and A. A. Kaminskii. Passively Q -switched ceramic Nd^{3+} :YAG/ Cr^{4+} :YAG lasers. *Applied Optics*, 43: 2944-2947, May 2004.
- [Findlay, 1966] D. Findlay, R. A. Clay. The measurement of internal losses in 4-level lasers. *Physics Letters*, 20: 277-278, 1966.

- [Fox, 1961] A. G. Fox and T. Li. Resonant modes in a maser interferometer. *Bell System Technical Journal*, 40:453-488, 1961.
- [Geusic, 1964] J. E. Geusic, H. W. Marcos, L. G. Van Uitert. Laser oscillations in Nd-doped yttrium aluminum, yttrium gallium, and gadolinium garnets. *Applied Physics Letters*, 4: 182–184, 1964.
- [Gordon, 1954] J. P. Gordon, H. J. Zeiger, and C. H. Townes. Molecular microwave oscillator and new hyperfine structure in the microwave spectrum of NH_3 . *Physical Review*, 95: 282–284, 1954.
- [Graham, 1985] I. G. Graham. Iterated galerkin versus iterated collocation for integral equations of the second kind. *IMA Journal of Numerical Analysis*, 5: 355-369, 1985.
- [Grivas, 2003] C. Grivas, D. P. Shepherd, T. C. May-Smith, R. W. Eason, M. Pollnau, A. Crunteanu, and M. Jelinek. Performance of Ar^+ -milled Ti:Sapphire rib waveguides as single transverse-mode broadband fluorescence sources. *IEEE Journal of Quantum Electronics*, 39: 501-507, 2003.
- [Hall, 1962] R. N. Hall, G. E. Fenner, J. D. Kingsley, T. J. Soltys, and R. O. Carlson. Coherent light emission from GaAs junctions. *Physical Review Letters*, 9: 366-368, 1962.
- [Hecht, 1992] Jeff Hecht. *Laser pioneers*. Academic Press, 2nd Revised edition, 1992.
- [Hercher, 1967] M. Hercher. An analysis of saturable absorbers. *Applied Optics*, 6: 947-954, 1967.
- [Holonyak Jr. 1962] N. Holonyak Jr., and S. F. Bevacqua. Coherent (Visible) light emission from Ga (As_{1-x}Px) junctions. *Applied Physics Letters*, 1: 82-83, 1962.
- [Hong, 2006] K. Hong, S. Kostritsa, T. Yu, J. Sung, I. Choi, Y. Noh, D. Ko, and J. Lee. 100-kHz high-power femtosecond Ti:sapphire laser based on downchirped regenerative amplification. *Optics Express*, 14: 970-978, 2006.
- [Hsieh, 1977] J. H. Hsieh and C. C. Shen. Room-temperature cw operation of buried-stripe double-heterostructure GaInAsP/InP diode lasers. *Applied Physics Letters*, 30: 429–431, 1977.

- [Hua, 1997] J. Hua, L. Liu, G. Li. Observing the fractional Fourier transform by free-space Fresnel diffraction. *Applied Optics*, 36: 512-513, 1997.
- [Huo, 2005a] Y. Huo and P. K. Cheo. Modeling of passively Q -switched $\text{Er}^{3+}/\text{Yb}^{3+}$ -codoped clad-pumped fiber lasers. *IEEE Journal of Selected Topics in Quantum Electronics*, 11: 658-666, 2005.
- [Huo, 2005b] Y. Huo. Modeling and experiments of actively Q -switched $\text{Er}^{3+}-\text{Yb}^{3+}$ -codoped clad-pumped fiber lasers. *IEEE Journal of Quantum Electronics*, 41: 573-580, 2005.
- [Ifflander, 2001] R. Ifflander. *Solid-state lasers for materials processing: fundamental relations and technical realizations*. Springer, 2001.
- [Iga, 1985] K. Iga, S. Ishikawa, S. Ohkouchi, and T. Nishimura. Room temperature pulsed scillation of GaAlAs/GaAs surface emitting junction laser. *IEEE Journal of Quantum Electronics*, QE-21: 663-668, 1985.
- [Iga, 2000] Kenichi Iga. Surface-emitting laser - Its birth and generation of new optoelectronics field. *IEEE Journal on Selected Topics in Quantum Electronics*, 6: 1201-1215, 2000.
- [Il'ichev, 1997] N. N. Il'ichev, E. S. Gulyamova, P. P. Pashinin. Passive Q -switching of a neodymium laser by a Cr^{4+} :YAG crystal switch. *Quantum Electronics*, 27: 972-977, 1997.
- [Ivanov, 2003] E. N. Ivanov, S. A. Diddams, and L. Hollberg. Experimental study of noise properties of a Ti:Sapphire femtosecond laser. *IEEE Transactions on Ultrasonics, Ferroelectrics, and Frequency Control*, 50: 355-360, 2003.
- [Javan, 1961] A. Javan, W. R. Bennett, Jr., and D. R. Herriott. Population inversion and continuous optical maser oscillation in a gas discharge containing a He-Ne mixture. *Physical Review Letters*, 6: 106-110, February 1961.
- [Johnson, 1961] L. F. Johnson and K. Nassau. Infrared fluorescence and stimulated emission of Nd^{3+} in CaWO_4 . *Proc. IRE*, 49: 1704-1705, 1961.
- [Kapon, 1999] Eli Kapon. *Semiconductor Lasers: Materials and structures*. Academic Press, 1999.

- [Kasper, 1965] J. V. V. Kasper, and G. C. F. Pimentel. hCI chemical laser. *Physical Review Letters*, 14: 352-354, 1965.
- [Keyes, 1964] R. J. Keyes and T. M. Quist. Injection luminescent pumping of $\text{CaF}_2:\text{U}^+$ with GaAs diode lasers. *Applied Physics Letters*, 4: 50–52, Feb. 1964.
- [Klinkhammer, 2009] S. Klinkhammer, T. Woggon, U. Geyer, C. Vannahme, S. Dehm, *et al.*. A continuously tunable low-threshold organic semiconductor distributed feedback laser fabricated by rotating shadow mask evaporation. *Applied Physics B: Lasers and Optics*, 97: 787-791, 2009.
- [Koch, 2007] B. R. Koch, J. S. Barton, M. Masanovic, Z. Hu, J. E. Bowers, and D. J. Blumenthal. Monolithic Mode-Locked Laser and Optical Amplifier for Regenerative Pulsed Optical Clock Recovery. *IEEE Photonics Technology Letters*, 19: 641-643, 2007.
- [Koechner, 2003] Walter Koechner, and Michael Bass. *Solid-state lasers: a graduate text*. Springer, 2003.
- [Koechner, 2006] W. Koechner. *Solid-State Laser Engineering*. Springer, sixth revised and updated edition, 2006.
- [Koester, 1964] C. J. Koester and E. Snitzer. Amplification in a fiber laser. *Applied Optics*, 3: 1182–1186, 1964.
- [Koyama, 1988] F. Koyama, S. Kinoshita, and K. Iga. Room temperature cw operation of GaAs vertical cavity surface emitting laser. *IEICE Transactions*, E71-E: 1089-1090, 1988.
- [Lando, 2000] M. Lando, Y. Shimony, Y. Noter, R. M. J. Benmair, and A. Yogev. Passive Q switching of a solar-pumped Nd:YAG laser. *Applied Optics*, 39: 1962-1965, 2000.
- [Langrock, 2002] C. Langrock, D. S. Hum, E. Diamanti, M. Charbonneau-Lefort, *etc.*. Laser diode cw pumped Nd:YAG laser. *IEEE Journal on Selected Topics in Quantum Electronics*, XX: 101-103, March 2002.
- [Larlsson, 2000] G. Karlsson, V. Pasiskevicius, F. J. A. Tellefsen, B. Denker, B. I. Galagan, V. V. Osiko and S. Sverchkov. Diode-pumped Er–Yb:glass laser passively Q

switched by use of $\text{Co}^{2+}:\text{MgAl}_2\text{O}_4$ as a saturable absorber. *Applied Optics*, 39: 6188-6192, 2000.

[Laroche, 2006] M. Laroche, H. Gilles, S. Girard, N. Passilly, and K. Ait-Ameur. Nanosecond pulse generation in a passively Q -switched Yb-doped fiber laser by Cr^{4+} :YAG saturable absorber. *IEEE Photonics Technology Letters*, 18: 764-766, 2006.

[Letellier, 2007] C. Letellier, M. Bennoud, G. Martel. Intermittency and period-doubling cascade on tori in a bimode laser model. *Chaos, Solitons and Fractals*, 33: 782-794, 2007.

[Li, 2004] G. Li, S. Zhao, H. Zhao, K. Yang, S. Ding. Rate equations and solutions of a laser-diode end-pumped passively Q -switched intracavity doubling laser by taking into account intracavity laser spatial distribution. *Optics Communications*, 234: 321-328, 2004.

[Li, 2005a] G. Li, S. Zhao, K. Yang, and J. Zou. Laser-Diode end-pumped passively Q -switched intracavity-frequency-doubling Nd:GdVO₄/KTP green laser with GaAs saturable absorber. *IEEE Journal of Selected Topics in Quantum Electronics*, 11: 638-644, 2005.

[Li, 2005b] G. Li, S. Zhao, K. Yang and P. Song. Control of the pulse width in a diode-pumped passively Q -switched Nd:GdVO₄/KTP green laser with a Cr^{4+} :YAG saturable absorber. *Applied Optics*, 44: 5990-5995, October 2005.

[Li, 2006a] J. Li, K. Ueda, J. Dong, M. Musha, A. Shirakawa. Maximum value of the pulse energy of a passively Q -switched laser as a function of the pump power. *Applied Optics*, 45: 5277-5384, 2006.

[Li, 2006b] M. Li, S. Zhao, G. Li, K. Yang, D. Li, J. Wang and J. An. Analysis of a laser-diode end-pumped intracavity frequency-doubled passively Q -switched and mode-locked Nd:GdVO₄/KTP laser. *Journal of Optics A: Pure and Applied Optics*, 8: 1007-1012, 2006.

[Li, 2006c] G. Li, S. Zhao, K. Yang and D. Li. Investigation of a diode-pumped double passively Q -switched Nd:GdVO₄ laser with a Cr^{4+} :YAG saturable absorber and a GaAs coupler. *Journal of Optics A: Pure and Applied Optics*, 8: 155-163, 2006.

- [Li, 2006d] G. Li, S. Zhao, K. Yang and D. Li. Diode-pumped passively Q -switched Nd:YVO₄ green laser with a periodically poled KTP and Cr⁴⁺:YAG saturable absorber. *Applied Optics*, 45: 1825-1830, 2006.
- [Liu, 1999] J. Liu, D. Kim. Optimization of intracavity doubled passively Q -switched solid-state lasers. *IEEE Journal of Quantum Electronics*, 35: 1724-1730, 1999.
- [Liu, 2001] J. Liu, D. Shen, S. Tam, Y. Lam. Modeling pulse shape of Q -Switched lasers. *IEEE Journal of Quantum Electronics*, 37: 888-897, 2001.
- [Liu, 2003] J. Liu, B. Ozygus, S. Yang, J. Erhard, U. Seelig, A. Ding, et al.. Efficient passively Q -switching operation of a diode-pumped Nd:GdVO₄ laser with a Cr⁴⁺:YAG saturable absorber. *Journal of the Optical Society of America B*, 20: 652-660, 2003.
- [Maiman, 1960] Theodore H. Maiman. Stimulated optical radiation in Ruby. *Nature*, 187: 493-494, August 1960.
- [McClung, 1962] F. J. McClung and R. W. Hellwarth. Giant optical pulsations from ruby. *Journal of Applied Physics*, 33(3): 828-829, 1962.
- [McDaniel, 1976] Earl W McDaniel, Harry W Ellis, Fred L Eisele, Michael G Thackston. *Bibliography on sources of information on phenomena of interest in gas laser research and development*. Defense Technical Information Center, 1976.
- [Mercer, 2007] C. J. Mercer, Y. H. Tsang, D. J. Binks. A model of a QCW diode pumped passively Q -switched solid state laser. *Journal of Modern Optics*, 54: 1685-1694, 2007.
- [Mirels, 1972] H. Mirels, R. Hofland, and W. S. King. Simplified model of CW diffusion type chemical laser. *AIAA Journal*, 11: 156-184, 1973.
- [Morris, 1990] J. A. Morris and C.R. Pollock. Passive Q -switching of a diode pumped Nd:YAG laser with a saturable absorber. *Optics Letters*, 15: 440-442, 1990.
- [Moulton, 1986] P. F. Moulton. Spectroscopic and laser characteristics of Ti:Al₂O₃. *Journal of the Optical Society of America B*, 3: 125-133, 1986.

- [Nathan, 1962] M. I. Nathan, W. Dumke, G. Burns, F. H. Dill Jr., and G. Lasher. Stimulated emission of radiation from GaAs p-n junctions. *Applied Physics Letter*, 1: 62-64, 1962.
- [Ng, 2006] S. P. Ng, D. Y. Tang, L. J. Qian, L. J. Qin. Satellite pulse generation in diode-pumped passively *Q*-switched Nd:GdVO₄ lasers. *IEEE Journal of Quantum Electronics*, 42: 625-632, 2006.
- [Patel, 1964] C. K. N. Patel. Continuous-wave laser action on vibrational-rotational transitions of CO₂. *Physical Review*, 136 (5A): A1187-A1193, 1964.
- [Patel, 2001] F. D. Patel and R. J. Beach. New formalism for the analysis of passively *Q*-switched laser systems. *IEEE Journal Quantum Electronics*, 37: 707-715, 2001.
- [Pavel, 2001] N. Pavel, J. Saikawa and T. Taira. Diode end-pumped passively *Q*-switched Nd:YAG laser intra-cavity frequency doubled by LBO crystal. *Optics Communications*, 195: 233-240, 2001.
- [Pellat-Finet, 1994] P. Pellat-Finet. Fresnel diffraction and the fractional-order Fourier transform. *Optics Letters*, 19: 1388-1390, 1994.
- [Peterson, 1970] O. G. Peterson, S. A. Tuccio, and B. B. Snavely. CW operation of an organic dye solution laser. *Applied Physics Letters*, 17: 245-246, 1970.
- [Petrov, 1999] V. Petrov, F. Rotermund, F. Noack, J. Ringling, O. Kittelmann, and R. Komatsu. Frequency conversion of Ti:Sapphire-based femtosecond laser systems to the 200-nm spectral region using nonlinear optical crystals. *IEEE Journal of Selected Topics in Quantum Electronics*, 5: 1532-1542, 1999.
- [Philippov, 2004] V. N. Philippov, A. V. Kir'yanov, S. Unger. Advanced Configuration of Erbium Fiber Passively *Q*-Switched Laser With Co²⁺:ZnSe Crystal as Saturable Absorber. *IEEE Photonics Technology Letters*, 16: 57-59, 2004.
- [Poppe, 1998] A. Poppe, L. Xu, F. Krausz, and C. Spielmann. Noise characterization of sub-10-fs Ti:Sapphire oscillators. *IEEE Journal of Selected Topics in Quantum Electronics*, 4: 179-184, 1998.
- [Powell, 1998] Richard C. Powell. *Physics of solid-state laser materials*. Springer, 1998.

- [Press, 1992] W. H. Press, B. P. Flannery, S. A. Teukolsky, W. T. Vetterling. *Numerical Recipes in C: The Art of Scientific Computing*. Cambridge University Press, second edition, October 1992.
- [Peterson, 1999] P. Peterson, A. Gavrielides, M.P. Sharma and T. Emeux. Dynamics of passively Q-switched microchip lasers. *IEEE Journal of Quantum Electronics*, 35: 1247-1256, 1999.
- [Quist, 1962] T. M. Quist, R. H. Rediker, R. J. Keyes, W. E. Krag, B. Lax, A. L. McWhorter, and H. J. Zeigler. Semiconductor maser of GaAs. *Applied Physics Letters*, 1: 91-92, 1962.
- [Ramaswamy, 1993] M. Ramaswamy, M. Ulman, J. Paye, and J. G. Fujimoto. Cavity-dumped femtosecond Kerr-lens mode-locked Ti:Al₂O₃ laser. *Optics Letters*, 18: 1822-1824, 1993.
- [Runge, 1972] P. K. Runge, R. Rosenberg. Unconfined flowing-dye films for cw dye lasers. *IEEE Journal of Quantum Electronics*, QE-8: 910, 1972.
- [Saleh, 1991] Bahaa E. A. Saleh, and Malvin C. Teich. *Fundamental of Photonics*. New York: John Wiley & Sons, 1991.
- [Schafer, 1966] F. P. Schafer, W. Schmidt, and J. Volze. Organic dye solution laser. *Applied Physics Letters*, 9:306-309, 1966.
- [Schibli, 2003] T. R. Schibli, O. Kuzucu, J. Kim, E. P. Ippen, J. G. Fujimoto, F. X. Kaertner, V. Scheuer, and G. Angelow. Toward single-cycle laser systems. *IEEE Journal of Selected Topics in Quantum Electronics*, 9: 990-1001, 2003.
- [Sennaroglu, 2007] Alphan Sennaroglu. *Solid-state lasers and applications*. CRC Press, 2007.
- [Shahruz, 1999] S. M. Shahruz and T. A. Mahavaraha. A system theoretic approach to the stability of passively Q-switched lasers. *IEEE Transactions on Circuits and Systems-I: Fundamental Theory and Applications*, 46: 512-517, April 1999.

- [Shahruz, 2000] S. M. Shahruz and T. A. Mahavaraha. A system theoretic approach to the stability of passively Q -switched lasers. *IEEE Transactions on Circuits and Systems I: Fundamental Theory and Applications*, 46: 512-517, 2000.
- [Shank, 1974] C. V. Shank, and E. P. Ippen. Subpicosecond kilowatt pulses from a modelocked cw dye laser. *Applied Physics Letters*, 24: 373, 1974.
- [Shank, 1975] C. V. Shank. Physics of dye lasers. *Reviews of Modern Physics*, 47: 649-657, 1975.
- [Shimony, 1995] Y. Shimony, Z. Burshtein and Y. Kalisky. Cr^{4+} :YAG as passive Q -switch and brewster plate in a pulsed Nd:YAG laser. *IEEE Journal of Quantum Electronics*, 31: 1738-1741, October 1995.
- [Siegman, 1986] A. E. Siegman. *Lasers*. University Science Books, 1986.
- [Sillard, 1998] P. Sillard, C. Grange, A. Brignon, J. P. Huignard, In-line Nd:YAG resonator using self-pumped phase conjugation in Cr^{4+} :YAG. *Optics Letter*, 23: 37-39, 1998.
- [Snitzer, 1961] E. Snitzer. Optical maser action of Nd^{+3} in barium crown glass. *Physical Review Letters*, 7: 444-446, 1961.
- [Soden,1965] Ralph R. Soden, Scotch Plains, and Le Grand G. Van Uitert. *Optical Maser Crystals*. Patent US 3177155 A, 1965.
- [Soffer, 1967] B. H. Soffer, B. B. McFarland. Continuously tunable, narrow-band organic dye lasers. *Applied Physics Letters*, 10: 266- 267, 1967.
- [Song, 2000] J. Song, C. Li, N.S. Kim, K. Ueda. Passively Q -switched diode-pumped continuous-wave Nd:YAG- Cr^{4+} :YAG laser with high peak power and high pulse energy. *Applied Optics*, 39: 4954-4958, 2000.
- [Sorokin, 1966] P. P. Sorokin, and J. R. Lankard. Stimulated emission observed from an organic dye, chloro-aluminum phtalocyanine. *IBM Journal of Research and Development*, 10: 162-163, 1966.

- [Spencer, 1969] D. J. Spencer, T. A. Jacobs, H. Mirels, and R. W. F. Gross. Continuous wave chemical laser. *International Journal of Chemical Kinetics*, 1: 493-494, 1969.
- [Spielmann, 1991] C. Spielmann, F. Krausz, T. Brabec, E. Wintner, and A. J. Schmidt. Femtosecond pulse generation from a synchronously pumped Ti:Sapphire laser. *Optics Letters*, 16: 1180-1182, 1991.
- [Spariosu, 1993] K. Spariosu, W. Chen, R. Stultz, M. Birnaum, A. V. Shestakov, Dual Q -switching and laser action at 1.04 and 1.44 μm in a $\text{Nd}^{3+}:\text{YAG}-\text{Cr}^{4+}:\text{YAG}$ oscillator at 300K. *Optics Letter*, 18: 814-816, 1993.
- [Staliunas, 2003] K. Staliunas, Victor J. Sanchez Morcillo. *Transvers patterns in nonlinear optical resonators*. Springer, 2003.
- [Sulc, 2004] J. Sulc, H. Jelinkova, M. Nemeč, K. Nejezchleb, V. Skoda. V:YAG saturable absorber for flash-lamp and diode-pumped solid state lasers. *Proceeding of the SPIE*, 5460: 292-302, 2004.
- [Szabo, 1965] A. Szabo and R. A. Stein. Theory of laser giant pulsing by a saturable absorber. *Journal of Applied Physics*, 36: 1562-1566, 1965.
- [Trester, 1999] S. Trester. Computer-simulated Fresnel diffraction using Fourier transform. *Computing in Science and Engineering*, 1:77-73, 1999.
- [Ujević, 2005] N. Ujević. A generalization of the modified Simpson's rule and error bounds. *ANZIAM J.*, 47 (E): E1-E13, 2005.
- [Vasilenko, 1975] L. S. Vasilenko, N. M. Dyuba, M. N. Skvortsov, and V. P. Chebotaev. Emission spectrum of a carbon dioxide laser with passive Q switching. *Soviet Journal of Quantum Electronics*, 5: 246-247, 1975.
- [Verschaffelt, 2003] G. Verschaffelt. Frequency response of polarization switching in vertical-cavity surface-emitting lasers. *IEEE Journal of Quantum Electronics*, 39: 1177-1186, 2003.
- [Voitkov, 2005] S. V. Voitkov, A. A. Demidovich, L. E. Batay, A. N. Kuzmin, M. B. Danailov. Sub-nanosecond pulse dynamics of Nd:LSB microchip laser Q -switched by Cr:YAG saturable absorber. *Optical Communication*, 251: 154-164, 2005.

- [Wagner, 1963] W. G. Wagner and B. A. Lengyel. Evolution of the giant pulse in a laser. *Journal of Applied Physics*, 34: 2040-2046, 1963.
- [Wang, 2002] C. Wang, Y. Weng, P. Huang, H. Cheng and S. Huang. Passively Q -switched quasi-three-level laser and its intracavity frequency doubling. *Applied Optics*, 41: 1075-1081, February 2002.
- [Welch, 2000] David F. Welch. A brief history of high-power semiconductor lasers. *IEEE Journal of Selected Topics in Quantum Electronics*, 6: 1470-1477, 2000.
- [Welford, 2003] D. Welford. Passively Q -switched lasers. *IEEE Circuits and Devices Magazine*, 19: 31-36, 2003.
- [White, 1962] A. D. White, J. D. Rigden. Continuous Gas Maser Operation in the Visible. *Proc. IRE*, 50: 1697, July 1962.
- [Xiao, 1997] G. Xiao and M. Bass. A generalize model for passively Q -switched lasers including excited state absorption in the saturable absorber. *IEEE Journal of Quantum Electronics*, 33: 41-44, 1997.
- [Xiao, 1998] G. Xiao and M. Bass. Additional Experimental Confirmation of the Prediction of a Model to Optimize Passively Q -Switched Lasers. *IEEE Journal of Quantum Electronics*, 34: 1142-1143, 1998.
- [Yang, 2004] K. Yang, S. Zhao, G. Li, and H. Zhao. A new model of laser-diode end-pumped actively Q -Switched intracavity frequency doubling laser. *IEEE Journal of Quantum Electronics*, 40: 1252-1257, 2004.
- [Yang, 2005] K. Yang, S. Zhao, G. Li, and H. Zhao. Theoretical and experimental study of a laser-diode-pumped actively Q -Switched Nd:YVO₄ laser with acoustic-optic modulator. *Optics and Laser Technology*, 37: 381-386, 2005.
- [Yang, 2006] K. Yang, S. Zhao, G. Li, M. Li, D. Li, J. Wang and J. An. Diode-pumped passively Q -switched mode-locked c-cut Nd:GdVO₄/KTP green laser with a GaAs wafer. *IEEE Journal of Quantum Electronics*, 42: 683-689, July 2006.
- [Yankov, 1994] P. Yankov. Cr⁴⁺:YAG Q -switching of Nd:host laser oscillators. *Journal of Physics D: Applied Physics*, 27: 1118-1120, 1994.

- [Zayhowshi, 2003] J. J. Zayhowski, A. L. Wilson, Jr.. Pump-induced bleaching of the saturable absorber in short-pulse Nd:YAG/Cr⁴⁺:YAG passively *Q*-switched microchip lasers. *IEEE Journal of Quantum Electronics*, 39: 1588-1593, 2003.
- [Zhang, 1994] X. Zhang, S. Zhao, Q. Wang, Y. Liu and J. Wang. Optimization of dye *Q*-switched lasers. *IEEE Journal of Quantum Electronics*, 30: 905–908, 1994.
- [Zhang, 1997] X. Zhang, S. Zhao, Q. Wang, Q. Zhang, L. Sun, S. Zhang. Optimization of Cr⁴⁺-Doped saturable-absorber *Q*-switched lasers. *IEEE Journal of Quantum Electronics*, 33: 2286-2294, 1997.
- [Zhang, 2003] S. Zhang, Q. Wang, X. Xu, C. Dong, X. Zhang and P. Li. Diode-laser pumped passively *Q*-switched green laser by intracavity frequency-doubling with periodically poled LiNbO₃. *Optics & Laser Technology*, 35: 233 – 235, 2003.
- [Zhang, 2006] L. Zhang, Z. Duan, J. Chen. Analytical solutions to rate equations of fiber lasers containing three-energy-level ions. *Optics Communications*, 267: 149-153, 2006.
- [Zhou, 1994] J. Zhou, G. Taft, C. Huang, M. M. Murnane, and H. C. Kapteyn. Pulse evolution in a broad-bandwidth Ti:sapphire laser. *Optics Letters*, 19: 1149-1151, 1994.
- [Zhou, 2006] X. Zhou, H. Kapteyn, and M. Murnane. Positive-dispersion cavity-dumped Ti:Sapphire laser oscillator and its application to white light generation. *Optics Express*, 14: 9750-9757, 2006.

University of Sussex

Doctor of Philosophy

Title: **Performance of Continuously Pumped, Passively Q-Switched, Solid State Lasers**

Summary

Min Lu

Department of Engineering and Design

This thesis studies the relationship between the selection of an output reflectivity and absorber initial transmission pair and the FWHM pulse duration of a continuously pumped passively Q -switched solid-state laser when the output energy is pre-determined. According to the different magnitude of the pumping power, three models based on the laser rate equations are proposed to get the proper output reflectivity and absorber initial pair with the corresponding FWHM pulse duration.

The working principle of the passively Q -switched laser decides that the pumping power and the output reflectivity and absorber initial pair determine the build-up time of the Q -switching and the repetition rate of the laser system. Hence, the models set up in this thesis based on two conditions: 1) the build-up time of the Q -switching; and 2) the recovery time of the absorber (which is assumed to be nearly equal to the repetition rate of the laser in the thesis).

When the build-up time of the Q -switching is short, but the recovery time of the absorber are long, *Model I* based on the simplified laser rate equations is used to get the output reflectivity and absorber initial pair to satisfy the pre-determined output energy and calculate the FWHM pulse duration. *Model II* is set up to study the case when both the build-up time of the Q -switching and the recovery time of the absorber are long. In *Model II*, the laser rate equations are solved by the Runge-Kutta method. *Model III* is suitable for the case when the recovery time of the absorber is short.

Generalizing the simulation results obtained from different passively Q -switched laser systems with different pumping power and different pre-determined output energy yields the general conclusions, which can help the designer to select the proper couple of output reflectivity and absorber initial transmission to control the FWHM pulse duration as the output energy is decided.